SIZE-SELECTED 2, 5, AND 10 NM GOLD NANOPARTICLES FOR LASER DESORPTION/IONIZATION MASS SPECTROMETRY

A Dissertation

by

KATHERINE ANNE STUMPO

Submitted to the Office of Graduate Studies of
Texas A&M University
in partial fulfillment of the requirements for the degree of

DOCTOR OF PHILOSOPHY

December 2008

Major Subject: Chemistry

SIZE-SELECTED 2, 5, AND 10 NM GOLD NANOPARTICLES FOR LASER DESORPTION/IONIZATION MASS SPECTROMETRY

A Dissertation

by

KATHERINE ANNE STUMPO

Submitted to the Office of Graduate Studies of
Texas A&M University
in partial fulfillment of the requirements for the degree of

DOCTOR OF PHILOSOPHY

Approved by:

Chair of Committee,	David H. Russell
Committee Members,	Paul S. Cremer
	John Fackler
	Gerard Coté
Head of Department,	David H. Russell

December 2008

Major Subject: Chemistry

ABSTRACT

Size-Selected 2, 5, and 10 nm Gold Nanoparticles for Laser Desorption/Ionization Mass Spectrometry. (December 2008)

Katherine Anne Stumpo, B.S., University of Northern Iowa

Chair of Advisory Committee: Dr. David H. Russell

The analytical utility of gold nanoparticles (AuNPs) for laser desorption/ionization mass spectrometry (LDI-MS) is examined here. An evaluation of the parameters that affect desorption/ionization show that careful treatments of AuNPs is needed, as subtle changes in the solution environment can result in subsequent changes in the mass spectra. A thorough evaluation of the parameters that affect desorption/ionization of peptides is presented here, and these parameters include: (i) AuNP-to-analyte ratio, (ii) AuNP size, (iii) solvent, (iv) AuNP surface composition, (v) pH and buffer effects, (vi) amino acid sequence, and (vii) additives such as fructose or glycerol. Specifically, controlling the AuNP-to-analyte ratio, pH, peptide composition, and AuNP size are important parameters for ionization. Additionally, effects of passivating the AuNP surface with halides or oxyanions was investigated. The presence of NaF, NaCl, NaBr, and NH_4X (X = F, Cl, Br, I) were shown to not significantly affect analyte ion abundances, whereas addition of NaI strongly suppressed analyte ion yields. Further physical characterization of the NPs showed that etching had occurred, which suggests that the surface chemistry of the NPs is important for desorption/ionization.

Throughout these investigations, questions remain as to what the internal energies of peptides are after the desorption/ionization event, and how energy is deposited. Peptide ion fragmentation is examined under different solution conditions to evaluate the relative internal energies of peptides, and the fragmentation pattern examined for insight into fragmentation mechanisms. The data suggest that radical species are important for fragmentation of peptides when using AuNPs. However, it is likely that multiple processes are actually directing the fragmentation. Finally, based on the data presented in this dissertation, a thermal desorption mechanism of pre-formed ions is proposed. This fundamental research is intended to lay foundations for optimizing the use of nanoparticles in routine LDI-MS analysis as well as giving insight into nanoparticle ionization mechanisms. Since very little work has been done in this area, this dissertation investigates, in detail, many of the subtle characteristics that affect desorption/ionization of biomolecules when using NPs.

DEDICATION

This dissertation is dedicated to various parts of my family. To my parents for always telling me I could go and do whatever I wanted, all I had to do was try. To JeFF for following me to Texas and for the good (and bad) days we both had during graduate school. And of course Stubby and Apple for much needed comic relief.

ACKNOWLEDGEMENTS

I thank my committee chair, Dr. David Russell for the opportunity to be a part of his research group, and all of his support and insight throughout my graduate career. Many current and past members of the Russell Research Group have been sources of guidance and support. In particular, I thank Dr. John McLean for early guidance on this project and in graduate school in general. I thank Stacy Sherrod, Stephanie Cologna, Dr. Chris Becker, and Kevin Kmeic for helpful discussions and a keen editing eye on various matters.

I would like to acknowledge Dr. Zhiping Luo at the Microscopy and Imaging Center and Mario Gomez of the Russell Group for time and assistance with Transmission Electron Microscopy. Dr. Garrett Slaton generously provided the synthesized peptides. Thanks goes to the sponsors of this work, The National Science Foundation, National Institutes of Health, and The Welch Foundation.

The women of Women in Science and Engineering provided a network of opportunities, and I thank all the members for good conversation and encouragement. Finally, I thank Dr. Nancy Magnussen and Dr. Marian Hyman for their friendship and a supportive ear, and especially for their invaluable advice about being a woman in science.

TABLE OF CONTENTS

CHAPTER Page

LIST OF FIGURES

FIGURE Page

FIGURE Page

FIGURE Page

FIGURE Page

FIGURE Page

FIGURE Page

LIST OF TABLES

CHAPTER I

INTRODUCTION

Mass spectrometry (MS) has long been a powerful tool in biomolecule structural analysis. However, until the advent of "soft" ionization techniques such as electrospray ionization (ESI) or matrix-assisted laser desorption/ionization (MALDI), analysis of intact biomolecules has been difficult. Both of these methods result in ions having low internal energies and very little fragmentation occurs during the ionization process. MALDI was pioneered by Karas and Hillenkamp, where they used small organic acid matrices to facilitate energy transfer to biomolecules, resulting in subsequent desorption and/or ionization.[1] Concurrently, Tanaka *et al.* developed a method by which small 30 nm cobalt particles suspended in glycerol promoted desorption and/or ionization of large, thermally labile proteins and protein aggregates.[2]

Since that time, much work has been done exploring the use of organic acid matrices, and determining optimum conditions for desorption/ionization of biomolecules,[3-10] and only a relatively few studies have been done using nanoparticulate materials. Early experiments with nanomaterials used graphite or other species suspended in glycerol. For example, Sunner *et al.* utilized large (2 – 150 μm) graphite particles suspended in glycerol, and successfully laser desorbed peptides with low limits-

---

This dissertation follows the style and format of the *Journal of the American Chemical Society*.

of-detection (pmol-nmol range), but low mass resolution (300). The authors claimed a thermal desorption/ionization mechanism similar to what Tanaka originally suggested.[2, 11] Dale and co-workers also investigated graphite particles (2 μm) in combination with a liquid matrix. They were able to ionize proteins, oligosaccharides, and synthetic polymers with detection limits as low as 50 fmol; the mechanism proposed was again thermal desorption.[12] Schürenberg *et al.* used several different nanomaterials suspended in glycerol, with the best results from 35 nm titanium nitride in glycerol, 19-55 nm tantalum in glycerol, and nano-soot in glycerol. The most important findings of this study were that mass spectra of cytochrome *c* (13 kDa) were obtained with comparable quality to organic acid matrices, detection limits were as low as a few tens of femtomoles for peptides, and desorption/ionization was achieved over a large range of wavelengths (337, 500-760, 1064 nm).[13]

Other nanomaterials, such as silicon nanopores or nanoparticles have also been shown to promote LDI.[14-19] While this is an alternative method for LDI-MS, these experiments typically involve surfaces that have been etched to create nanofeatures, and none of the surface is desorbed/ionized. Therefore, the mechanistic considerations from these experiments are less relevant, and will not be discussed further unless directly applicable.

Very few examples of noble metal (copper, silver, gold) particles or thin films exist. Lai *et al.* deposited a sample overlayer on a thin silver film substrate, and then illuminated the sample by backside irradiation, resulting in desorption/ionization of small biomolecules.[20] Li *et al.* determined that desorption/ionization from thin gold films

was possible.[21] Finally, Chen and co-workers described LDI of biomolecules on gold-coated porous silicon and gold nanorods (~15 nm diameter with lengths from 50-200 nm). They were able to desorb/ionize small peptides and sugars and primarily observed the $[M + Na]^+$ ion, which they suggested was a result of gas-phase cationization.[22] In a related study using dissociation spectroscopy, large metal clusters irradiated with a laser resulted in desorption of atoms or photoemission of electrons. Whole clusters were even evaporated from the surface owing to thermal heating. Desorbed species were detected using a quadrupole mass spectrometer.[23]

All of these studies used nanomaterials larger than 35 nm or thin films. Interestingly, noble metal nanoparticles exhibit unique optical and electronic properties at smaller sizes, specifically in the 2 – 5 nm size regime. Therefore, the studies discussed in this dissertation use 2, 5, and 10 nm gold nanoparticles (AuNPs) in order to investigate size-related effects on LDI of biomolecules.

Nanoparticle Optical and Electronic Properties

The unique optical properties of AuNPs have been used for coloration of glass, ceramics, and pottery[24] dating back to the middle ages. The Lycurgus cup was crafted by the Romans in the 4th century BC[25] and changes color from green in reflected light to red in transmitted light as a result of the colloidal material in it. In 1857 Faraday reported the synthesis of gold colloidal solutions with colors varying from ruby red to amethyst. He correctly postulated that the color indicated the presence of aggregates of gold atoms and his work is now marked as the beginning of colloid science.[26]

The physical origin for the color observed in small metal NPs is the coherent oscillation of the conduction band electrons interacting with an electromagnetic field. This resonance is known as a surface plasmon resonance (SPR) band. The electric field of an incoming light wave induces polarization of the electrons with respect to the heavy core of the NP. A net charge difference only occurs at the NP surface, and interaction of the electrons with the electric field creates a dipolar oscillation of the electrons, as Figure 1 depicts. When the frequency of electromagnetic radiation is resonant with the electron motion, a strong absorption band in the UV-Visible absorption spectrum is observed (see Figure 2), and this is the origin of the NP color. A number of factors influence the frequency and width of the SPR band, including: size, shape, monodispersity, composition, the dielectric constant of the surrounding medium, stabilizing ligands, and interactions between the ligands. [24, 27]

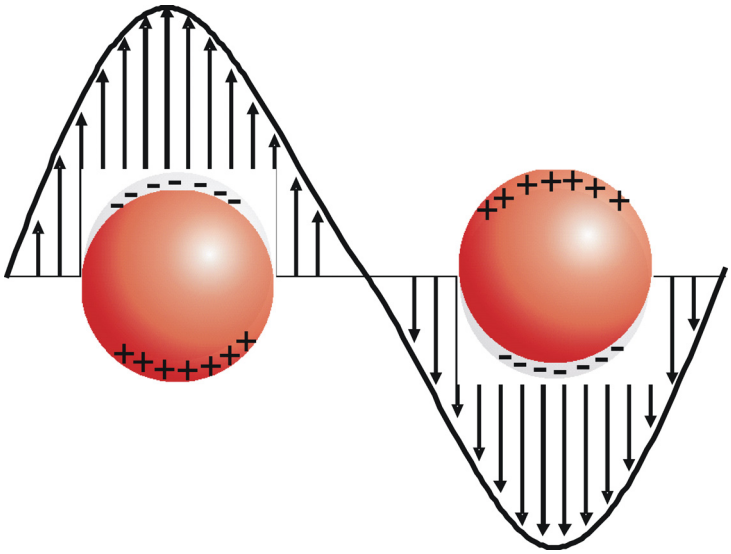

Figure 1. Pictoral representation of NP electron motion in an electric field.

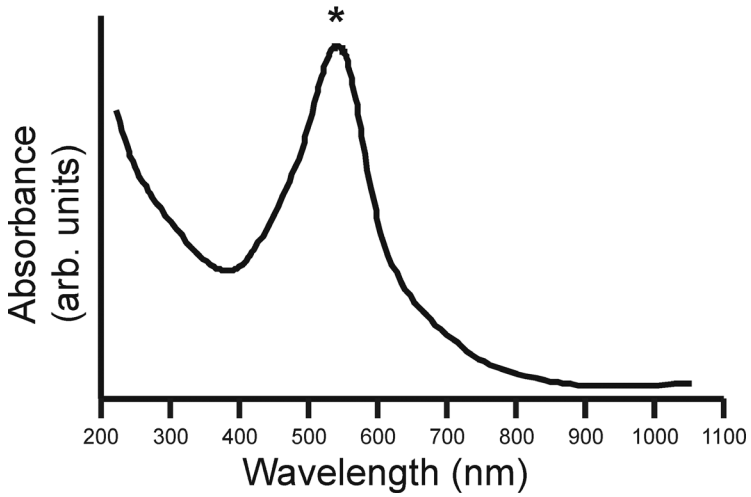

Figure 2. Pictoral representation of a surface plasmon resonance band (*).

Noble metals have very strong plasmon resonances, making them widely used in optical and electronics applications. Most other transition metals have only a broad and poorly resolved absorption band.[28] This difference is due to the "free" motion of the electrons in the conduction band, giving the electrons a higher polarizability, which in turn makes the plasmon resonance shift to lower frequencies.

The optical properties that account for surface plasmon resonance were theorized by Mie in 1908.[29] Mie's solution for Maxwell's equations of electromagnetism aimed to describe the optical absorption and scattering of light by a cluster, and was broken into two parts: the electromagnetic and the material part. Mie's solution treated the material properties in a new way where only the complex dielectric constants entered the calculation. He also introduced the phenomenological dielectric functions $\varepsilon(\omega, R)$, which incorporated the radius of a particle into the equation. These phenomenological optical material functions resulted in wide applicability, as they can incorporate all important

cluster effects for many different materials (*e.g.*, metal NPs, ionic crystals, semiconductor materials).[30,31]

For NPs much smaller than the wavelength of light (< 20 nm), Mie's theory reduces to the following expression:

$$\sigma = \frac{9 \cdot V \cdot \varepsilon_m^{3/2}}{c} \cdot \frac{\omega \cdot \varepsilon_2(\omega)}{[\varepsilon_1(\omega) + 2 \cdot \varepsilon_m]^2 + \varepsilon_2(\omega)^2}, \quad 30$$

where V is the particle volume, ω is the angular frequency of the exciting light, and c is the speed of light. The dielectric function of the surrounding medium and the metal are ε_m and $\varepsilon(\omega) = \varepsilon_1(\omega) + i\varepsilon_2(\omega)$, respectively. The dielectric function of the metal is complex and depends on the frequency. This equation does have limitations; it does not accurately describe effects for NPs less than ~2 nm, which are better treated as molecular clusters with discrete electronic states.[27] Secondly, it only takes into account dipolar resonances, and while multipolar oscillations can occur as Mie predicted, they are typically only of importance when dealing with non-spherical or very large particles.[27]

As NPs become smaller the energy level spacing within the system is affected, specifically for particles smaller than 2 nm. Similarly to particle-in-a-box, as NP dimension decreases the energy spacing between adjacent levels increases. Eventually this leads to quantum size effects owing to the quantization of energy levels, but in order to observe localization of the energy levels the size must be well below 2 nm. A

theoretical investigation of quantum size effects is beyond the scope of this research and will not be discussed further.

The dynamics of electrons in NPs < 2 nm have been investigated by various groups, and have some relevance here. Using ultrashort laser pulses electrons of metal NPs can be selectively excited, and electron processes followed in real time.[32] A discussion on the role of electrons emitted from NPs is discussed in detail in Chapter VI.

Time-of-Flight Mass Spectrometry

The concept of time-of-flight (TOF) mass spectrometry was first proposed in 1946 by W.E. Stephens[33] and the first instrument of this type was built in 1948 by Cameron and Eggers.[34] In 1955 Wiley and McLaren introduced a pulsed ion extraction TOF instrument that specifically addressed issues relating to mass resolution, and the first commercial TOF instrument was produced.[35] There was not much progress in TOF development from this time until the 1980s, when improved electronics simplified data handling. The discovery of LDI and MALDI techniques in the late 1980s[1, 2] also renewed interest in TOF, as the pulsed nature of these ionization techniques are well suited to TOF.

In a basic LDI-TOF instrument, ions are formed at the surface of the backing plate, accelerated through the entire source-extraction region to the same final kinetic energy, enter the field-free drift region where they separate based on their mass-to-charge ratio (*m/z*), and are then detected (see Figure 3). The kinetic energy of the ions is described by:

$$KE = \frac{1}{2}mv^2.$$

Ions cross the drift region with velocities:

$$v = \left(\frac{2KE}{m}\right)^{1/2},$$

and flight times:

$$t = \left(\frac{m}{2KE}\right)^{1/2} D,$$

which depend on the square root of their masses.

Mass resolution in a TOF instrument depends on a number of factors, including: time resolution (and therefore laser pulse widths), detector response, digitizing rates, and ion initial kinetic energies. Mass resolution is defined as:

$$R = \frac{m}{\Delta m} = \frac{t}{2\Delta t}.$$

TOF instruments have long been considered low resolution instruments and several factors contribute to this; however, new instrument designs have significantly improved resolution in TOF instruments. The major contributors to low resolution are time, space, and kinetic energy distributions.[36]

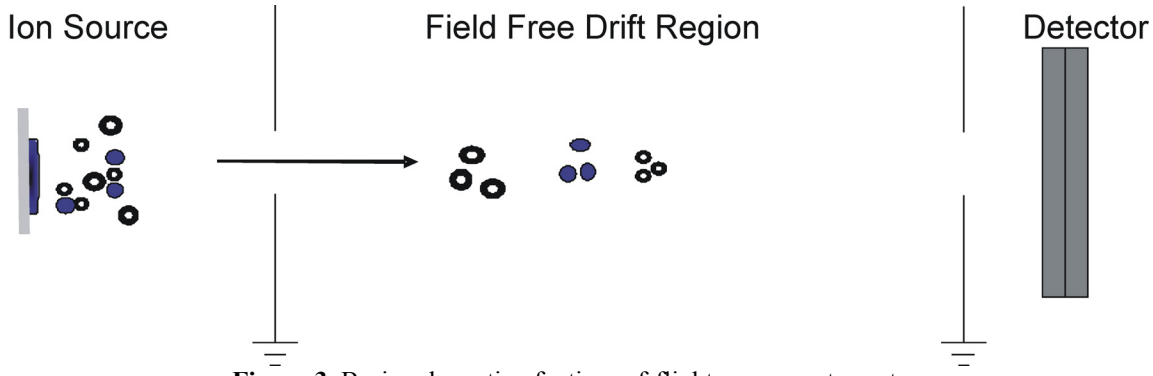

Figure 3. Basic schematic of a time-of-flight mass spectrometer.

Temporal distributions include differences in the time of ion formation, as well as differences in ion detection time. Ions of the same *m/z* that are formed at different times can enter the drift region at different times, but maintain a constant time difference, Δt, as they approach the detector. Since mass resolution is dependent on $t/2\Delta t$, longer flight tubes result in longer flight times, and will increase t while maintaining a constant Δt.[36]

Spatial distributions include ions that are formed in different regions of the source and are thereby accelerated through different distances in the extraction field, resulting in a distribution of final kinetic energies. For example, ion A is formed directly on the surface of the sample plate and ion B at some distance above the surface of the sample plate. Ion B will exit the source region sooner and with a lower velocity, and will arrive at the detector later than ion A. This appears in the mass spectrum as peak tailing. Delayed extraction can help correct spatial distributions, and is illustrated in Figure 4. With continuous extraction ions are immediately pulsed into the drift region and reach the detector at slightly different times because of the difference in kinetic energy, these

ions are focused at some point in the drift region (Figure 4A). Delayed extraction allows the ions to expand into a field free region in the source, and after a certain time delay (typically hundreds of nanoseconds) a voltage pulse is applied to extract the ions from the source; ions have a narrower final kinetic energy distribution and are focused just before entering the detector (Figure 4B).[36, 37]

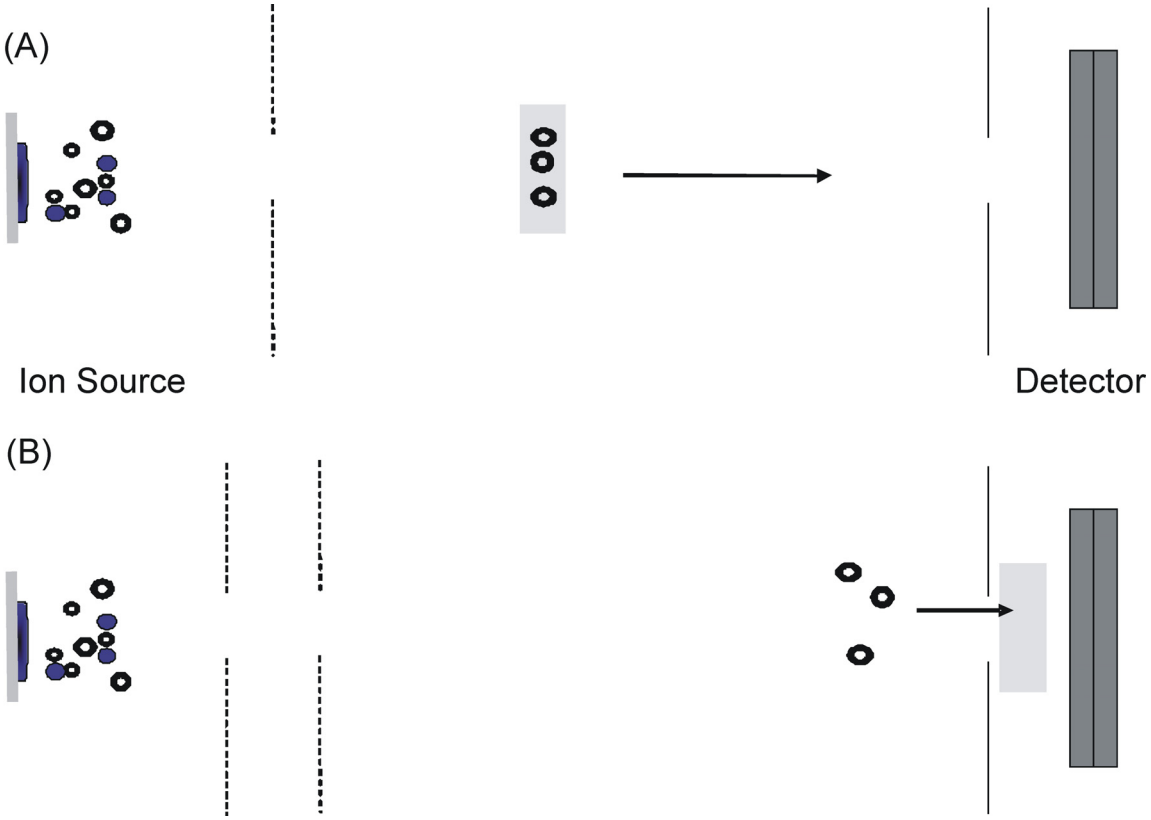

Figure 4. Schematic of (A) a continuous extraction source and (B) a delayed extraction source.

Initial kinetic energy distributions arise from 2 main sources: (i) the ionization process,[38-40] and (ii) in instruments where spatial distributions dominate, as delayed extraction can increase the final kinetic energy spread.[36] The best way to improve mass

resolution and to counteract the energy spread is by using an electrostatic reflector, or a reflectron. The reflectron is an ion mirror which reverses the direction of ion motion by means of a retarding electric field. This corrects the kinetic energy distribution of ions leaving the source with the same *m/z*, as ions with higher kinetic energy will spend more time in the reflectron, thereby allowing them to reach the detector at the same time as ion with lower kinetic energies, which spend less time in the reflectron.[36]

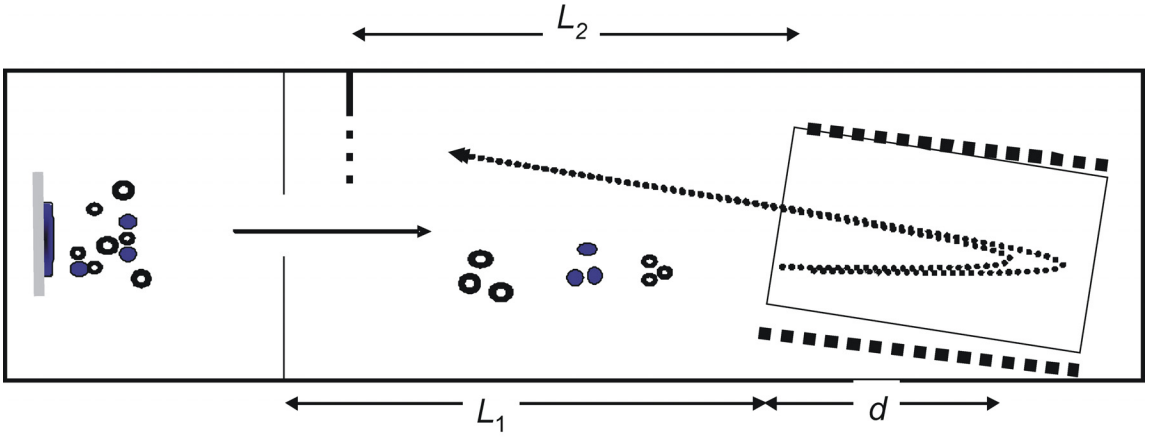

Figure 5. Schematic of a reflectron time-of-flight instrument.

The total flight time of ion is now represented by:

$$t = \left(\frac{m}{2KE}\right)^{1/2} [L_1 + L_2 + 4d],$$

where L_1 is the distance from the exit of the source to the entrance of the reflectron, L_2 is the distance from the exit of the reflectron to the detector, and d is the penetration depth into the reflectron, which will vary with kinetic energy.

Peptide Fragmentation

As previously stated, MALDI typically results in low ion internal energies and little fragmentation occurs during desorption/ionization. However, ions can be collisionally activated which results in ion fragmentation. LDI of analytes using AuNPs also produces a similar effect, as Chapters IV and V describe. Therefore, it is useful to have a description of peptide fragmentation here. Ion dissociation typically occurs through the lowest energy pathways and for peptides this typically results in breaking bonds along the backbone. Fragment ion nomenclature is illustrated in Figure 6, as given by Roepstorff and Fohlman.[41] Cleavage of the peptide amide backbone that results in charge retention at the N-terminus yields a-, b-, and c-type ions; charge retention at the C-terminus results in x-, y-, and z-type ions. Ions that result from simple bond cleavage are denoted with capital letters (*e.g.*, B_n-, Y_n-type ions). The addition of 2 hydrogens to a Y_n- type ion results in a y_n-, type ion; the y-type product ion is more commonly observed than the Y-type ion. Odd-electron species can also be observed, and ions are denoted here with a radical symbol (*e.g.*, $a^{\bullet}$). Further to this work, Biemann identified other fragment ions which consist of cleavage of the amino acid side chain.[42] Partial or complete elimination of side chains yields d-, v-, and w-type ions (see Figure 6). Partial side chain loss of an a-type ion yields a d-type ion, complete side chain loss of a y-type ion results in a v-type ion, and partial side chain loss of a z-type ion yields a w-type ion. The amino acids isoleucine and threonine are branched at the β-carbon and ions are labeled depending on which brand is cleaved (*e.g.*, d_a-, d_b-, w_a-, and w_b-type ions).

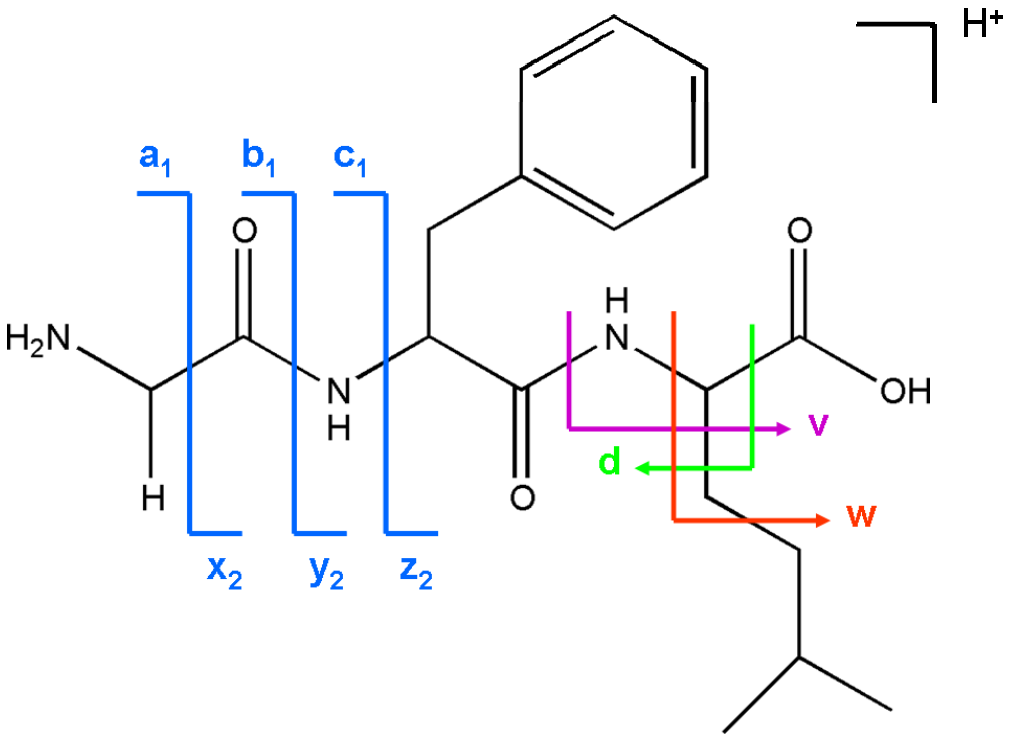

Figure 6. Peptide fragmentation nomenclature.

Peptides typically fragment in a predictable manner depending on the excitation method. Low-energy activation methods such as collision induced dissociation (CID) involves accelerating ions into a neutral background gas. Low energy collisions (1 keV) typically yield b- and y-type ions, as the carbonyl-amide bond is the most labile. Other techniques have been shown to induce unique peptide ion fragmentation of other backbone bonds. Electron transfer dissociation (ETD) and electron capture dissociation (ECD) typically result in cleavage of the N-C_α bonds of the peptide backbone, yielding c- and z-type ions.[43-45] Photodissociation utilizes high energy photons (*e.g.*, 157 nm or

193 nm) to directly excite the peptide backbone, and yields a variety of fragment ions, with x-type ions and side chain cleavages typically dominating the mass spectra. [46-49]

A physical description of peptide ion dissociation (or unimolecular ion decomposition) is given by quasi-equilibrium theory.[50] Upon ionization the ion is in an excited state and does not initially have a change in bond length. Energy is rapidly redistributed throughout the degrees of freedom of the molecule and a "quasi-equilibrium" among the energy states is established before ion fragmentation occurs. Rice-Ramsperger-Kassel-Marcus (RRKM) theory states that the rate constant for a particular reaction is the population of energy states of the excited molecule relative to the population of all the other energy states of the decomposing ions. This is simplified to the expression:

$$k(E) = v\left(\frac{E - E_0}{E}\right)^{n-1},$$

where v is the frequency factor, E is the internal energy of the ion, E_0 is the critical energy of the reaction required for bond dissociation, and n is the number of vibrational degrees of freedom.[51]

The relationship between internal energy of the ion and dissociation is shown in Figure 7 (adapted from McLafferty and Turecek[51]). The energy deposition function ρ(E), describes the distribution of internal energy in an ensemble of ions after the ionization event. As the internal energy of the ion increases, fragment ion products (*e.g.*, AB^+ and CD^+) may become favored to form. The relationship between ion internal energy and rate of dissociation is illustrated by the lower half of Figure 7. As the internal energy of

the ion increases, the pathway for dissociation of the ion into the products A^+ and B becomes more favorable. At even higher internal energies, the rate of dissociation to C^+ and D becomes greater than that of A^+ and B.

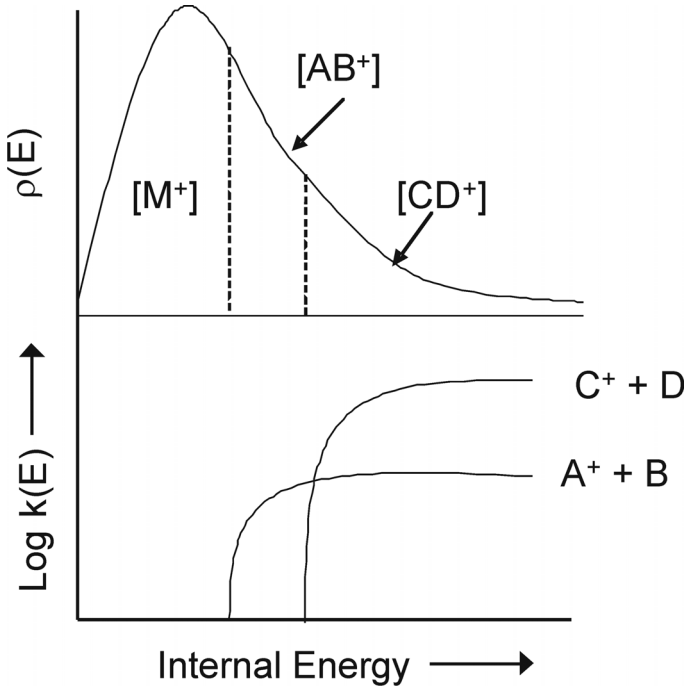

Figure 7. Wahrhaftig diagram describing the relationship between internal energy of ions and rate of dissociation.

Research Direction

Many aspects of mass spectrometry and NP chemistry are relevant to the research in this dissertation. The purpose of this research is fourfold: (i) to investigate the utility of AuNPs as matrices for LDI-MS and parameterize the factors that affect desorption/ionization, (ii) to determine the effects of passivating the AuNP surface, (iii) to determine how changing the solution conditions can affect internal energy deposited

in peptides, and (iv) to propose a mechanism of ion formation. Chapter II details the solution parameters that affect ionization, including how to enhance ionization of the $[M + H]^+$ ion. Chapter III focuses on conditions that passivate the AuNP surface and the subsequent effects on the mass spectra. Chapters IV and V describe energy transfer to the analyte and peptide ion fragmentation mechanisms. Chapter VI broadly focuses on the mechanism of desorption/ionization.

CHAPTER II

PARAMETERIZATION OF IONIZATION OF BIOMOLECULES USING GOLD NANOPARTICLES FOR LDI-MS*

Introduction

In order to determine parameters that may be important for desorption/ionization of biomolecules using AuNPs in laser desorption/ionization (LDI) mass spectrometry, one can first look to traditional matrix-assisted LDI (MALDI) mass spectrometry experiments to identify variables in sample preparation that affect ion yield and mass spectral complexity in TOF instruments. A number of factors have been identified that are important for ionization of biomolecules using MALDI, such as: (i) sample preparation and deposition method,[1, 7, 52-59] (ii) choice of matrix or mixed matrices,[10, 59-64] (iii) presence of impurities such as detergents or buffers,[59, 65-70] (iv) solution pH,[10, 59, 64, 71] (v) solvent composition,[9, 59, 70] (vi) various matrix additives,[72-74] and (vii) biomolecule composition.

Of the parameters listed above that can affect ionization in MALDI, only a few have been investigated with regards to NPs. First, AuNPs can be synthesized in a variety of different solvents and with different surfactants, some of which are not compatible with LDI. For example, the two most common synthesis methods are the Brust[75] and

---

*Parts of this chapter are reprinted from "Size-Selected (2-10 nm) Gold Nanoparticles for Matrix Assisted Laser Desorption Ionization of Peptides" by J. A. McLean, K. A. Stumpo, and D. H. Russell, *J. Am. Chem. Soc.*, **2005**, *127*, 5304-5305, Copyright [2005] American Chemical Society.

the Turkevich[76] methods. The Brust method is a two-phase synthesis that transfers $AuCl_4^-$ to toluene using tetraoctylammonium bromide, and is then reduced using sodium borohydride in the presence of dodecanethiol. There are several issues that may complicate the use of NPs from the Brust method in LDI: (i) the presence of detergents can complicate the mass spectrum or suppress analyte ion signal and (ii) the resultant NPs are in toluene, which is not a compatible solvent with many biological samples. In contrast to this, the Turkevich method is an aqueous reduction of $AuCl_4^-$ with sodium citrate. Citrate capped AuNPs are readily miscible with biological samples and do not have surfactants; the main complicating factor is excess sodium. Most of the experiments in this dissertation utilize citrate capped AuNPs.

A number of the additives that are used in MALDI (*e.g.*, sugars, ammonium salts, etc.) have been used in different NP syntheses, but are typically involved in NP formation, not as stabilizing ligands for the NPs. Also, aqueous environments are not always used in NP syntheses, as discussed above, making the effects of additives difficult to understand at times. Specific cases are discussed where relevant.

Next, the effects of pH on NPs have been investigated somewhat. Several studies have focused on ordered assembly processes by pH manipulation, which is typically a result of hydrogen-bonding interactions.[25, 77] Since analyte is also present with AuNPs in an LDI experiment, H-bonding interactions between AuNPs and analyte are already complicated. Therefore, it is initially unclear what affect lowering the pH may have. Aggregation of AuNPs as the pH is lowered may be an issue, as the stability of citrate

capped AuNPs is dependent on the electrostatic repulsion between NPs that arises from the charged citrate molecules.

This chapter will detail basic parameters of ionization, including, (i) AuNP-to-analyte ratio, (ii) effects of peptide composition, (iii) effects of solution pH, (iv) AuNP surface modification, and (v) effects of methanol addition. In MALDI analyses a number of solution additives (*e.g.*, ammonium,[78, 79] fructose[80, 81]) have been found to improve spectral clarity and promote higher abundances of $[M + H]^+$ ions, so a brief evaluation of some common MALDI additives is also presented in this chapter.

Experimental

LDI-MS experiments were performed on an Applied Biosystems Voyager DE-STR (Framingham, MA) equipped with a N_2 laser (Spectra-Physics) for irradiation at 337 nm. Positive and negative mode experiments were performed in the reflected mode using 200 laser shots with internal calibration. All of the mass spectra shown used laser energies at 7-12% above the threshold for desorption/ionization.

Samples were prepared by mixing solutions containing the AuNPs with solutions containing analyte. Any other additions were then added to this solution. Typically, solutions were allowed to sit for 5 to 10 minutes prior to depositing an aliquot of sample on to a stainless steel plate, which was then vacuum dried and analyzed.

Modification of Angiotensin I to Angiotensin I methyl ester was done according to literature procedures.[82] Briefly, 800 μL of acetyl chloride was added very slowly to 5 mL of anhydrous methanol and stirred. After approximately 5 minutes, 500 μL of the

resulting solution was added to 5 mg of peptide and stirred at room temperature for 2 hours. The peptide was then dried by lyophilization. The modification of free acid on the C-terminus and aspartic acid side chain to the methyl ester was confirmed by tandem mass spectrometry. Acetylation of the N-terminus consisted of very slowly adding 200 μL of acetic anhydride to a peptide solution consisting of 200 ng of peptide in 200 μL water:acetonitrile (1:1 v/v) and allowing this to react for 10 minutes at 37°C, and was then dried by lyophilization.[83] This reaction results in two products, N-terminal acetylation, and double acetylation (N-terminus and arginine side chain). By quenching the reaction at the proper time, a high abundance of only the N-terminal acetylated product is produced, with minimal doubly acetylated product. The two products were separated by fast performance liquid chromatography (FPLC), where samples were applied in 50 mM ammonium bicarbonate and eluted with 500 mM sodium chloride. Modification site(s) were confirmed using tandem mass spectrometry. See Figures 8 and 9 for structures of peptide modification.

Protein digestion was done according to standard procedures. Briefly, 10 μL of protein solution in water was added to 50 μL of a 50 mM ammonium bicarbonate solution and heated to 90°C for 15 minutes. Protein denaturation was quenched by cooling the solution at 0°C for 10 minutes. Next, 5 μL of trypsin was added and the solution warmed at 37°C for 4 hours.

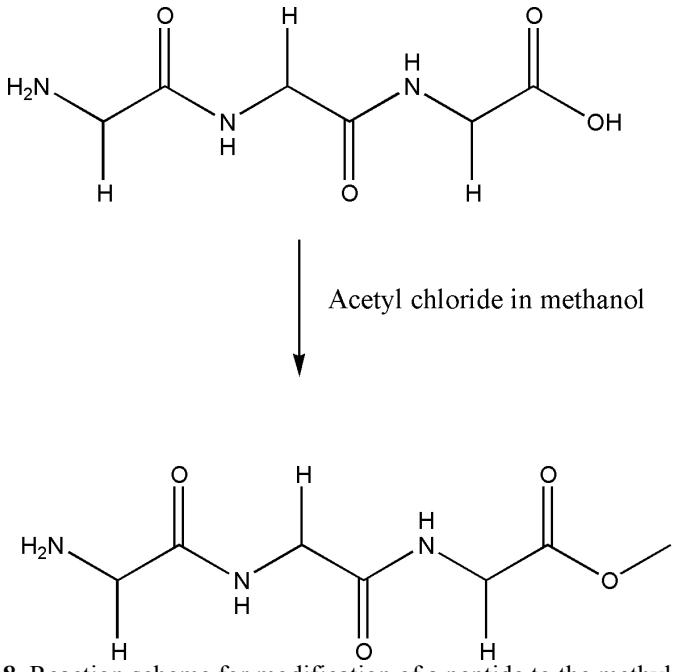

Figure 8. Reaction scheme for modification of a peptide to the methyl ester.

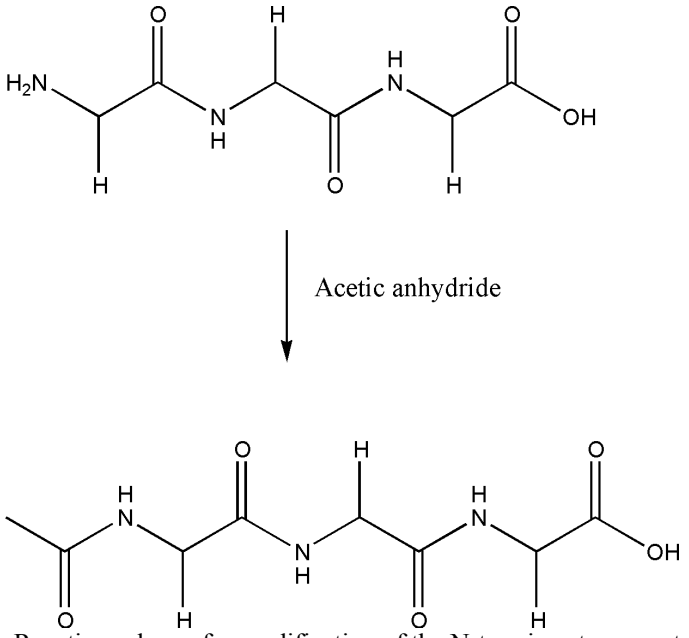

Figure 9. Reaction scheme for modification of the N-terminus to an acetyl group.

The pH of citrate capped AuNP solutions was adjusted to 3, 4, and 5.2 using citric acid. These pH values were chosen because they bracket the pK_a values of citrate, (pK_{a1} = 3.13, pK_{a2} = 4.76, pK_{a3} = 6.4) giving different charge states on the surface of the AuNP, as is shown in Table 1.

Table 1. Citrate chemical formulae at varying pH values.

Solution pH	Citrate formula
3	$HOCCH_2(COOH)_3$
4	$HOCCH_2(COOH)_2COO^- + H^+$
5.2	$HOCCH_2(COOH)(COO^-)_2 + 2H^+$
7	$HOCCH_2(COO^-)_3 + 3H^+$

AuNPs were modified using standard gold-thiol chemistry.[84] Tiopronin (TP), glutathione (GSH), and β-mercaptoethanol (β-me) were chosen for these studies because of differences in ligand bulk. In each case the modified NPs were prepared by mixing an aqueous solution containing the modifying reagent (ranging in concentration from 10-15 mM) with a solution of AuNPs 1:1 (v/v), and allowed the resulting solution to sit for 0.5 to 2 hours at room temperature. Excess modifying reagent was removed by using Millipore Microcon Centrifugal Filters (Billerica, MA); however, no significant differences in the mass spectral data for filtered versus non-filtered NP solutions were observed. LDI mass spectra of the modified AuNPs contain primarily Au_x^+ cluster species and low abundance signals for Au_xS^+ and fragment ions of the modifying reagent adducted to Au. Although exact surface coverage has not been determined, estimates based on molecule size and unit packing efficiency were used to give an upper limit of

bound ligands. For example, using 20 $Å^2$ as the approximate size for TP, it is estimated that there are ~60 TP molecules attached to the gold surface, assuming that there are about 150 surface gold atoms in a 2 nm AuNP. Using a similar approach for GSH, with estimated molecule size of *ca.* 120 $Å^2$, it is estimated that 10 GSH molecules per 2 nm AuNP and about 120 β-me molecules (10 $Å^2$) per 2 nm AuNP.

UV-Vis spectroscopy and TEM were used to characterize the modified AuNPs. Absorption spectra were obtained on an Agilent 8453 UV-Visible Spectrophotometer (Foster City, CA) to monitor changes in the surface plasmon band of the AuNPs. Samples of AuNPs and any additives were mixed and spectra recorded at $t = 0$ min, 2 min, and 5 min. Electron microscopy images were obtained on a JEOL 2010 Hi-Resolution Transmission Electron Microscope with an acceleration voltage of 200 kV.

2 nm, 5 nm, and 10 nm citrate capped gold nanoparticles were purchased from Ted Pella, Inc. (Redding, CA). Val^4-Angiotensin III (RVYVHPF), Angiotensin I (DRVYIHPFHL), Substance P (RPKPQQFFGLM-NH_2), Dynorphin A (1-6) (YGGFLR), Oxytocin (CYIQNCPLG-NH_2), Bradykinin 2-9 (PPGFSPFR), Dynorphin A (1-13) (YGGFLRRIRPKLK), C-telopeptide (EDAHDGGR), [Ala-Pro-Gly-(Ile^3,Val^5)] Angiotensin II (APGDRIYVHPF), Cys^8-Renin Substrate (DRVYIHPCHLLYYS), and Flag peptide (DYKDDDK) were purchased from American Peptide Co. (Sunnyvale, CA) and were prepared in water. RVGVAGG was synthesized in-house using standard solid phase Fmoc chemistry. HPLC grade methanol, citric acid, *p*-toluenesulfonic acid, ascorbic acid, acetic acid, tris(hydroxymethyl)aminomethane (Tris), hydrochloric acid, ammonium acetate, glycerol, ammonium chloride, N-(2-mercaptopropionyl)glycine

(tiopronin), glutathione, and β-mercaptoethanol were obtained from Sigma (St. Louis, MO) and used as received. Water used was distilled and deionized using a Barnstead water purification system (Dubuque, IA).

Results and Discussion

The absorption spectra of 2 nm, 5 nm, and 10 nm AuNPs are shown in Figure 10. An SPR band is present for 5 nm and 10 nm AuNPs at 522 nm and 524 nm, respectively; 2 nm AuNPs do not have an SPR band. LDI is typically performed using a UV laser (*e.g.*, nitrogen laser at 337 nm), and while there is not a plasmon band at this wavelength, there is still some absorption by the NPs. LDI at the plasmon band is beyond the scope of this research.

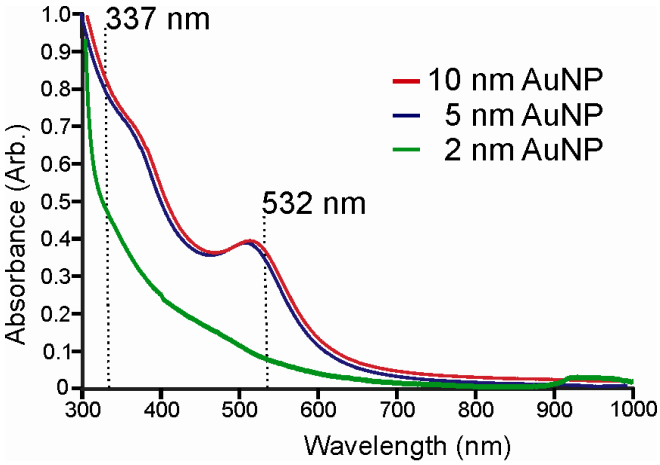

Figure 10. UV-Visible absorption spectra of 2, 5, and 10 nm citrate capped AuNPs.

The utility of AuNPs for LDI using size distributions of 2, 5, and 10 nm was examined. Figure 11 shows transmission electron microscopy images and size

distribution measurements of 2, 5, and 10 nm AuNPs. When co-deposited with peptide, both positive- and negative-ion LDI spectra are observed for all three size distributions (Figure 12). In the positive ion spectra $[M + H]^+$, $[M + Na]^+$, and $[M + K]^+$ are observed, as well as peaks corresponding to Au-cluster species (*e.g.,* Au_3^+, Au_5^+). The relatively high abundances of cationized analytes are attributed to the metal salts used to prepare the NPs. The negative ion spectra contain abundant $[M - H]^-$ as the AuNP size decreases (*i.e.*, 2 nm > 5 nm > 10 nm), whereas the abundances of higher order Au-clusters increase as the AuNP size increases (*i.e.,* 10 nm > 5 nm > 2 nm).

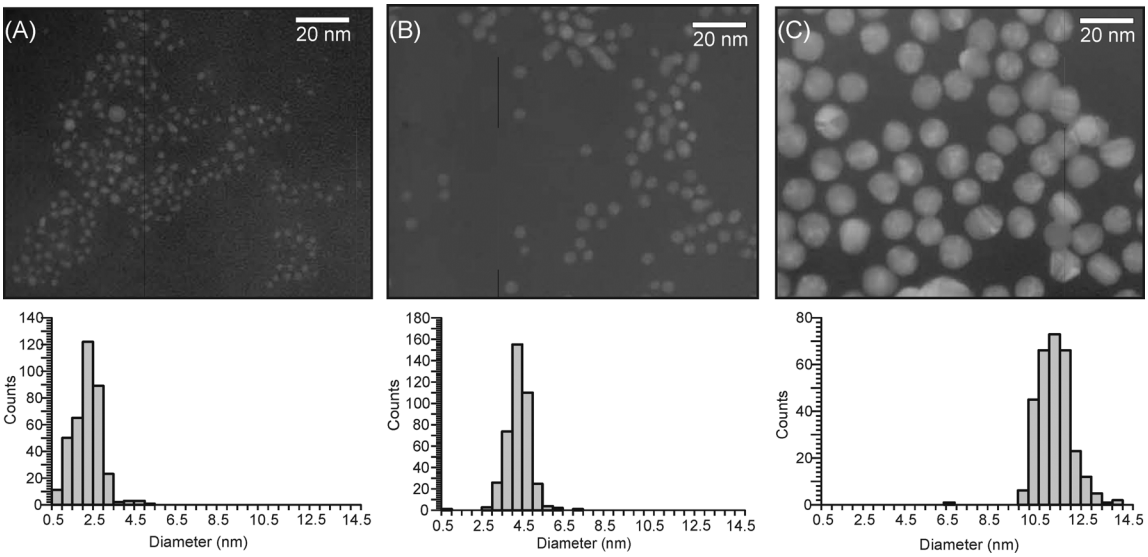

Figure 11. Transmission electron micrographs and size distribution of (A) 2 nm (B) 5 nm and (C) 10 nm citrate capped AuNPs.

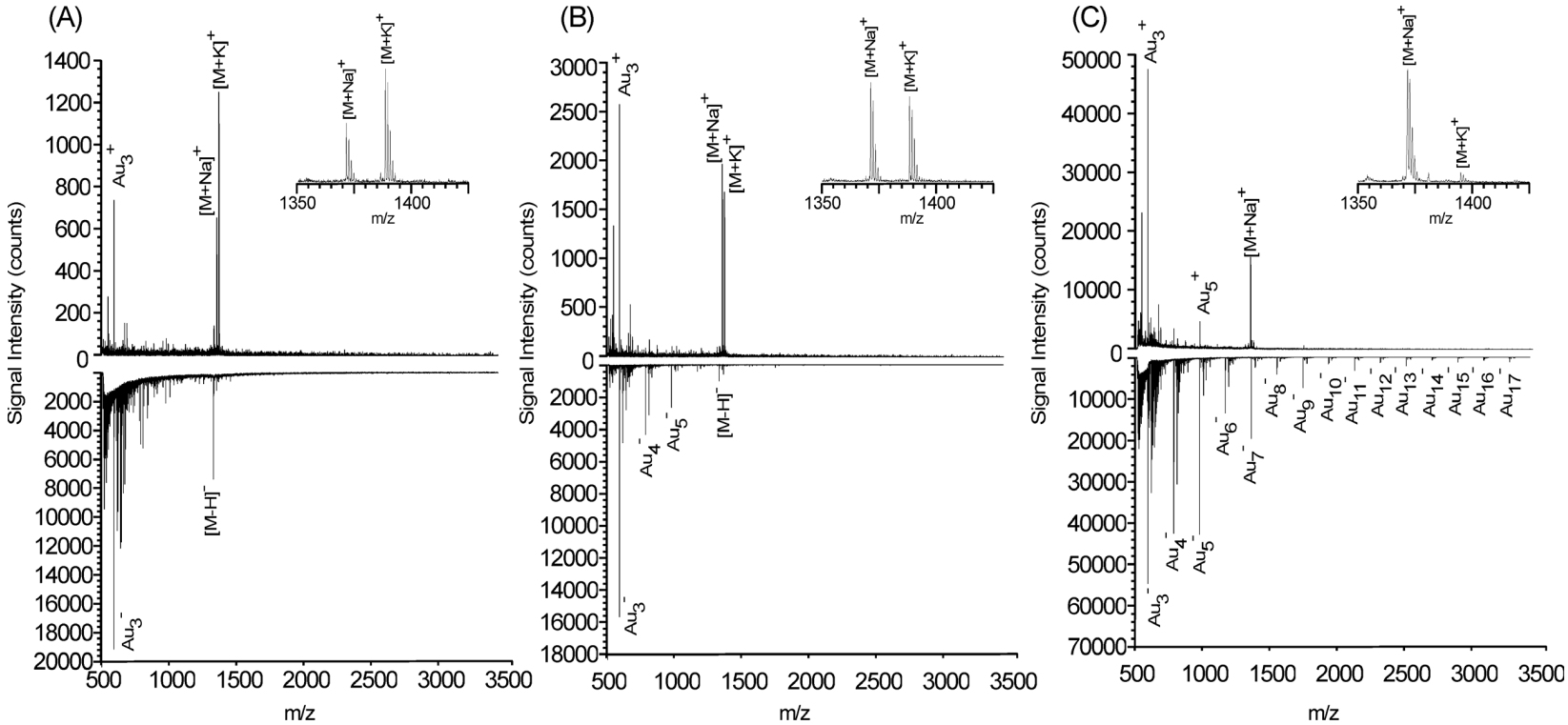

Figure 12. Positive and negative ion LDI-TOF mass spectra of substance P (RPKPQQFFGLM-NH_2, M_r = 1347.64 Da) obtained by using citrate capped AuNPs: (A) 2 nm, (B) 5 nm, and (C) 10 nm.

The molar AuNP-to-analyte ratio (AuNP:A) used here is 1 AuNP: 10^7 peptide molecules. It is especially interesting to compare the AuNP:A to the matrix-to-analyte ratio for conventional UV-MALDI using organic acid matrices.[1] The molar matrix-to-analyte ratio for organic acid matrices is 10^3-10^5 matrix molecules:1 analyte molecule.

As the spectra in Figure 12 show, 2 and 5 nm AuNPs yield high relative abundances of analyte in the positive ion spectra, with little chemical noise in the background. Further work in this dissertation will focus on 2 and 5 nm AuNPs.

Desorption/ionization of a biomolecule is represented by the cartoon illustration in Figure 13 using citrate capped AuNPs. The AuNP is mixed with analyte, and depending on the chemical properties, some may adsorb to the AuNP surface. Since peptides have amines or carbonyl oxygens, it is reasonable to claim affinity for the AuNP surface.[77] Next, the sample is irradiated with a laser and either positive or negative ions can be detected using the mass spectrometer. This cartoon model will be used throughout this dissertation as different solution or NP conditions are used.

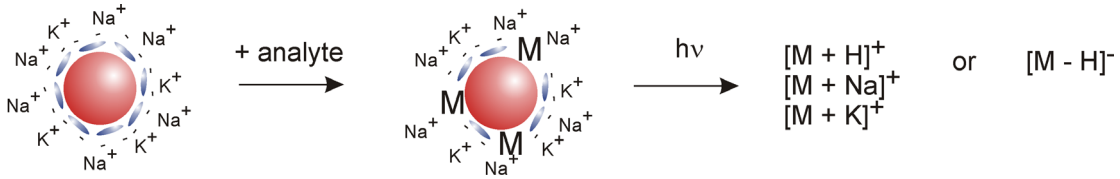

Figure 13. Cartoon illustration of desorption/ionization using citrate capped AuNPs.

AuNP-to-analyte ratio

Peptides follow a general trend of ionization within the range of 1 AuNP: 10^4 analyte molecules to 1 AuNP: 10^9 analyte molecules, with the best results occurring for 1 AuNP: 10^5-10^8 peptide molecules. Figure 14 shows the peptide Angiotensin I methyl ester at solution pH 7 using 2 nm citrate capped AuNPs at varying AuNP: A. For the ratios 1 AuNP: 10^5 analyte molecules and 1 AuNP: 10^6 analyte molecules, $[M + alkali]^+$ ions are predominate in the spectra. Using ratios of 1 AuNP: 10^7 analyte molecules and 1 AuNP: 10^8 analyte molecules, the protonated molecule, $[M + H]^+$, dominates. The data shown is representative of several peptides that were examined. The spectra shown are normalized to each other, so 100% relative abundance is 1200 counts for each spectrum. The enhancement of the $[M + H]^+$ ion is of interest, as numerous $[M + alkali]^+$ ions complicates the mass spectrum, and partitions the ion signal into multiple channels; this is not ideal because it can make spectral interpretation more difficult and time consuming. The main contribution of alkali in solution is from the AuNPs (a consequence of the synthesis), and so by increasing the AuNP-to-analyte ratio, the amount of alkali per peptide in a given area is reduced, resulting in less alkali adduction, *i.e.*, the salt concentration is reduced, resulting in fewer $[M + alkali]^+$ ions being observed. Issues pertaining to sample cleanup are discussed later in this chapter.

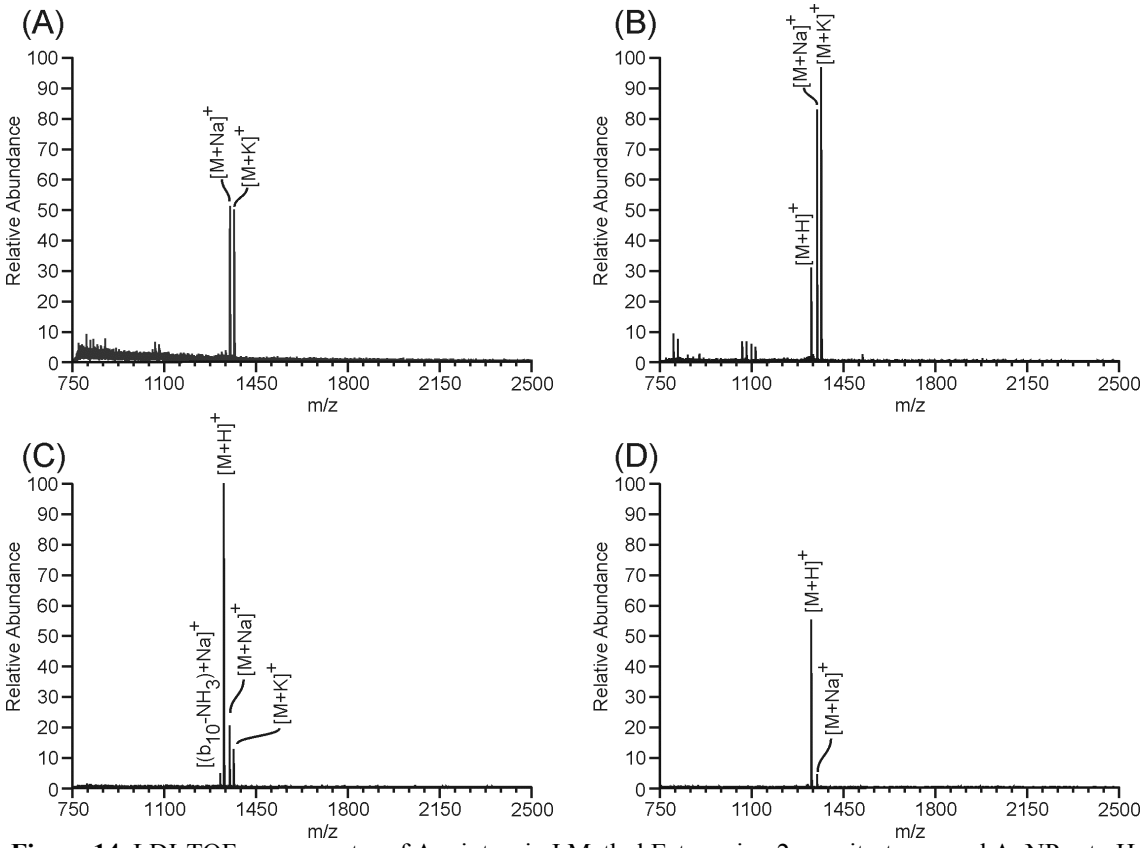

Figure 14. LDI-TOF mass spectra of Angiotensin I Methyl Ester using 2 nm citrate capped AuNPs at pH 7 with a ratio of (A) 1 AuNP: 10^5 analyte molecules, (B) 1 AuNP: 10^6 analyte molecules, (C) 1 AuNP: 10^7 analyte molecules, and (D) 1 AuNP: 10^8 analyte molecules.

Peptide composition

The two analytes shown so far (Substance P and Angiotensin I methyl ester) both have high ionization efficiencies, meaning that a high relative abundance of the peptide is observed. In traditional MALDI experiments it has been shown that peptide sequence can affect how well a peptide is ionized.[85-89] Basic amino acids, or peptide with a high isoelectric point (pI) tend to desorb/ionize more readily than acidic peptides, or those with low pI values. A small library of peptides has been investigated in order to evaluate any ionization trends based on physical parameters or peptide composition.

Table 2. Peptide library information

Peptide Sequence	*Peptide Name/Abbreviation*	M_r[1]	*pI*[1]
RVYVHPF	Val[4]-Angiotensin III	917.1	8.75
RVGVAGG	Peptide 1	614.7	9.75
YGGFLR	Dynorphin A (1-6)	711.8	8.75
CYIQNCPLG-NH_2	Oxytocin[2,3]	1007.2	5.51
(D-OMe)RVYIHPFHL-OMe	Angiotensin I Methyl Ester[2,4]	1324	> 6.92
PPGFSPFR-OMe	Bradykinin 2-9 Methyl Ester[2,4]	918.5	> 10.18
RPKPQQFFGLM-NH_2	Substance P[2]	1347.7	> 11
PPGFSPFR	Bradykinin 2-9	904.02	10.18
DRVYIHPFHL	Angiotensin I	1296.4	6.92
YGGFLRRIRPKLK	Dynorphin A (1-13)	1604.2	11.73
APGDRIYVHPF	Peptide 2	1271.6	6.79
EKAHDGGR	C-telopeptide	868.9	6.85
DVGVAGG	Peptide 3	573.6	3.80
DRVYIHPCHLLYYS	Cys[8]-Renin Substrate	1779.4	6.91
DYKDDDDK	Flag peptide	1013	3.97

[1]calculated by the ExPASy ProtParam tool, found at http://ca.expasy.org/tools/protparam.html
[2]values are approximate; calculation does not take modified termini or disulfide bonds into consideration
[3]Peptide has a disulfide bond between Cys[1] and Cys[6]
[4]acidic residues and C-terminus modified to the methyl ester

As Table 2 shows, the peptides analyzed have been grouped into three categories. Group 1 (green) peptides are defined as: (i) having high relative abundances at the threshold for desorption/ionization, where the analyte is often the dominant peak, (ii) maintaining a high analyte ion abundance as laser fluence increases, and (iii) counts increase to over 10,000 when the laser fluence is 10% above the threshold laser fluence for desorption/ionization. Group 2 (yellow) peptides typically have: (i) low relative abundances at the desorption/ionization threshold (often lower than 40%), (ii) have an increase in relative abundances as laser fluence increases, but counts do not go above 10,000, and (iii) the intact analyte may or may not be the dominant peak in the spectrum.

Group 3 (red) peptides have very low analyte ion abundances (often less than 20%) at any laser fluence, or do not desorb/ionize at all. Figure 15 shows an example mass spectrum for a peptide from each of these groupings. At higher laser fluence, fragmentation of the peptide may occur and this is discussed further in Chapter IV.

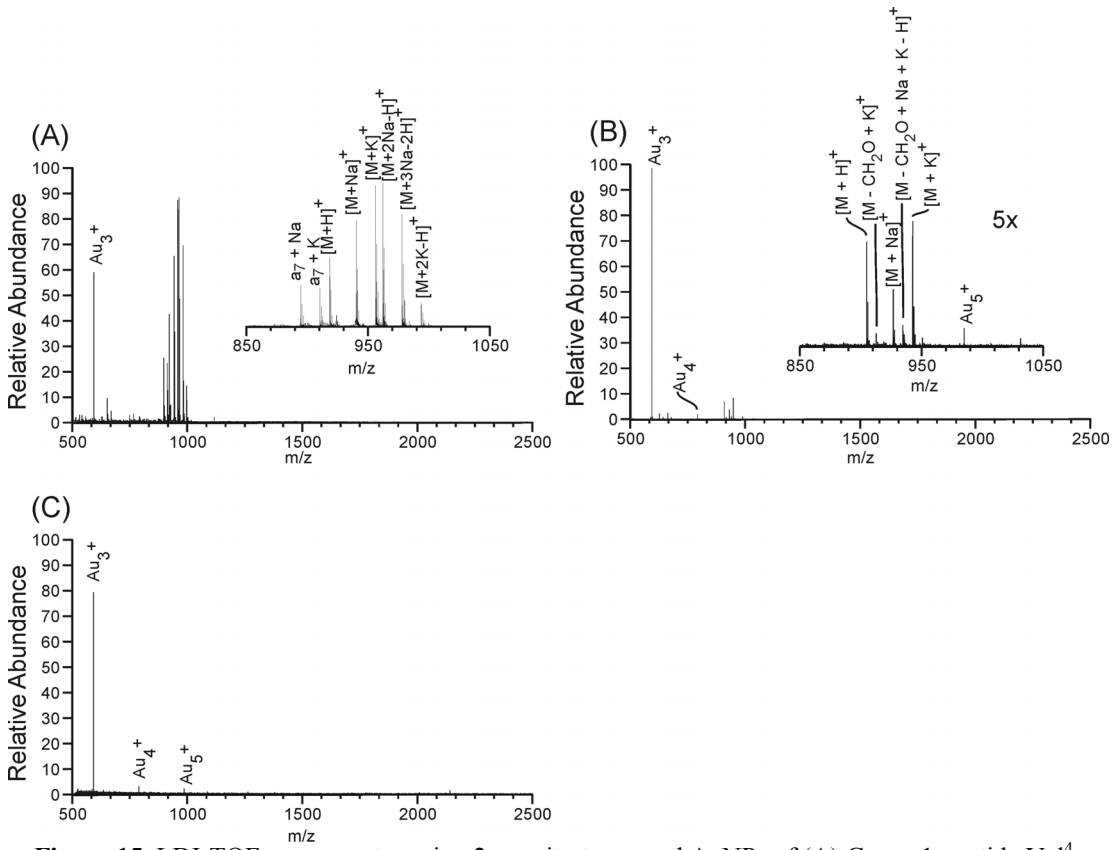

Figure 15. LDI-TOF mass spectra using 2 nm citrate capped AuNPs of (A) Group 1 peptide Val^4-Angiotensin III, (B) Group 2 peptide Bradykinin 2-9, and (C) Group 3 peptide Cys^8-Renin substrate.

These peptide groupings were made based on qualitative aspects because very little commonality exists based on physical parameters of the peptides (*e.g.*, pI, aliphatic index, hydrophobicity). The only correlation to physical parameters is that peptides with a basic and acidic site near each other do not desorb/ionize well (*e.g.*, Angiotensin I,

Bradykinin 2-9, C-telopeptide, Flag). To determine if desorption/ionization could be improved, peptides with basic and acidic sites near each other were modified to the methyl ester. The methyl ester peptides have a lower threshold for desorption/ionization, and at a comparable laser fluences, the methyl ester peptides exhibit much higher analyte ion abundances, as Figure 16A and 16B shows. This suggests that the acid-base properties of the peptides are important for ionization. Angiotensin I modified to N-terminal acetylation was also investigated to further evaluate the acid-base properties of the peptide. As Figure 16C shows, similar sample loading of Acetylated Angiotensin I does not result in desorption/ionization of the peptide. The general trend of ionization efficiency for these three peptides is Angiotensin I methyl ester > Angiotensin I > Acetylated Angiotensin I. The preferential desorption/ionization of the methyl ester and free acid Angiotensin support the idea that basic sites are important for ionization,[85] especially with pre-formed ions, which will be discussed in detail in Chapter VI.

Peptide mixtures and protein digests

The utility of AuNPs for ionization of a mixture was also evaluated. A peptide mixture composed of 3.33 pmol each of Ac-Angiotensin I, Angiotensin I, and Angiotensin I methyl ester results in desorption/ionization of all three analytes, as is shown in Figure 16D. This is markedly different to analysis of each peptide separately, where the free acid and methyl ester of Angiotensin are the only two peptides that desorb/ionize (see Figure 16A-C). The interaction of the three different peptides may enhance overall desorption/ionization due to simple acid-base interactions and proton

transfer in solution. The observation of increased analyte ion abundances is in contrast to traditional MALDI matrices, where multi-component mixtures often result in lower internal energies of all analyte ions, and less ionization.[90]

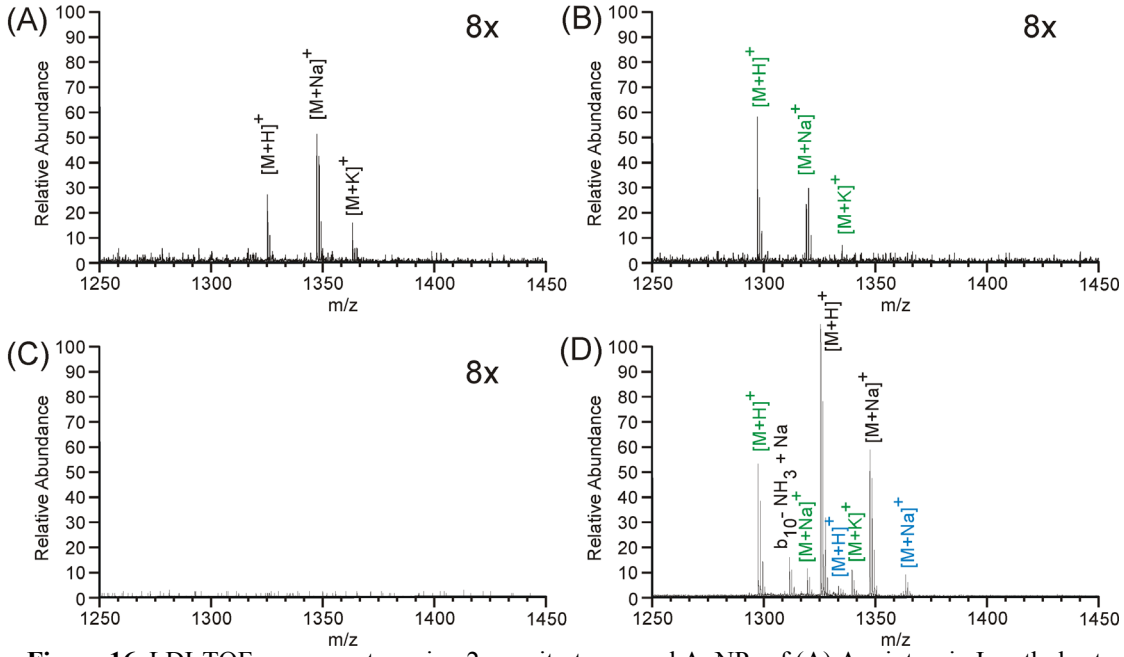

Figure 16. LDI-TOF mass spectra using 2 nm citrate capped AuNPs of (A) Angiotensin I methyl ester, (B) Angiotensin I, (C) Acetylated Angiotensin I, and (D) mixture of Angiotensin I methyl ester (black labels), Angiotensin I (green labels), and Acetylated Angiotensin I (blue labels).

An even more complex mixture is a tryptic digest, which was also analyzed. The proteins cytochrome *c*, bovine serum albumin, β-casein, and aldolase were evaluated using a series of AuNP-to-analyte ratios. No identifiable peptide peaks were observed for any of these proteins; Figure 17A shows the LDI-TOF mass spectrum of a tryptic digest of cytochrome *c* using 2 nm citrate capped AuNPs. Several control experiments were done to determine if the buffer or trypsin were interfering with

desorption/ionization. Figure 17B shows a standard peptide (Angiotensin I) with addition of ammonium bicarbonate at pH 8. Figure 17C shows a Angiotensin I with added trypsin, and Figure 17D shows Angiotensin I with both components added. The ammonium bicarbonate does not reduce ion signal compared to none added, in fact it enhances the protonated molecule, which may be due to the additional proton source from the ammonium ion. Addition of trypsin reduces the resolution and overall ion signal, suggesting this maybe affecting the desorption/ionization process. However, addition of trypsin and ammonium bicarbonate again has improved ion signal, making the effects of trypsin unclear. There is difficulty in getting a larger component mixture to work, and addition of enzymes complicates the issue even more. While peptide digests have not been a major focus of research, this experiment represents an area where the utility of citrate capped AuNPs is limited, and further investigation is needed in order to understand these effects.

pH and buffer effects

Solution pH was found to affect ionization of peptides when using AuNPs in LDI. Citrate capped AuNP solutions were modified from pH 7 to pH 5, 4, and 3 using citric acid. These values were chosen because they bracket the three pK_a values of citrate, the NP surface capping agent (see Table 1). A significant change was noted between the spectra for pH 7 and 5 vs. pH 4 and 3. As is shown in Figure 14, at pH 7 the mass spectrum is predominately $[M + alkali]^+$ ions, and at pH 3 (Figure 18), the

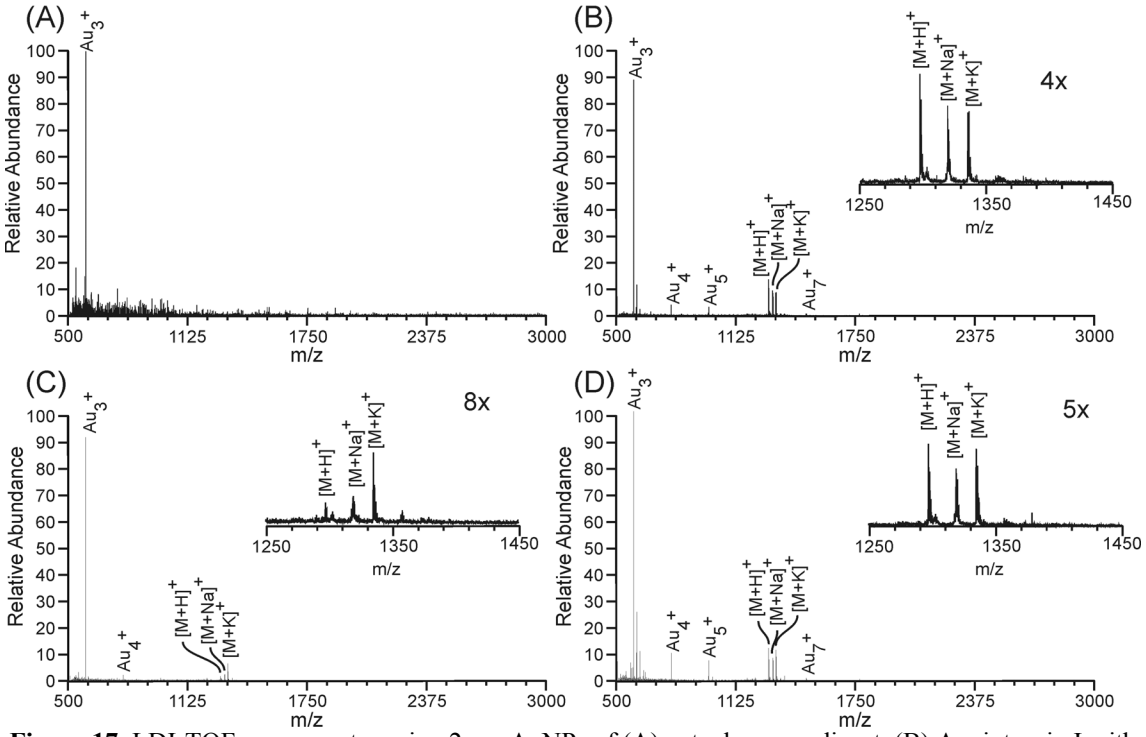

Figure 17. LDI-TOF mass spectra using 2 nm AuNPs of (A) cytochrome *c* digest, (B) Angiotensin I with added ammonium bicarbonate, (C) Angiotensin I with added trypsin, and (D) Angiotensin I with added trypsin and ammonium bicarbonate.

protonated molecule dominates. The increase of $[M + H]^+$ is attributed to the addition of a proton source. To confirm the effects of an additional proton source, several other acids were used to lower the pH. Acetic acid, ascorbic acid, and *p*-toluenesulfonic acid (see Figure 19) all yield higher analyte ion abundances for the protonated molecule.

AuNPs were also treated with buffers to determine compatibility for biological mass spectrometry. As previously shown for the peptide Angiotensin I, addition of ammonium bicarbonate increased analyte ion abundances (see Figure 17B). AuNP solutions were adjusted to pH 6.5, 7.5, and 8.5 using Tris-HCl. Solutions of AuNPs were lowered to pH 5.91 and 4.12 using ammonium acetate-acetic acid. Figure 20 shows LDI mass spectra of these solutions, where analyte is marked with an asterisk, which is

present at all of these solution conditions. The cartoon in Figure 21 depicts how the ions near the surface of the AuNP may change when the pH is lowered.

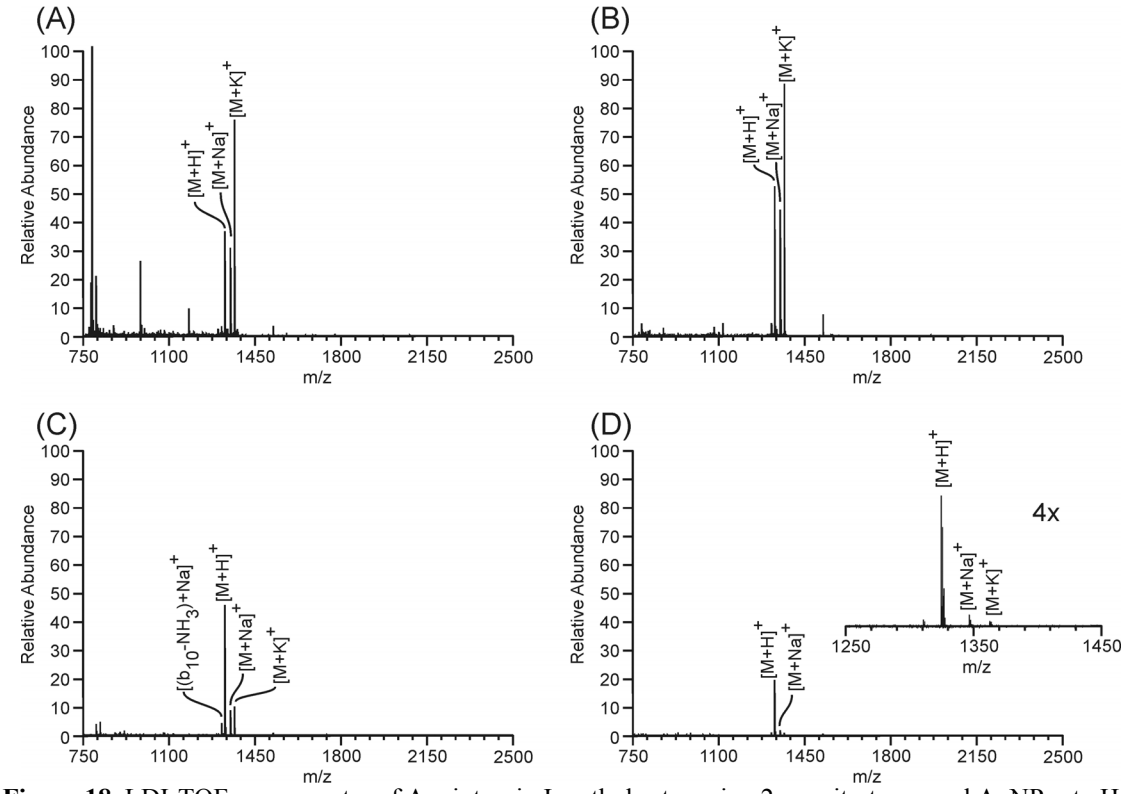

Figure 18. LDI-TOF mass spectra of Angiotensin I methyl ester using 2 nm citrate capped AuNPs at pH 3 with a ratio of (A) 1 AuNP: 10^5 analyte molecules, (B) 1 AuNP: 10^6 analyte molecules, (C) 1 AuNP: 10^7 analyte molecules, and (D) 1 AuNP: 10^8 analyte molecules.

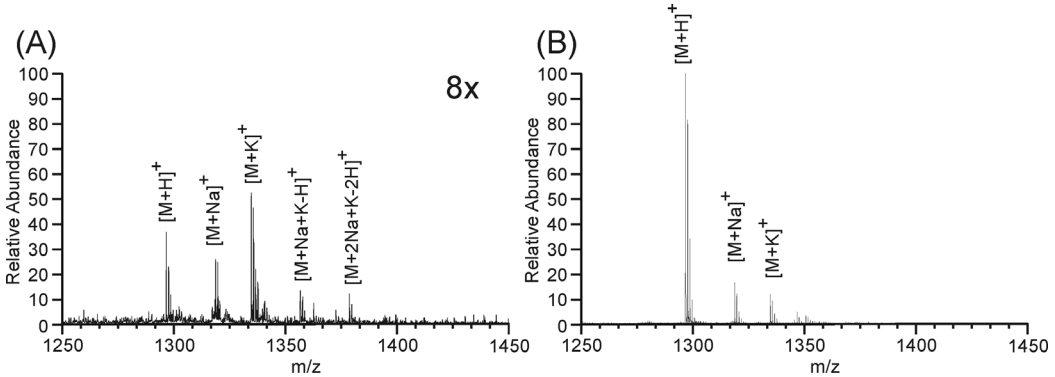

Figure 19. LDI-TOF mass spectra of Angiotensin I using 2 nm citrate capped AuNPs (A) without and (B) with *p*-toluenesulfonic acid.

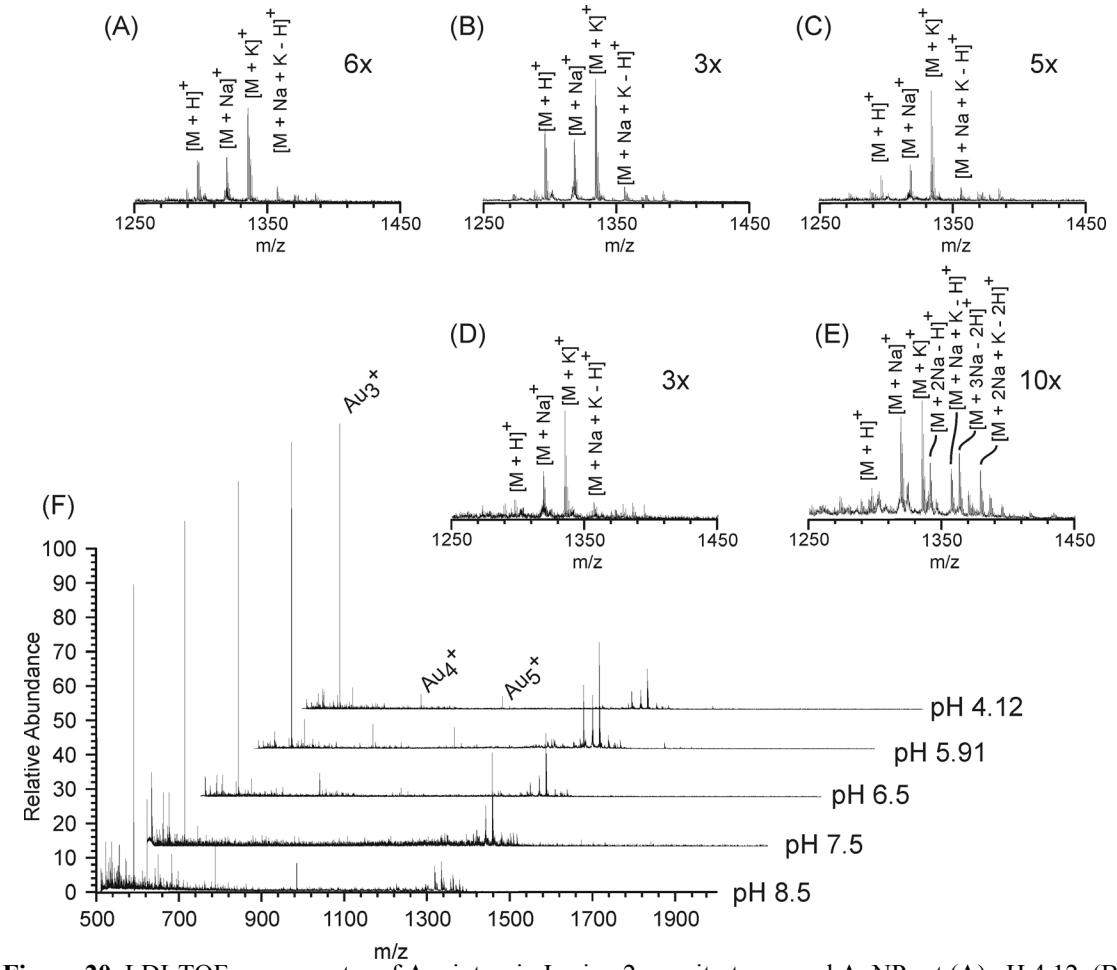

Figure 20. LDI-TOF mass spectra of Angiotensin I using 2 nm citrate capped AuNPs at (A) pH 4.12, (B) pH 5.91, (C) pH 6.5, (D) pH 7.5, (E) pH 8.5, and (F) at all pH values.

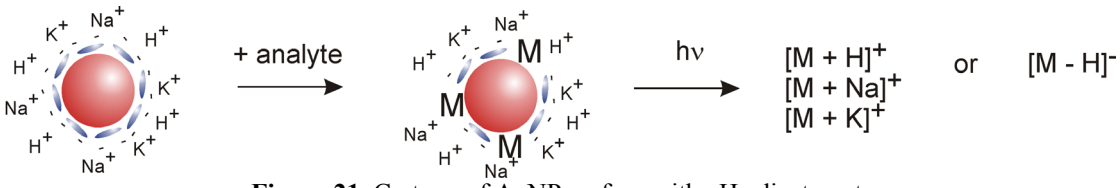

Figure 21. Cartoon of AuNP surface with pH adjustment.

Reducing salt content

As many of the mass spectra in this chapter have shown, $[M + alkali]^+$ ions are very abundant when using citrate capped AuNPs. As previously mentioned, having the

ion signal partitioned is less than desirable because it can complicate the mass spectrum and make peak assignment difficult. Several experiments were done to attempt to reduce the contribution of $[M + alkali]^+$ ions. Dialysis, size-exclusion chromatography, and centrifugal filters of AuNPs all resulted in little improvement in the ion signal, and AuNP concentration was difficult to determine after all of these experiments, which is a significant issue because AuNP:A is important. The 'cold water sling', a method shown to decrease salt content in traditional MALDI experiments was also tried.[91] The method consists of first depositing and drying the sample (1-2 μL), and then placing a 0.5-1 μL drop of cold water over the dried sample, and slinging the water off quickly. As Figure 22A shows, significant alkali adduction is present in the control sample, and Figure 22B (cold-water sling applied) shows some reduction in alkali adduction. However, owing to the solubility of the AuNPs and analyte, significant sample loss is observed, most likely accounting for the reduction in Au-cluster species and overall ion abundances. None of the described methods were successful in significantly depleting $[M + alkali]^+$ ions.

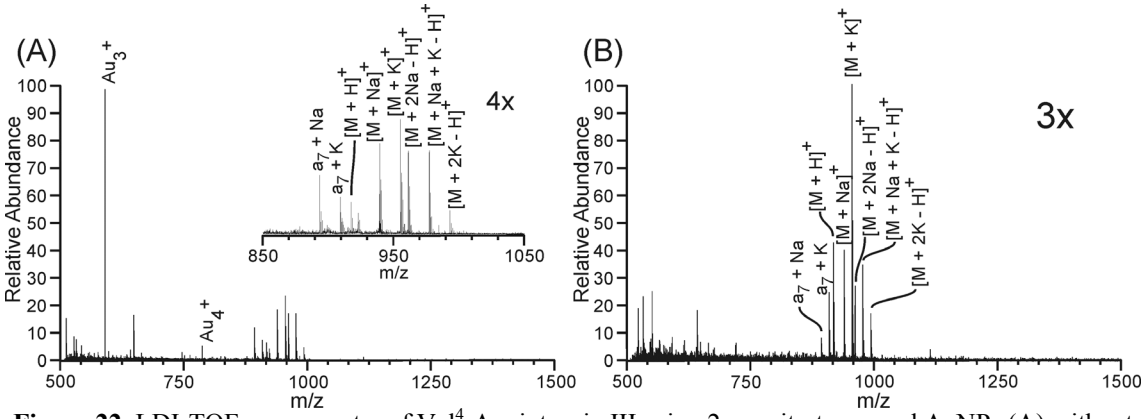

Figure 22. LDI-TOF mass spectra of Val[4]-Angiotensin III using 2 nm citrate capped AuNPs (A) without any further sample treatment and (B) using the cold water sling method.

Methanol addition

Methanol was added to determine (i) if hydrogen-bonding between the analyte, solvent, and NP are important for ionization, (ii) if alkali adduction could be reduced, and (iii) if similar results occur for different AuNP-to-analyte ratios. Angiotensin I methyl ester was analyzed using a ratio of 1 AuNP: 10^6 analyte molecules. With no methanol present, $[M + H]^+$ and $[M + alkali]^+$ ions are present (see Figure 16A). As methanol content increases from 20% to 40%, $[M + alkali]^+$ ions are still present, as is shown in Figure 23. At 50% methanol content only traces of $[M + alkali]^+$ ions are present, and the $[M + H]^+$ ion dominates the mass spectrum. At 60% and 70% methanol content, $[M + H]^+$ remains the dominant ion, but overall analyte ion abundances decrease compared to 50% methanol content.

Using 1 AuNP: 10^7 analyte molecules, very little $[M + alkali]^+$ ions are present to begin with, as has previously been demonstrated with changing AuNP: A (see Figure 14C). Methanol addition results in further reduction of $[M + alkali]^+$ ions starting with 20% methanol addition, as Figure 24 shows. Analyte ion abundances are greatest with 40% methanol addition, and no $[M + alkali]^+$ ions are present with 70% methanol content.

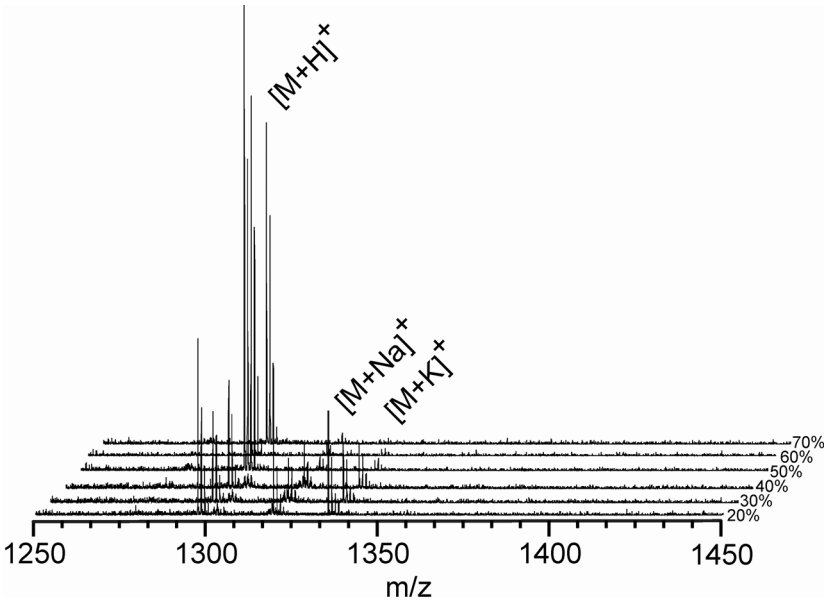

Figure 23. LDI-TOF mass spectra of Angiotensin I methyl ester using citrate capped 2 nm AuNPs with varying percentages of methanol. AuNP: analyte ratio is 1 AuNP: 10^6 analyte molecules; 20 pmol of peptide deposited on the sample plate.

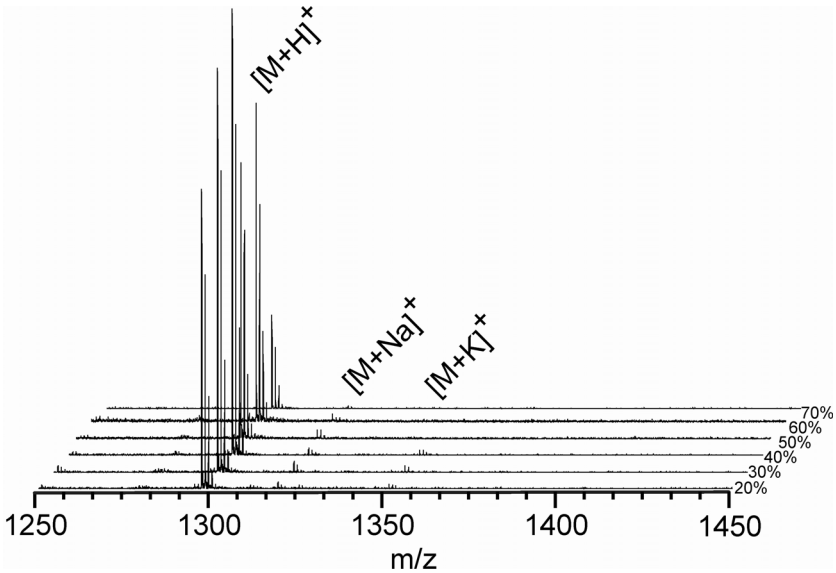

Figure 24. LDI-TOF mass spectra of Angiotensin I methyl ester using citrate capped 2 nm AuNPs with varying percentages of methanol. AuNP: analyte ratio is 1 AuNP: 10^7 analyte molecules; 20 pmol of peptide deposited on the sample plate.

These data suggest that if any disruption of hydrogen bonding between the various solution components occurs during the drying process, it does not affect the overall desorption/ionization process. Methanol is effective at reducing $[M + alkali]^+$ ions, perhaps due to a partitioning of the alkali into the methanol, resulting in less alkali per peptide in a given area, similar to the effect with AuNP-to-analyte. Alternately, alkali cations have a high affinity for methanol, resulting in the alkali drying away from the peptide as methanol dries faster.

Mixtures of peptides with methanol addition were also investigated to determine if changes in desorption/ionization occur. For the peptides Angiotensin I and Angiotensin I methyl ester, with no methanol addition the methyl ester dominates the spectrum, and only very low relative abundances of Angiotensin I is observed, as is shown in Figure 25A. With 10% methanol content, the abundances of $[M + alkali]^+$ ions for Angiotensin I methyl ester is decreased, and no change in abundances for Angiotensin I occurs, as is shown in Figure 25B. At 20% methanol content (Figure 25C), a significant increase in analyte abundances is observed for Angiotensin I with respect to Angiotensin I methyl ester, and $[M + alkali]^+$ ions are reduced significantly compared to 10% methanol content. At 30% - 60% methanol content, only trace amounts of $[M + alkali]^+$ ions are present; 60% methanol addition is shown in Figure 25D. As discussed with previous peptide mixtures, it appears that peptide-peptide interactions are affecting analyte desorption/ionization.

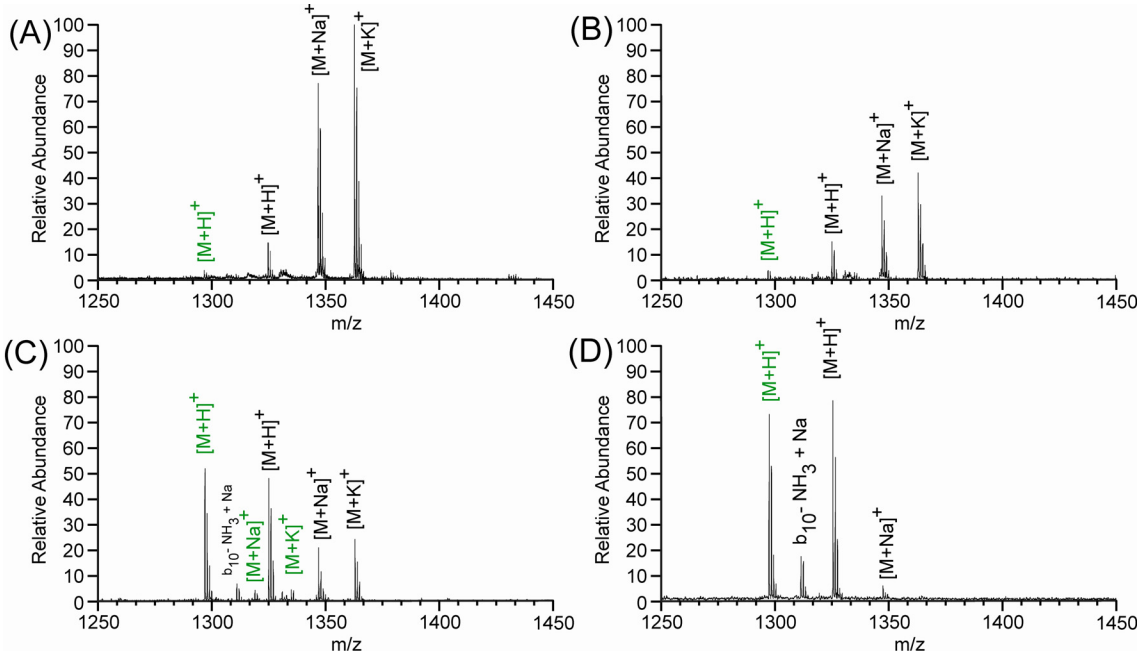

Figure 25. LDI-TOF mass spectra of Angiotensin I (green labels) and Angiotensin I methyl ester (black labels) (A) with no methanol, (B) with 10% methanol, (C) with 20% methanol, and (D) with 60% methanol. AuNP: analyte ratio is 1 AuNP: 10^6 analyte molecules; 20 pmol of peptide deposited on the sample plate.

Glycerol addition

The addition of glycerol in LDI stems from fast atom bombardment (FAB) MS, and early experiments done by Tanaka and coworkers.[2] Here, differing amounts of glycerol have been added to determine if ionization is affected. The relative abundances of the $[M + H]^+$ ion for the peptide Angiotensin I methyl ester in glycerol compared to no addition (see Figure 16A) increases, but there is little effect on reduction of $[M + alkali]^+$ ions, as is shown in Figure 26. The ratio of $[M + H]^+$ to $[M + alkali]^+$ ions does not dramatically change from 10% - 50% glycerol content; also, overall ion abundances decrease at higher glycerol content. Glycerol can serve as an additional proton source, accounting for the increase in the $[M + H]^+$ ion.

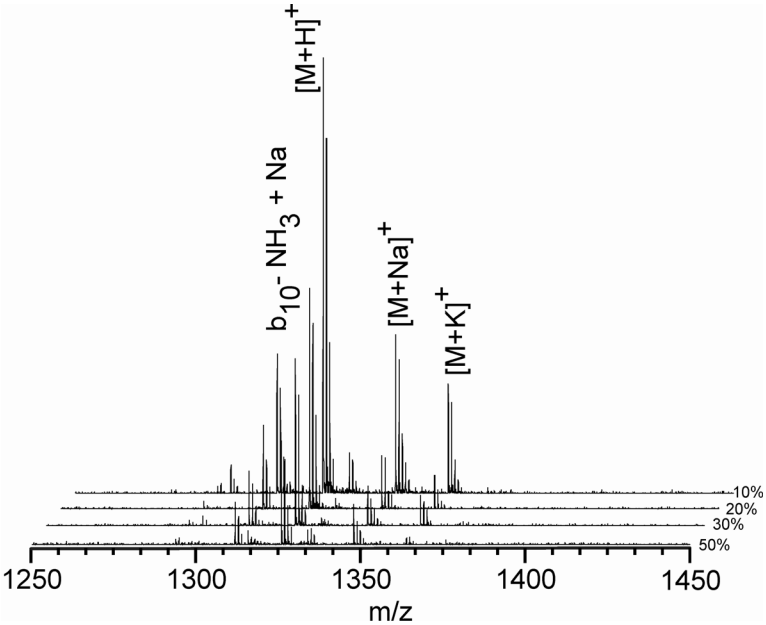

Figure 26. LDI-TOF mass spectra of Angiotensin I methyl ester using citrate capped 2 nm AuNPs with different percentages of glycerol solution composition.

As previously suggested with liquid matrices, analyte at the surface of the droplet is desorbed/ionized, making pre-formed ions a possibility here.[92] With glycerol present the sample spot is not actually dry, so the amount of alkali per given area is also fluid, most likely accounting for the lack of reduction of $[M + alkali]^+$ ions compared to previous conditions discussed here.

Fructose addition

Fructose has previously been used as an additive for MALDI to reduce the amount of internal energy of ions, *i.e.*, to lessen the amount of in-source fragmentation. A small amount of fragmentation is observed when using AuNPs for LDI (see Figure 18C), but it is not the dominant pathway. Figure 27 shows the LDI mass spectra of Val^4-

Angiotensin III with and without fructose addition. Overall ion signal is decreased, and fewer [M + alkali]$^+$ ions are observed. Fructose addition will be revisited in Chapter IV.

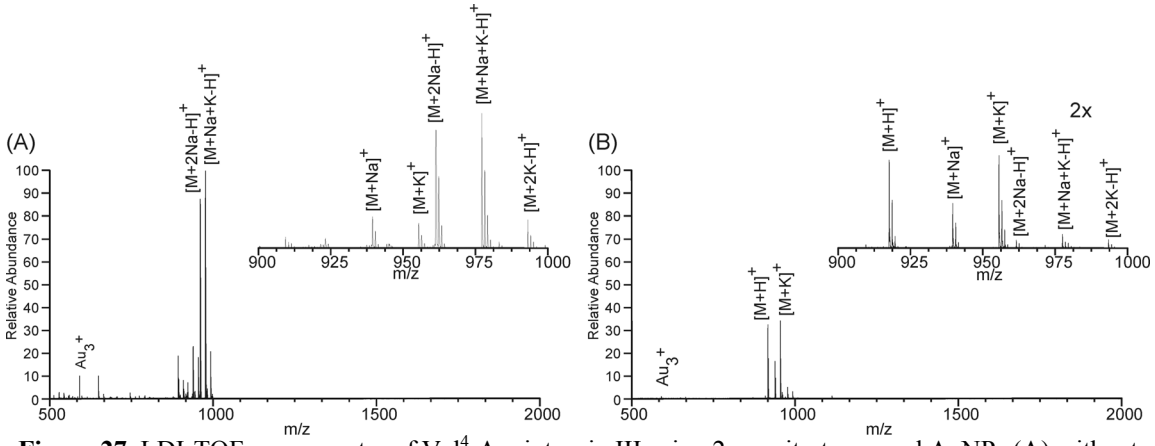

Figure 27. LDI-TOF mass spectra of Val^4-Angiotensin III using 2 nm citrate capped AuNPs (A) without fructose added and (B) with fructose added.

Ligand effects

Capping reagents play important roles in the chemical and physical properties of NPs, owing to the fact that NPs need stabilization of some type to prevent aggregation to the thermodynamically favorable bulk material.[32] NPs are typically stabilized in one of three ways: (i) electrostatically via charged species (*e.g.*, citrate), (ii) by steric hindrance (*e.g.*, dodecanethiol), or (iii) through encapsulation (*e.g.*, within a dendrimer).[25, 32, 93] Most of the AuNPs used in this dissertation are citrate capped, however here AuNPs were modified using standard gold-thiol chemistry.[84] Tiopronin (TP), glutathione (GSH), and β-mercaptoethanol (β-me) were chosen for these studies because of differences in ligand bulk, the possibility of proton donation, and some peptide like structure (for tiopronin and glutathione). Figure 28 shows the structures of these ligands. LDI of

Angiotensin I using citrate capped AuNPs (see Figure 19A) results in multiple [M + alkali]$^+$ ions, while TP modified AuNPs (Figure 28A) result in higher abundances of the [M + H]$^+$ ion, but still with a significant amount of [M + alkali]$^+$ ions present. LDI of Angiotensin I using GSH modified AuNPs yield much higher abundances of [M + H]$^+$ than citrate capped AuNPs, as is shown in Figure 28B. Finally, β-me capped AuNPs (see Figure 28C) does not significantly improve the abundance of the protonated molecule, however spectra obtained when using this ligand are not always repeatable, as some results have shown improvement in the ion signal of the [M + H]$^+$ ion. The higher abundances of [M + H]$^+$ for tiopronin and glutathione addition can be attributed to the availability of protons: the pK_a of tiopronin is estimated to be 5.2 and the pK_a of the glutamic acid side chain in glutathione is 4.07. The pK_a of β-me is 9.4, making it less likely to be a proton donor.

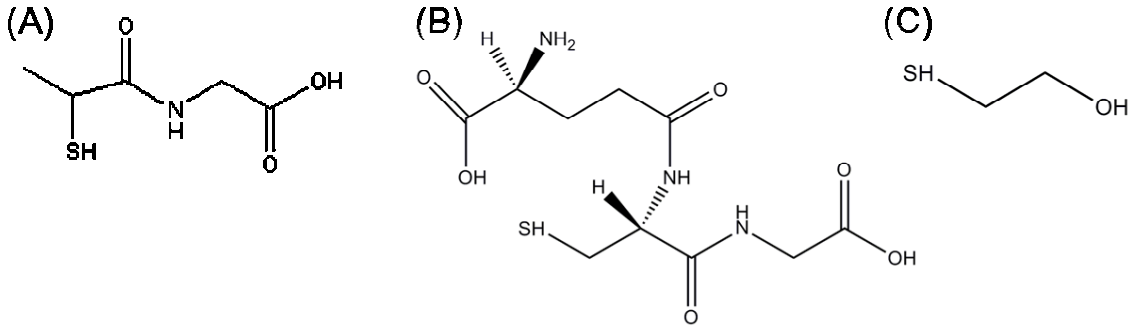

Figure 28. Structure of (A) tiopronin, (B) glutathione, and (C) β-mercaptoethanol.

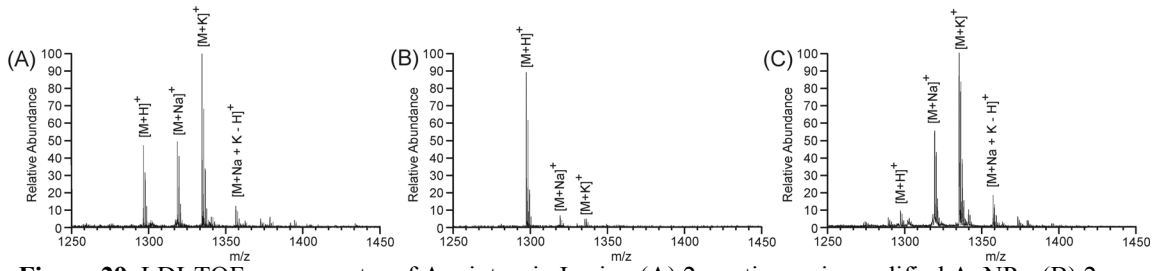

Figure 29. LDI-TOF mass spectra of Angiotensin I using (A) 2 nm tiopronin modified AuNPs, (B) 2 nm glutathione modified AuNPs, and (C) 2 nm β-mercaptoethanol modified AuNPs.

Different synthesis methods use different thiol ligands, and some NP extraction procedures from dendrimers use long chain alkanethiols. Here, several different thiols were mixed with citrate capped AuNPs to determine any affects on desorption/ionization. Figure 30 shows LDI-TOF mass spectra of the peptide Angiotensin I with hexanethiol, dodecanethiol, mercaptoundecanol, and mercaptoundecanoic acid modified AuNPs. The two alkanethiols (Figure 30A and 30B) do not result in analyte desorption/ionization. The two ligands with potential proton donors (mercaptoundecanol in Figure 30C and mercaptoundecanoic acid in Figure 30D) do result in desorption/ionization, although with relatively low ion yield. While the peptide Angiotensin I typically results in low ion yields, other peptides (Substance P and Val^4-Angiotensin III) were also evaluated and similar results were observed.

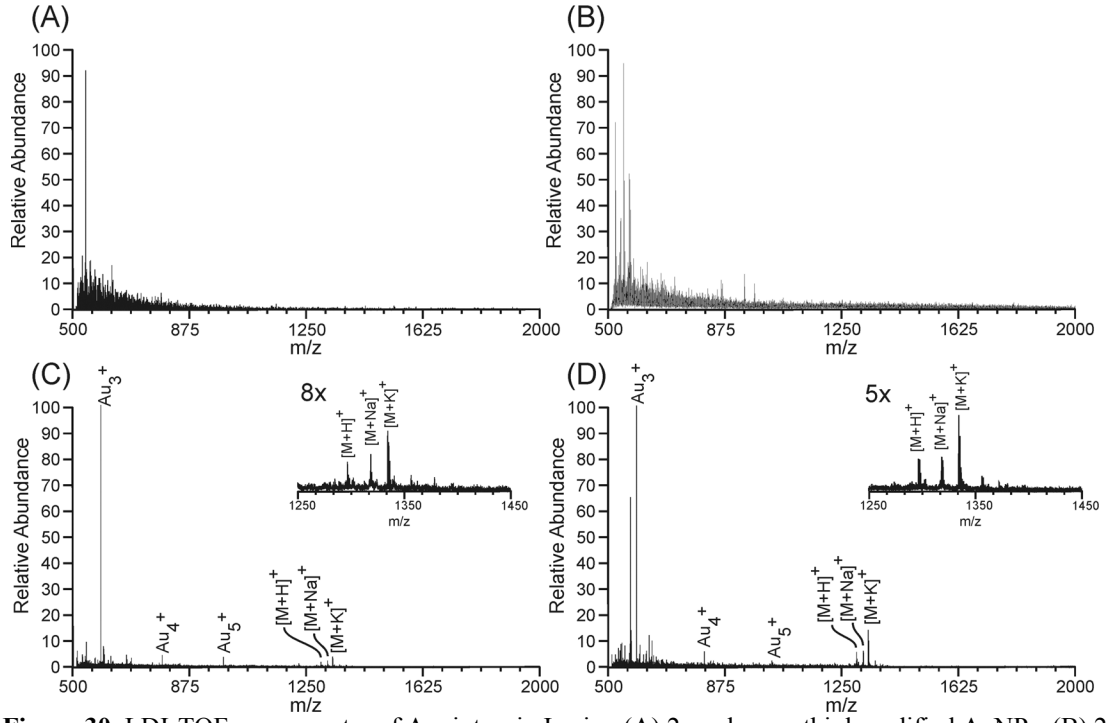

Figure 30. LDI-TOF mass spectra of Angiotensin I using (A) 2 nm hexanethiol modified AuNPs, (B) 2 nm dodecanethiol modified AuNPs, (C) 2 nm mercaptoundecanol modified AuNPs, and (D) 2 nm mercaptoundecanoic acid modified AuNPs.

Figure 31 shows a cartoon representation of the AuNP surface with ligand modification. The ligands discussed in this section are all thiols, which form a covalent bond with the Au surface.[94-98] A peptide can not displace a bound ligand, and so will interact with the ligand. Ligands such as hexanethiol or dodecanethiol are not miscible with aqueous analyte solutions, making interaction between the AuNP and analyte difficult, and may be part of the reason that desorption/ionization does not occur.

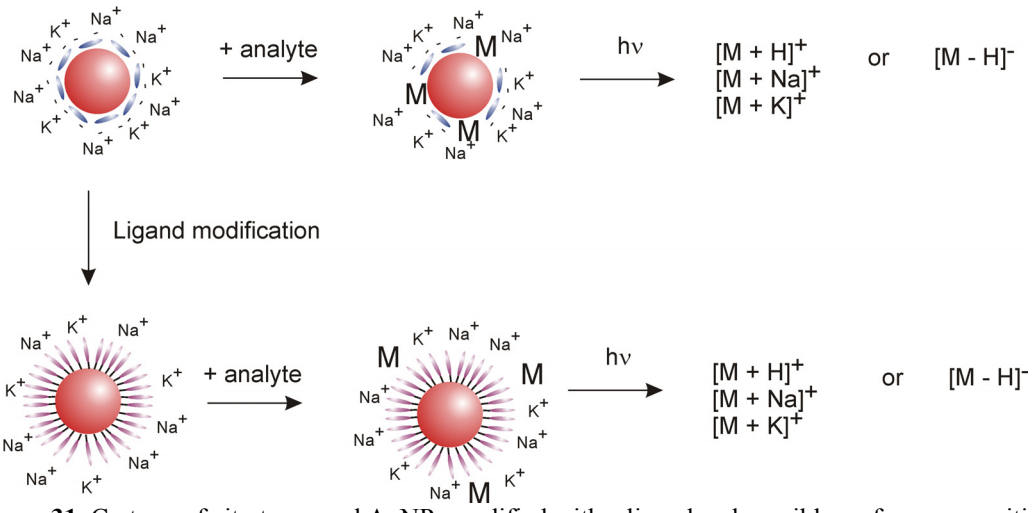

Figure 31. Cartoon of citrate capped AuNPs modified with a ligand and possible surface composition.

Summary

Three key points have been highlighted in this chapter: ionization of biomolecules using AuNPs varies dramatically depending on (i) analyte, (ii) solution conditions, and (iii) NP surface ligands. Analyte composition, specifically amino acid composition, can affect desorption/ionization when using AuNPs, just as in regular MALDI experiments. Peptides that are more basic (*i.e.*, have a high pI) generally tend to desorb/ionized more easily than acidic peptides (*i.e.*, have a low pI), as the pI values in Table 2 shows; the Angiotensin series of peptides that is contained in Figure 16 supports this statement as well. This is a result of the basic sites of the peptide (*e.g.*, N-terminus, arginine side chain, or lysine side chain) having a higher affinity for protons or alkali cations than other amino acids. A model peptide (*e.g.*, Angiotensin I methyl ester, Angiotensin I) was used to determine effects of solution conditions and NP surface conditions. Changes in solution conditions or composition, such as AuNP-to-analyte

ratio, pH, or addition of buffers or methanol, can be tuned to result in higher analyte ion abundances. The optimum AuNP-to-analyte ratio was determined to vary from peptide to peptide, but generally the highest analyte ion abundances are observed for 1 AuNP: 10^6-10^7 analyte molecules (Figure 14). Lowering the pH results in less desorption/ionization of the $[M + Na]^+$ or $[M + K]^+$ ions, and higher abundances of the $[M + H]^+$ ion (see Figure 18). Methanol additions reduces the abundances of the $[M + Na]^+$ and $[M + K]^+$ ions (Figure 23). Changes to the surface of the AuNP can also affect ionization. For example, covalent attachment of ligands, such as tiopronin or glutathione generally increase analyte ion yield compared to citrate capped AuNPs (see Figure 29). Conversely, alkanethiols do not result in desorption/ionization of analyte, but an alkanethiol with a terminal carboxylic acid or alcohol does result in desorption/ionization of analyte (Figure 30). These results suggest that interaction of the analyte with the AuNP is important for desorption/ionization, but can still occur if a viable proton source (*e.g.*, proton from a carboxylic acid, alcohol, amine) is present. There are important implications for a desorption/ionization mechanism here, and that topic is explored further in Chapter VI. Differences in desorption/ionization based on peptide composition is also important to that discussion, and highlighted more in Chapter VI. Finally, there are several examples in this chapter where desorption/ionization does not occur. While some of these effects are not fully understood, they can still provide insight into the overall mechanism of desorption/ionization of biomolecules.

CHAPTER III

ANION EFFECTS ON IONIZATION OF BIOMOLECULES USING GOLD NANOPARTICLES AS MATRICES FOR LDI-MS

Introduction

Although LDI mass spectra obtained using AuNPs are less congested in the low mass range and a greater range of sample deposition conditions (*e.g.*, pH, solvents) can be used, it has also been observed that specific changes in the solution environment can dramatically affect LDI ion yields. For example, in some cases the presence of salts and buffers do not significantly affect analyte ion abundances, whereas small amounts of alkali metal salts and/or buffers and changes in the amino acid composition of the peptide strongly suppresses analyte ion yields. It is unclear if these effects are the result of a change in the physicochemical properties of the NPs or if they arise solely from alteration of analyte-NP interactions. Therefore, this chapter presents a systematic study as to how specific changes in the composition of the solution, and thereby changes in the physicochemical NP surface environment, affects ion yields for size-selected AuNPs.

It is quite possible that the sample preparation methods that are essential for LDI of biomolecules could alter the surface capping and/or lead to aggregation of the NPs. Therefore, examination of NPs by TEM is necessary to determine if any aggregation has occurred. In addition, the presence of impurities (*e.g.*, buffers or detergents) as well as polar amino acids that comprise the peptide could displace the capping group and lead to changes in the physical/chemical properties of the NP. Here, the effects of various salts

on the physical properties of the AuNPs and on LDI ion yields are examined, as well as the sensitivity of "salt effects" on the chemical nature of the capping group.

Experimental

All mass spectrometry experiments were performed on an Applied Biosystems Voyager DE-STR (Foster City, CA) with a Spectra-Physics (Irvine, CA) N_2 laser (337 nm). Positive and negative mode experiments were performed in the reflected mode using 200 laser shots with internal calibration. All of the mass spectra shown used laser energies at 7-12% above the threshold for ionization. The positive and negative ion spectra within each figure are all normalized to each other, *i.e.*, the relative ion abundance at 100% represents the same number of counts.

As previously discussed in Chapter II, the optimum AuNP-to-analyte ratio for LDI from AuNPs is approximately 1 AuNP: 10^6 analyte molecules, and for the studies in this chapter that ratio was used because this gives consistent results for the selected analyte. While only data for Val^4-Angiotensin III is shown here several analytes were tested; Val^4-Angiotensin III is representative of the trends observed here.

Samples were prepared by mixing solutions containing the AuNPs with salt solutions and solutions containing analyte and let sit for 5 to 10 minutes to allow time for equilibration between NP and salt. Under optimum conditions, meaning samples contain minimum amounts of salt content, peptide ion detection levels of 10-50 femtomoles can be achieved; however, for the studies reported here relatively high sample loadings (~9 pmol of total analyte) were used to minimize data acquisition times.

It is estimated that this sample loading corresponds to approximately 8-10 attomoles of analyte (10^5 molecules) per NP. The final salt concentration of the sample solution was 0.44 M. A 1 μL aliquot of the solution was deposited on to a stainless steel plate (9 pmol peptide), vacuum dried, and analyzed. A positive ion spectrum of a control sample consisting of AuNPs and peptide (9 pmol peptide deposited) contains abundant $[M + alkali]^+$ ions, and very low analyte ion abundances in the negative ion spectrum (data not shown). Previous work has also shown that $[M + alkali]^+$ ions dominate the mass spectrum. Several sample cleanup methods have been investigated, but as Chapter II described, sample loss and decrease in ion signal are problematic. AuNPs were modified using standard gold-thiol chemistry, and the procedure was reported in Chapter II.[84]

UV-Vis spectroscopy and TEM were used to characterize the modified AuNPs, and AuNPs with salts added. Absorption spectra were obtained (Agilent 8453 UV-Visible Spectrophotometer (Foster City, CA)) to monitor changes in the surface plasmon band of the AuNPs. Samples of AuNPs and salts were mixed and spectra recorded at t = 0 min, 2 min, and 5 min. TEM images were obtained on a JEOL 2010 Hi-Resolution Transmission Electron Microscope with an acceleration voltage of 200 kV. The absorption spectra of the modified NPs shows a slight red-shift in the surface plasmon band with no change in the plasmon band width, indicating a change in the NP environment consistent with a change in ligand, as opposed to particle aggregation (see Figure 32). Results from TEM do not indicate any significant changes in particle size upon ligand adsorption (Figure 33) or particle aggregation.

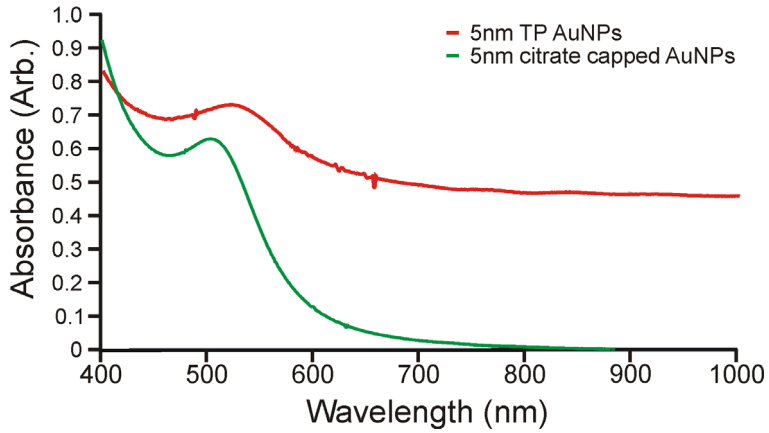

Figure 32. UV-Visible absorption spectra of citrate capped and tiopronin modified 5 nm AuNPs.

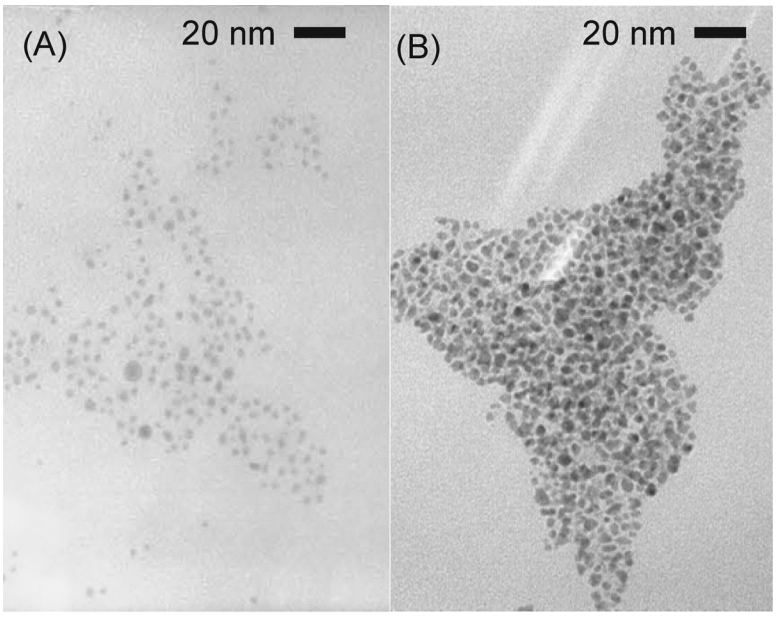

Figure 33. TEM images of (A) 2 nm citrate capped AuNPs and (B) 2 nm tiopronin modified AuNPs.

99% Sodium fluoride, ≥ 99% sodium chloride, 99% sodium bromide, ≥ 99.5% sodium iodide, 99% ammonium fluoride, 99% ammonium chloride, ≥ 99.5% ammonium bromide, ≥ 99% ammonium iodide, 99% sodium nitrate, 99% sodium sulfate, 99% sodium carbonate, N-(2-mercaptopropionyl)glycine (tiopronin), glutathione, and β-

mercaptoethanol were obtained from Sigma (St. Louis, MO) and used as received. 2 nm, 5 nm, and 10 nm citrate capped gold nanoparticles were purchased from Ted Pella, Inc. (Redding, CA). Val^4-Angiotensin III (RVYVHPF) was purchased from American Peptide Co. (Sunnyvale, CA) and was prepared in water.

Results

We first examined the electronic and physical properties of the AuNPs using UV-Vis absorption measurements and TEM. For example, shifts in the surface plasmon resonance (SPR) band for the 5 nm particles would indicate possible changes in NP size, shape, capping molecules, and dielectric environment, but similar measurements cannot be performed on 2 nm particles owing to the absence of an SPR band. Figure 34 contains absorption spectra for 5 nm AuNPs with halide salt addition, and we observe a slight red-shift in the SPR band upon addition of F^- and Cl^-. Br^- addition results in a broadening of the SPR band, and the SPR band is absent for I^- treated particles. We assume that similar effects occur for the 2 nm AuNPs owing to the fact that TEM images for 2 nm citrate capped AuNPs (Figure 35A) with added chloride (Figure 35B), bromide (Figure 35C), and iodide (Figure 35D) support the observations for UV-Vis of 5 nm AuNPs with halides added. In the TEM images for 2 nm AuNPs with halides added it appears that addition of Cl^- or Br^- does not result in changes of particle size or induce any aggregation; conversely, addition of I^- results in dramatically different particle sizes, shapes, and aggregation does occur.

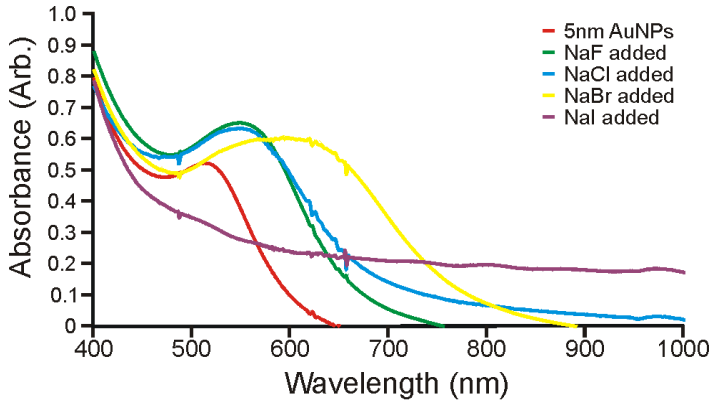

Figure 34. UV-Visible absorption spectra of 5 nm citrate capped AuNPs with the addition of NaF, NaCl, NaBr, and NaI.

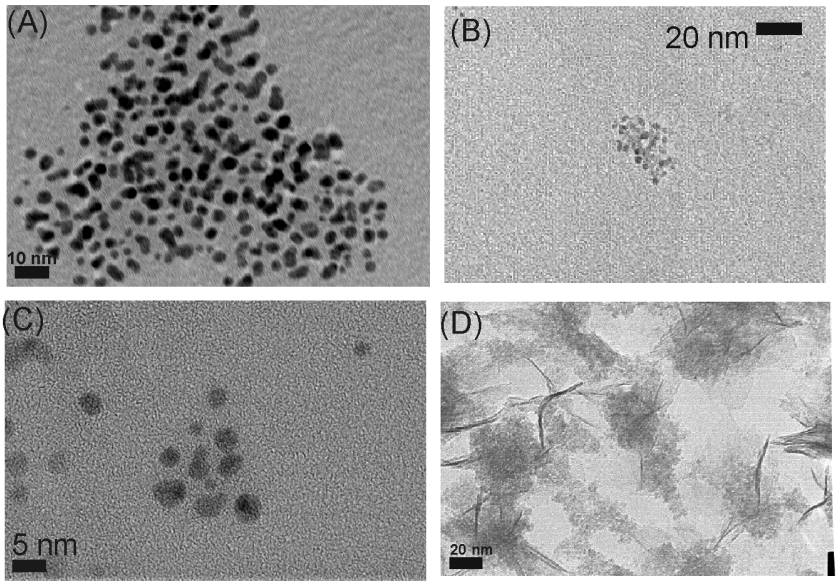

Figure 35. TEM images of (A) 2 nm citrate capped AuNPs, (B) 2 nm citrate capped AuNPs with NaCl added, (C) 2 nm citrate capped AuNPs with NaBr added, and (D) 2 nm citrate capped AuNPs with NaI added.

Figure 36 contains positive and negative ion 337 nm LDI mass spectra for citrate capped 2 nm AuNPs mixed with Val^4-Angiotensin III and NaF, NaCl, NaBr, or NaI. Although positive ion spectra for samples containing F^- and Cl^- are very similar to spectra from untreated samples, the yield for $[M - H]^-$ ions is increased. Addition of Br^-

has little affect on the positive ion spectrum, but Br^- addition completely suppresses the $[M - H]^-$ ion yield.

Addition of I^- (as NaI) results in complete loss of positive and negative analyte ion signals; however, abundant analyte ion signals are observed upon addition of I^- (as NH_4I). Figure 37 contains AuNP LDI mass spectra for Val^4-Angiotensin III with addition of NH_4X (X = F, Cl, Br, and I). Note that analyte ion signals are observed from samples containing NH_4X salts in both positive and negative ion spectra. In fact, we observe an increase in the abundance of $[M + H]^+$ ions compared to citrate capped AuNPs.

The UV-Visible absorption spectra in Figure 38A show plasmon bands for all salt additions, whereas previously addition of iodide as NaI resulted in loss of the SPR band. Also, TEM of NH_4I addition (Figure 38B) shows very little NP aggregation or dissolution.

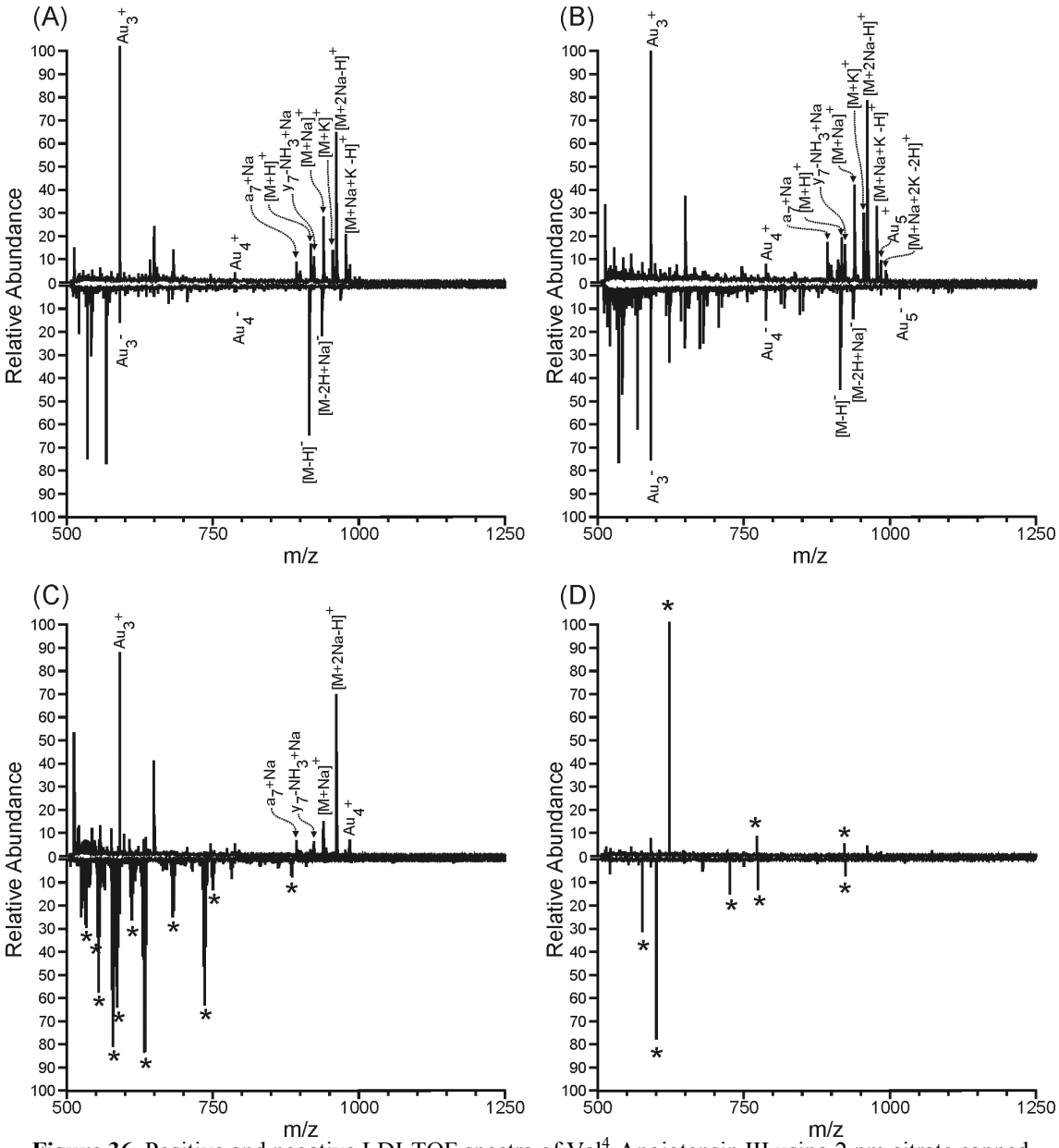

Figure 36. Positive and negative LDI-TOF spectra of Val^4-Angiotensin III using 2 nm citrate capped AuNPs with the addition of (A) NaF, (B) NaCl, (C) NaBr, and (D) NaI. (*) denote salt clusters.

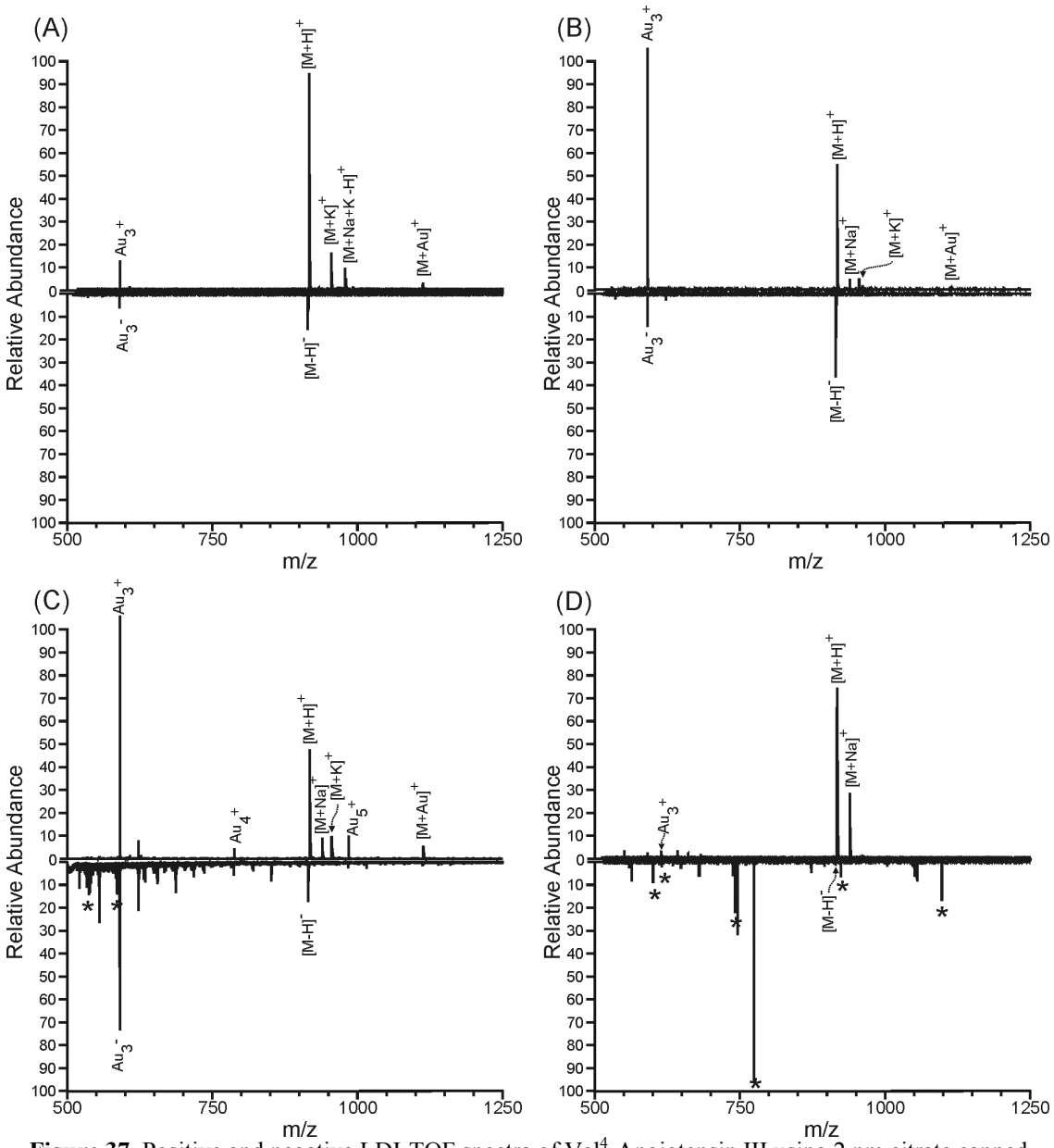

Figure 37. Positive and negative LDI-TOF spectra of Val^4-Angiotensin III using 2 nm citrate capped AuNPs with added (A) NH_4F, (B) NH_4Cl, (C) NH_4Br, and (D) NH_4I.

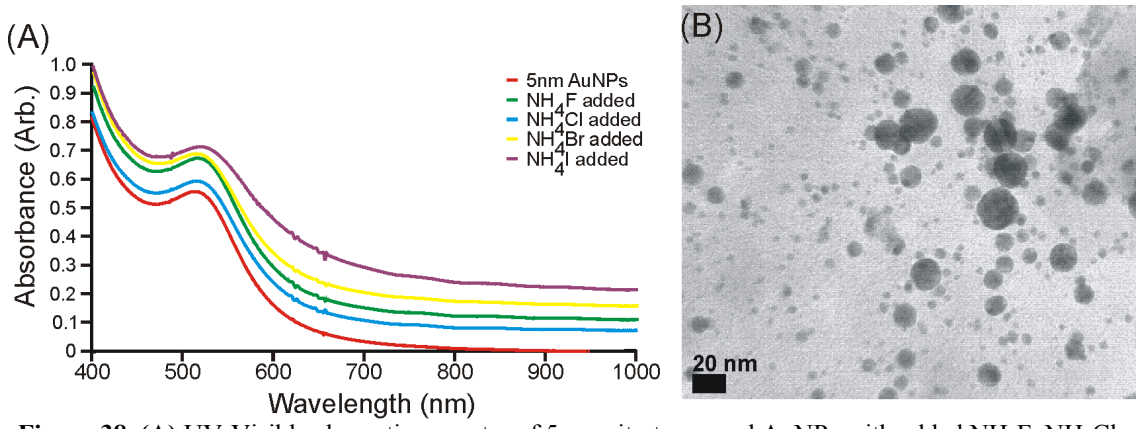

Figure 38. (A) UV-Visible absorption spectra of 5 nm citrate capped AuNPs with added NH_4F, NH_4Cl, NH_4Br, and NH_4I. (B) TEM image of 2 nm citrate capped AuNPs with NH_4I added.

Positive and negative ion spectra for Val^4-Angiotensin III from citrate capped AuNPs treated with TP and NaX (X = F, Cl, Br, I) were also examined as Figure 39 shows. Similar ion yields are found for 2 nm and 5 nm AuNPs modified with GSH and β-me. There is enhancement in the $[M - H]^-$ ion yield with added F^- and Cl^- similar to that for citrate capped AuNPs, and abundant $[M - H]^-$ ion yields are observed if Br^- is added. Interestingly, analyte signal is observed for AuNPs treated with I^-, in marked contrast to results for I^- addition to citrate capped AuNPs. The UV-Visible absorption spectra in Figure 40A show plasmon bands for all salt additions, in contrast to citrate capped AuNPs where addition of NaI resulted in loss of the SPR band. Also, TEM of TP modified AuNPs with NaI addition (Figure 40B) shows very little NP aggregation or dissolution.

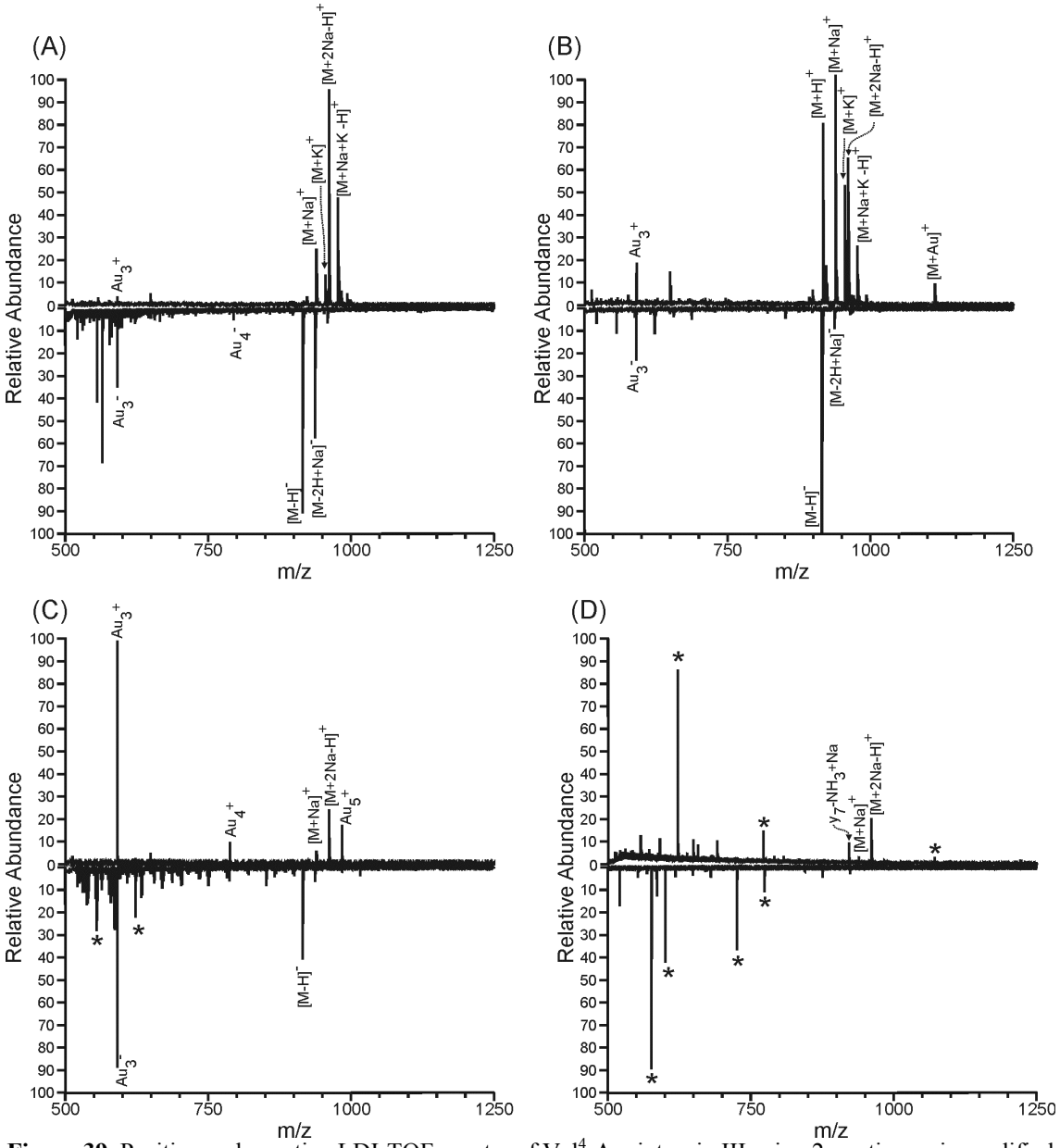

Figure 39. Positive and negative LDI-TOF spectra of Val^4-Angiotensin III using 2 nm tiopronin modified AuNPs with the addition of (A) NaF, (B) NaCl, (C) NaBr, and (D) NaI.

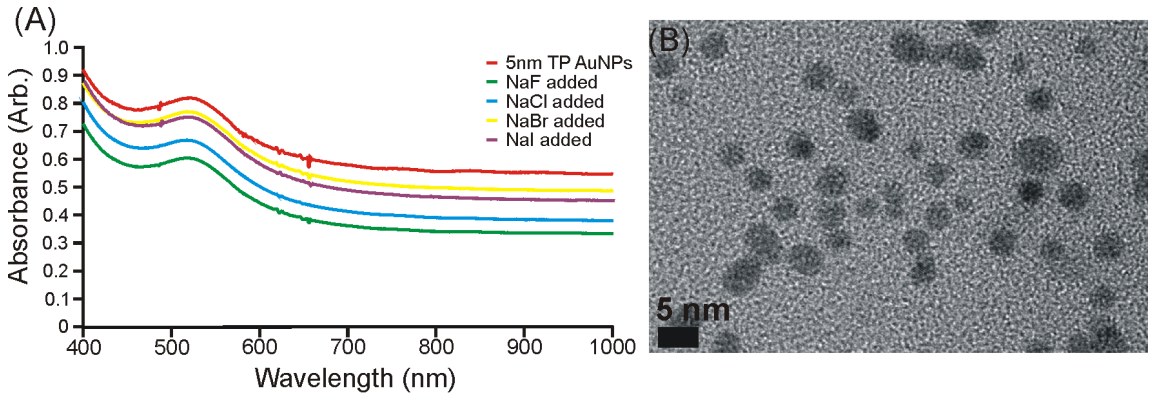

Figure 40. (A) UV-Visible absorption spectra of 5 nm tiopronin modified AuNPs with addition of NaF, NaCl, NaBr, and NaI. (B) TEM image of 2 nm tiopronin modified AuNPs with NaI addition.

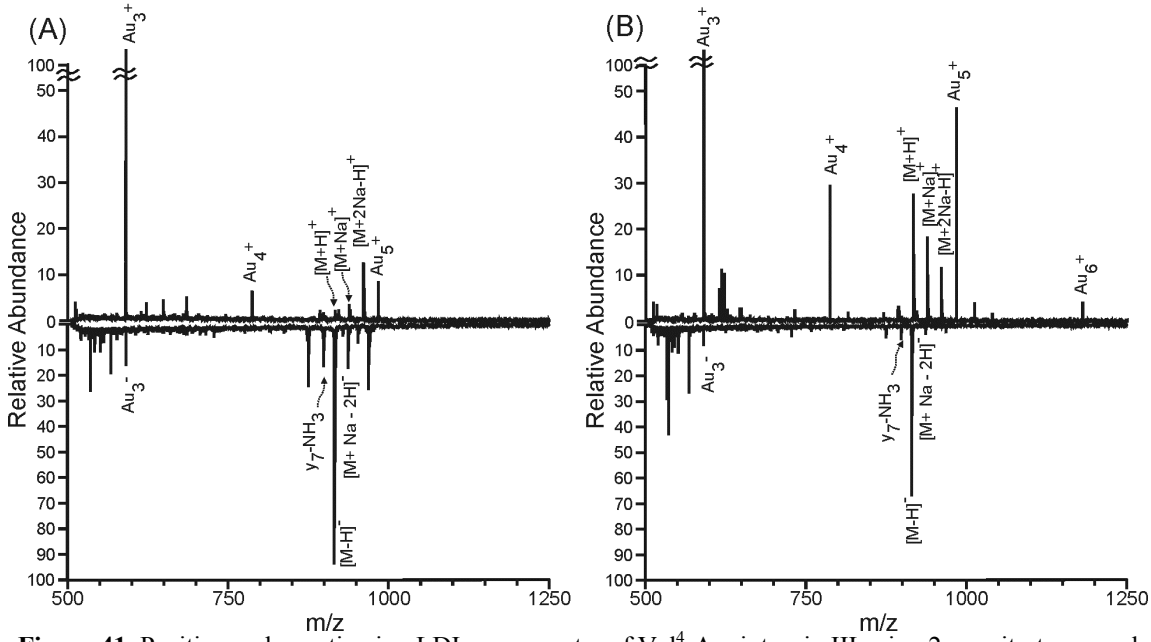

Figure 41. Positive and negative ion LDI mass spectra of Val^4-Angiotensin III using 2 nm citrate capped AuNPs with the addition of (A) $NaNO_3$ and (B) Na_2SO_4.

Figure 41 contains LDI spectra for Val^4-Angiotensin III citrate capped AuNPs with added $NaNO_3$ and added Na_2SO_4. Although there is an overall decrease in analyte ion abundances in the positive ion spectra, there is a pronounced enhancement in the abundance of the $[M - H]^-$ ion in the negative ion spectra. Similar trends are observed

for 5 and 10 nm AuNPs. UV-Visible absorption spectra in Figure 42 shows no loss of plasmon band.

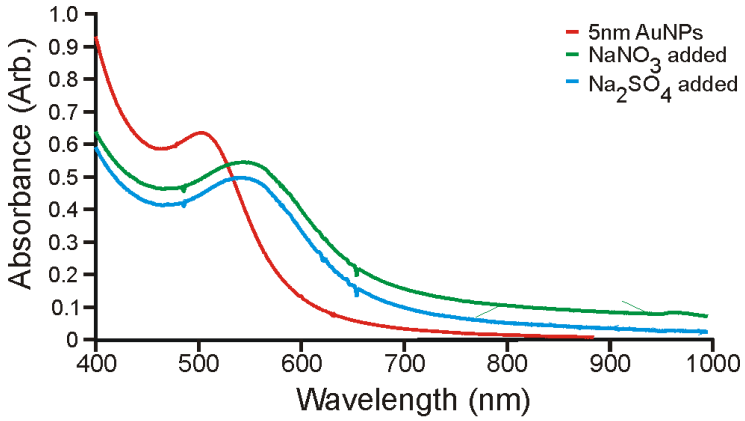

Figure 42. UV-Visible absorption spectra of 5 nm citrate capped AuNPs with addition of $NaNO_3$ and Na_2SO_4.

It is also interesting to compare the effects of oxyanions on citrate capped AuNPs versus TP, GSH, and β-me modified AuNPs. For example, Figure 43 contains positive and negative LDI mass spectra for Val^4-Angiotensin III with added $NaNO_3$ using β-me modified AuNPs (the data is representative of TP and GSH modified AuNPs as well as 5 nm AuNPs modified with all three ligands). Note the dramatic decrease in the negative ion signal and the abundance of positive ion signal, specifically $[M + H]^+$, $[M + Na]^+$ and $[M + K]^+$ ions. Figure 44 contains UV-Visible absorption spectra, which show the SPR band is still present.

Modified AuNPs were also treated with ammonium halide salts. The data included in Figure 45 are for GSH modified AuNPs, and this is representative of data for TP and β-me modified AuNPs as well as 5 nm AuNPs modified with all three ligands.

Analyte ions are observed for all the ammonium halide salts; the increase in $[M + H]^+$ ions is attributed to the additional proton source from the ammonium cation. F^- and Cl^- addition result in an enhancement of the $[M - H]^-$ ion. Finally, UV-Visible absorption spectroscopy (Figure 46) shows that the SPR band is retained.

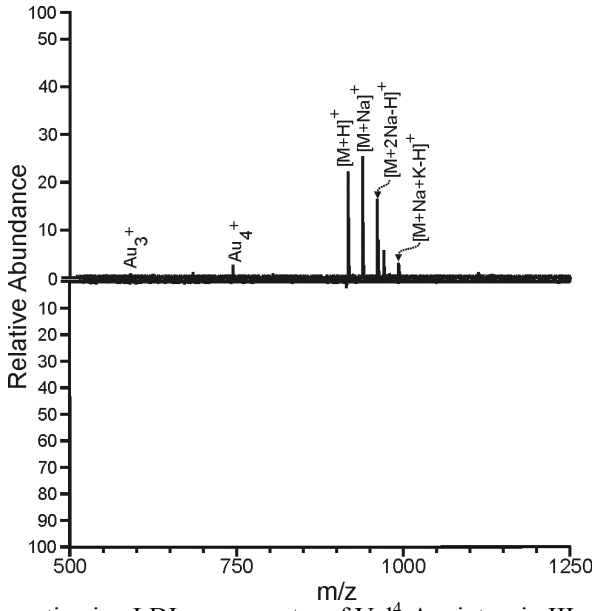

Figure 43. Positive and negative ion LDI mass spectra of Val^4-Angiotensin III using 2 nm β-me modified AuNPs with the addition of $NaNO_3$.

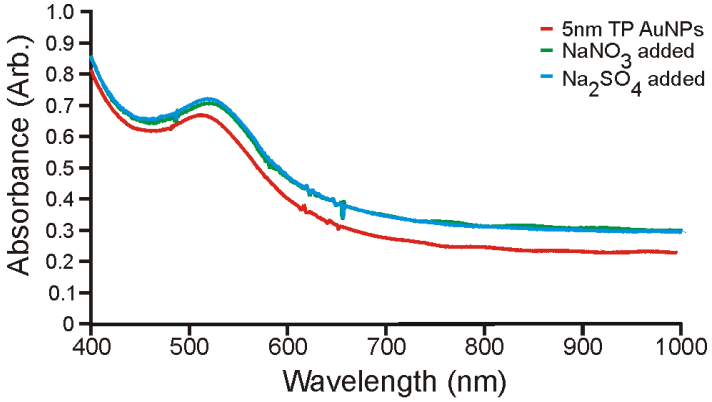

Figure 44. UV-Visible absorption spectra of 5 nm tiopronin modified AuNPs with $NaNO_3$ and Na_2SO_4.

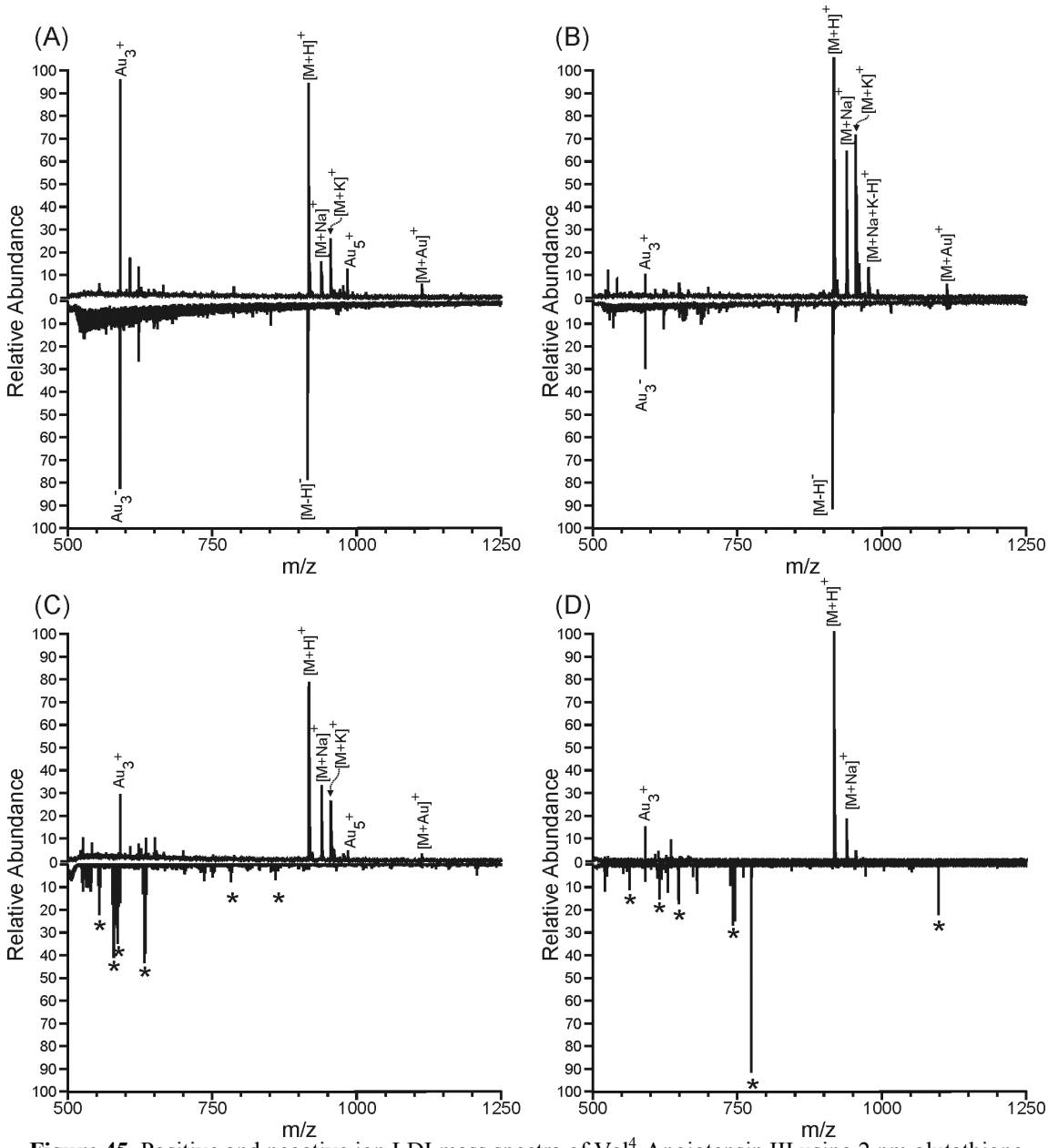

Figure 45. Positive and negative ion LDI mass spectra of Val^4-Angiotensin III using 2 nm glutathione modified AuNPs with the addition of (A) NH_4F, (B) NH_4Cl, (C) NH_4Br, and (D) NH_4I.

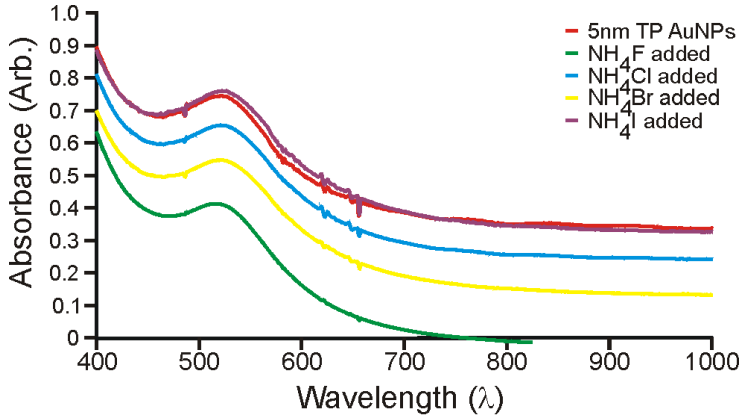

Figure 46. UV-Visible absorption spectra of 5 nm tiopronin modified AuNPs with added NH_4F, NH_4Cl, NH_4Br, and NH_4I.

Discussion

It has previously been shown that size-selected (2 nm, 5 nm, 10 nm) citrate capped AuNPs serve as effective matrices for LDI-MS,[99] and that various solution parameters, *i.e.*, buffer anions, surfactants, solution pH, and other common additives, influence both positive and negative ion yields. These effects are clearly illustrated in the data presented above; additionally, these data highlight three important points: (i) the addition of species that do not interact with the AuNPs or species that interact but are unreactive do not affect the LDI process, (ii) species which interact and are reactive with the AuNP have dramatic effects on the LDI ion yields, and (iii) capping the AuNP with organic ligands such as TP, β-me, and GSH minimize or even eliminate the effects of species that possess high affinity for or react with AuNPs. Also, addition of capping reagents such as oxyanions, NH_4^+, or thiourea enhance the relative abundances of $[M - H]^-$ and $[M + H]^+$ ions, respectively. These effects on ion yield appear to be the result of reaction chemistry with the analyte, *i.e.*, oxyanions react with peptides to enhance the

yield of $[M - H]^-$ and NH_4^+ and thiourea enhance the yields for $[M + H]^+$ ions. These trends in LDI ion yields are independent of AuNP size. That is, similar results are obtained with 2 nm, 5 nm, and 10 nm citrate capped AuNPs and modified (β-me, GSH and TP) AuNPs.

UV-Vis absorption spectra and TEM of NaX addition to citrate capped AuNPs shown in Figures 34 and 35 confirm that no significant change in particle size occurs for F^- and Cl^- addition. A slight red-shift in the absorption spectrum for F^- and Cl^- addition is expected, as the ionic strength and dielectric environment of the solution changed.[24] The UV-Vis absorption spectrum of AuNPs with Br^- addition shows a broadening of the SPR band, suggesting that aggregation may be occurring, but TEM shows only a very small amount of change in AuNP size. UV-Vis absorption spectrum of I^- added to citrate capped AuNPs shows loss of the SPR band, indicating aggregation or dissolution of the particles. TEM shows extensive networking of particles treated with I^-. Given the reduced size of the AuNPs, it seems most likely that the NPs were fragmented via reactions with the surrounding medium, and then formed a network, versus fusing into a network structure first, which would appear as larger NPs.

The spectra contained in Figure 36 show that addition of F^- and Cl^- has little effect on the positive ion spectra of Val[4]-Angiotensin III, but addition of F^- and Cl^- significantly enhances the yield of $[M - H]^-$ ions. The results for positive ion LDI are not surprising because F^- does not efficiently bind to gold,[100] thus displacement of citrate is unlikely. Although Cl^- has a significant affinity for gold surfaces and most likely displaces citrate, Cl^- does not disrupt the surface morphology[100, 101] owing to similar

ionic and atomic radius, chloride ion (1.81Å)[102] and gold (1.74Å), respectively.[103] On the other hand, the results for negative ion LDI suggests that both F^- and Cl^- promote formation of $[M - H]^-$ ions, thus these anions must be interacting with the AuNP or influencing the peptide-AuNP interactions in a manner that enhances negative ion formation. It is feasible that $[M + F^-]^-$ or $[M + Cl^-]^-$ species, which can be formed in relatively high yields by electrospray ionization and dissociate by loss of HF or HCl, may also be formed as transient species by LDI. Breuker *et al.* have also investigated the dissociation chemistry of $[M + F]^-$ and $[M + Cl]^-$ ions[104] and we are continuing this work.[105]

The spectra obtained for Br^- treated and untreated AuNPs show some differences (Figure 36C); Br^- has a high affinity for gold and displaces citrate from the AuNP surface.[101] Although the positive ion spectra for untreated and treated AuNP are similar, the negative ion spectra are quite different because $[M - H]^-$ ions are not detected. We see evidence of small changes in size for AuNP treated with Br^- in both TEM and UV-Vis data, but such small changes should not have a strong effect on ion yields. By analogy with the explanation for $[M + F^-]^-$ and $[M + Cl^-]^-$, we do not observe any product from formation of $[M + Br^-]^-$.

Addition of I^- to the AuNPs has the strongest effect on $[M + H]^+$ and $[M - H]^-$ ion yields. I^- has a high affinity for gold and can cause aggregation as well as dissolution of the particles.[106-109] Cheng and co-workers[107] interpreted TEM and UV-Vis absorption data as evidence that I^- displaces citrate from the AuNPs owing to a weakened and broadened SPR band. They also propose that reactions occur on the NP surface, resulting

in etching or fragmentation of the AuNPs, followed by aggregation. Wanner and Gerthson[108] also showed that citrate is displaced from AuNPs by I^-, and suggested that the product of reaction is I_3^-, which then acts as a capping agent. The I_3^- on the NP surface reacts further with I^- to yield $[AuI_2]^-$ and I_2. Singh *et al.*[109] suggest that AuI forms on the surface after iodide adsorption, causing a mismatching lattice structure of the NP surface and AuI, leading to deformation of the particles. Figure 47 is a cartoon that illustrates how the different halide additives may displace the citrate on the AuNP surface.

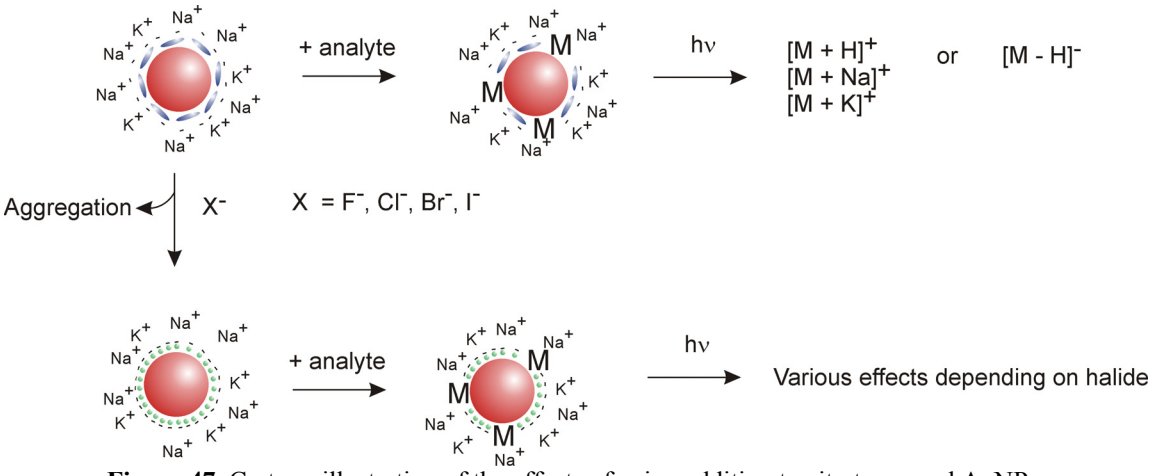

Figure 47. Cartoon illustration of the effects of anion addition to citrate capped AuNPs.

Addition of I^- presents the most dramatic change in ion signal, with Figure 36D showing no analyte signal detected, however addition of I^- as NH_4I results in abundant analyte ion signals (see Figure 37D). With this quaternary ammonium ligand the anion interacts with the AuNP surface, and the ammonium cation coordinates with the anion, this interaction is termed anion-induced cation adsorption.[110, 111] Fink and co-workers[112]

proposed that AuNPs capped with ammonium salts (*i.e.*, $R_4N^+Br^-$) exist as Br^- adsorbed directly to the surface, with R_4N^+ electrostatically coordinated to the bromide. Such ion pairs stabilize the Au surface in solution. Addition of ammonium halide salts (NH_4X, X= F, Cl, Br, I) results in analyte ion signals for all the salts. There is also an increase in $[M + H]^+$ ion abundances, which may be the result of additional proton source from the ammonium ion because similar effects are observed for samples treated with thiourea. Note that even though I^- is adsorbing to the surface, it does not appear to cause significant amounts of etching or aggregation, as suggested by the change in the SPR band in the UV-Vis data. The TEM image in Figure 38B shows that NPs are still present with I^- addition as NH_4I, compared to complete particle etching with addition of NaI. The difference in NP morphology is probably the result of the I^- being capped on the surface of the AuNP by the ammonium cation, making it difficult for secondary reactions that are responsible for the destructive etching of the surface to occur, or the kinetics of surface etching has been altered.[107-109]

Addition of NaX (X = F, Cl, Br, I) to modified AuNPs results in analyte ion signals in the positive ion spectra for all halide salts (see Figure 39). The ionization of analyte in the presence of I^- suggests that the covalently bound ligands protect the NP surface from complete halide adsorption. However, the analyte ion abundances are still low, meaning that competing processes may be occurring. In contrast to halide addition to citrate capped AuNPs, $[M - H]^-$ ion signal is enhanced upon addition of F^-, Cl^-, and Br^-. It is unclear why $[M - H]^-$ ion signal is enhanced for Br^- addition, but in contrast to citrate capped AuNPs with Br^- addition fewer salt clusters are observed, which would

result in less ion suppression. Figure 48 is a cartoon that illustrates AuNPs covalently modified with a ligand, addition of halide salts, and the subsequent effects of halide addition.

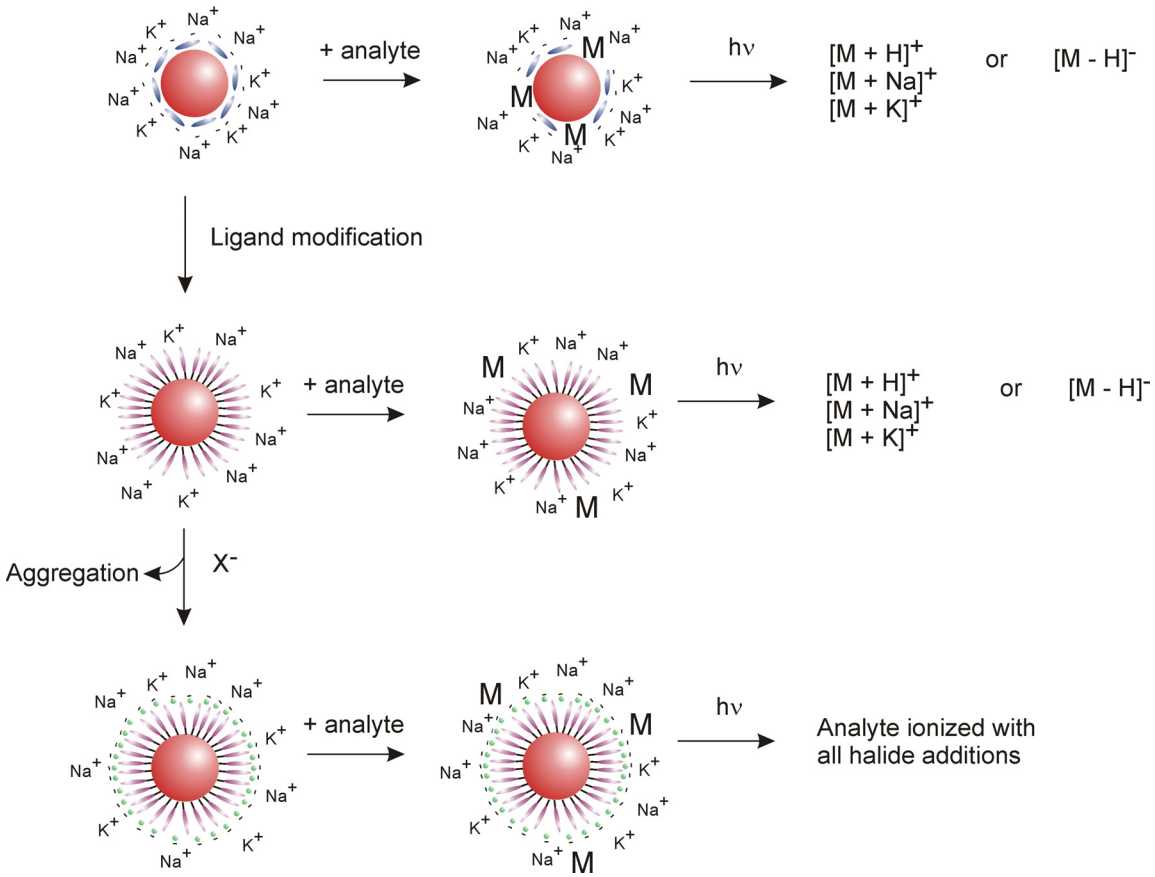

Figure 48. Cartoon illustration of halide addition to ligand modified AuNPs.

Figure 41 contains addition of oxyanions to citrate capped AuNPs and results in an enhancement of the $[M - H]^-$ ion. Cumberland and Strouse[113] and Enusten and Turkevich[76] have shown that oxyanions can coordinate with metal surfaces through electrostatic interaction of the anion, specifically by coordination of the oxygen donor

atoms which back-bond with the metal surface. As with I^- and Br^-, such interactions can displace citrate from the AuNP surface. The red-shift in the UV-Vis absorption spectra (see Figure 42) suggest a change in the electronic interactions between the ligand and the NP, most likely due to displacement of the citrate, and the broadening of the SPR band suggest some aggregation or dissolution of the NPs.[24] TEM confirms that there is a limited amount of aggregation or fusing of the NPs. The peptide reacts with the oxyanion coordinated on the AuNP surface and produces a deprotonated peptide molecule and oxyanion acid. The enhancement of $[M - H]^-$ supports this reaction scheme, as does the aggregation or fusing of the NPs, as loss of charge on the NP surface would result in some aggregation. Enhancement of the $[M - H]^-$ ion is not observed for oxyanion addition to modified NPs (see Figure 43). While the oxyanion is still interacting with the peptide, the addition of a ligand that is chemically peptide-like on the NP surface results in a competing process for deprotonation. Figure 49 is a cartoon depicting oxyanion addition to citrate capped AuNPs.

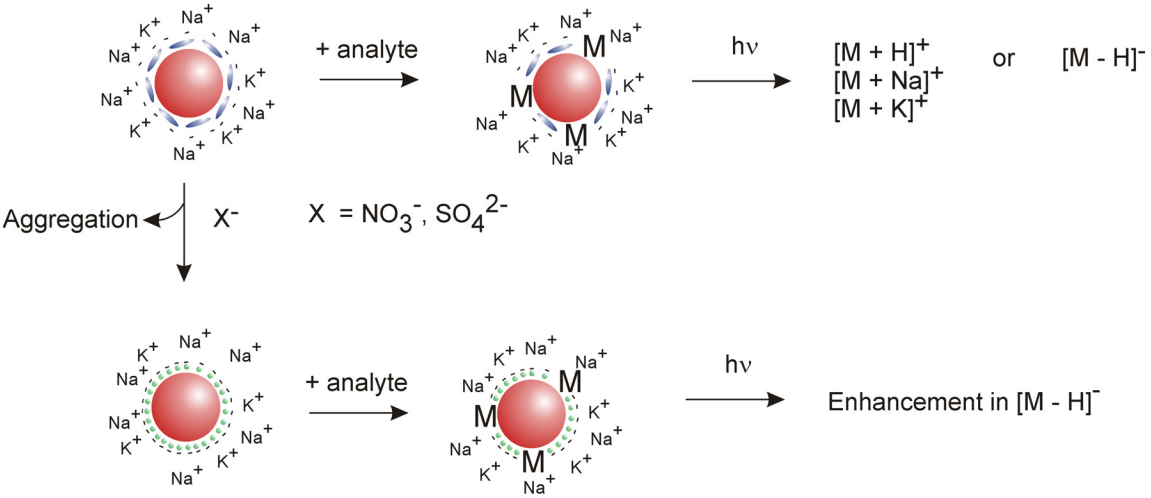

Figure 49. Cartoon illustration of oxyanion addition to AuNPs.

Summary

This chapter illustrates three key issues regarding surface chemistry of AuNPs on LDI ionization efficiency. First, species that don't interact with the AuNP or interact but are unreactive toward the AuNP surface do not affect the LDI process, which is demonstrated by the addition of fluoride and chloride, respectively. Second, species that are reactive with the AuNP surface have dramatic effects on the LDI ion yields, both increase and decreases in ion yields. Increase in ion yield is observed upon addition of oxyanions, and decreases in ion yields is observed with addition of iodide and to some extent bromide. Third, modification of the AuNP surface with organic ligands such as TP, GSH, or β-me minimize or eliminate the effects of said reactive species. There are two additional points of interest that are observed. Iodide addition as NH_4I instead of NaI results in no loss of ion signal, indicating that (i) the effects on the ionization process are not just of initial ligand reactivity, *i.e.*, the etching effects of iodide alone are not responsible for the loss of ion signal, but the secondary reactions or kinetics of the secondary reactions are what ultimately affect the ionization process, and (ii) *the increase in ion abundances of* $[M + H]^+$ *suggests that* NH_4^+ *may be interacting with the analyte to make a pre-formed ion*. The results from oxyanion addition also suggests that ionization may be occurring from pre-formed ions. These results show the utility of subtle changes in the AuNP environment for general use, *i.e.*, non-specific selectivity.

CHAPTER IV

RADICAL DRIVEN IN-SOURCE DECAY FRAGMENTATION OF PEPTIDES USING GOLD NANOPARTICLES AS MATRICES FOR LDI-MS

Introduction

Peptide ion fragmentation is a important tool in mass spectrometry-driven proteomics experiments. There are numerous techniques that induce fragmentation of biomolecules, and most produce distinctive ion types. Collision induced dissociation (CID) is the most common method of activation used to gain sequence information of peptides and proteins. The internal energy transferred during collisions is vibrationally redistributed throughout the molecule, resulting in ion dissociation occurring through low energy pathways; *i.e.*, the amide backbone in the case of peptides. All backbone fragment ions (*i.e.*, a-, b-, c-, x-, y-, and z- type ions) are a result of cleavage along the amide backbone of the peptide, but the most commonly observed fragment ions in CID are b- and y-type ions. Furthermore, most of the ions that are observed involve H-transfer from even electron species. Extensive research has been done to investigate how peptide composition and charge site affects the CID fragmentation process.[114-118] The most common charge-directed fragmentation process in CID is typically referred to as the "mobile proton" model, where charge transfer of the ionizing proton initiates fragmentation.[114, 118] Charge-remote fragmentation typically requires higher internal energies of peptide ions, and is accomplished by high-energy CID, photodissociation, or collisions with surfaces. Other techniques have been shown to induce unique peptide ion

fragmentation, including electron-based methods (*e.g.*, electron transfer dissociation (ETD) and electron capture dissociation (ECD)), photodissociation, and collisions with surfaces.[119-121] Of the methods of ion activation listed here, photodissociation and collisions with surfaces, along with high-energy CID, can deposit more internal energy into the peptide ion, and charge-remote fragmentation processes can occur.

The ion types that are generated from the ion activation methods listed above differ from CID. ETD and ECD typically result in cleavage of the N-C_α bonds of the peptide backbone, yielding c- and z-type ions.[43-45] Often the c- and z- ions are complementary, with the c-ion observed as an even-electron species and the z-ion as a radical species, denoted as $z^{\bullet}$. Recent photodissociation experiments have shown that peptides with a charge sequestered at the N-terminus yield a nearly complete a-ion series along with some side chain cleavages, and peptides with the charge sequestered at the C-terminus yield complete sequence coverage in the form of x-type ions.[47, 122] Radical fragment ions have also been observed in photodissociation of peptide ions, with secondary reactions occurring to yield d-, w-, or v-type ions, possibly accounting for the relatively high abundance of these side chain fragment ions.[46, 47]

Fragmentation of parent odd-electrons species (*e.g.*, $M^{+\bullet}$, $[M + nH]^{(n-1)+\bullet}$) has also been studied. Siu and coworkers have suggested in a number of papers that distonic ions, where the radical site is separated from the charge site, play an important role in fragmentation of peptide radical cations.[123-126] Wee *et al.* have described radical-initiated reactions that occur in small glycine-containing peptides, and they suggest that fragmentation is a competitive process between charge-directed processes and radical-

driven processes.[127] Karnezis *et al.* further demonstrated that radical-driven processes dominate when peptides incorporate a fixed-charge group.[128] Laskin *et al*. have also suggested that charge-remote radical-driven fragmentation pathways occur in the fragmentation of odd-electron peptide ions.[129]

Fragmentation of peptide ions can also occur in the source of the mass spectrometer, instead of in a collision cell, and is termed in-source decay (ISD). ISD has been demonstrated for sequencing of peptides and proteins, but is less common as the yield of fragment ions is low.[130-132] Interestingly, the primary ion types that have been observed are c- and z-type ions, which is similar to ECD and ETD. Köcher *et al.* suggested that ISD is a radical initiated event, with the radicals generated from a photochemical reaction of the matrix upon laser irradiation.[133]

It is important to note that much of the research that has been done on peptide fragmentation has focused on dissociation of the $[M + H]^+$ ion, however, metal ions can induce conformational changes and affect the stability of the biomolecule, thus altering the fragmentation pattern of a peptide or protein. A substantial amount of research has been done to determine metal ion binding sites, metal ion binding energies,[134] and fragmentation mechanisms.[135-138] ISD experiments have typically also focused on the $[M + H]^+$ ion as the parent ion, and so effects that may be a result of cation adduction have not been explored.

Our interest in fragmentation of peptides stems from the observation that AuNPs, esp. 5 nm AuNPs in LDI readily facilitate ISD. The use of AuNPs in LDI has recently been established, and there is evidence for a thermally driven desorption/ionization

mechanism.[2, 139] This chapter aims to (i) determine the extent of ISD that can be achieved using AuNPs, (ii) determine if amino acid sequence affects fragmentation of $[M + Na]^+$ ions, and (iii) propose a mechanism for fragmentation using AuNPs.

Experimental

Mass spectrometry experiments using AuNPs were performed on an Applied Biosystems Voyager DE-STR (Foster City, CA) with a Spectra-Physics (Irvine, CA) N_2 laser (337 nm). Experiments were performed in the positive ion reflected mode averaging spectra from 200 laser shots; each spectrum was internally calibrated. All of the mass spectra shown used laser energies 10-15% above the threshold for ionization. Tandem mass spectrometry was performed on an Applied Biosystems 4700 Proteomics Analyzer (Foster City, CA). Collision-induced dissociation spectra were acquired using 10-20% greater laser power than MS acquisition in order to generate sufficient ion signal. Collision gas (air) was used at the medium air pressure setting with 1 kV collision energy.

AuNP-to-analyte ratios are important to achieve analyte ionization; the optimum ratio determined for these peptides is 1 AuNP: 10^6 analyte molecules, which is consistent with previous reports.[99, 139] Samples were prepared by mixing solutions containing the AuNPs with solutions containing analyte and any additives, and immediately deposited onto a stainless steel plate and vacuum dried. Relatively high sample loadings were used in order to observe in-source decay (~10-20 pmol of analyte).

Fructose was added to give a final ratio of 1 AuNP: 10^6 analyte molecules: 10^1 fructose molecules.

Derivitization of free acid peptides to produce the methyl ester was performed according to literature procedures,[82] and was described in detail in Chapter II. Modification of AuNPs was done according to previously published procedures.[139]

Peptide fragmentation nomenclature proposed by Roepstorff and Fohlmann[41] and later modified by and Johnson and co-workers[140] is employed here. Briefly, for clarification, a Y-type ion is defined as the product of the simple bond cleavage between the carbonyl carbon and the amide nitrogen with the charge retained on the C-terminus, to yield a radical species. A y-type ion is defined as a Y-type ion with addition of 2 hydrogen atoms, with a mass of Y + 2H, see Chapter I for a more detailed review of nomenclature. Data analysis of fragmentation efficiency was performed by taking the peak area of the desired fragment ion or group of fragment ions divided by the peak area of all peaks in the fragment ion area, *i.e.*, the area of all peaks with a lower *m/z* than the intact parent ion.

Fructose, glycerol, N-(2-mercaptopropionyl)glycine (tiopronin), glutathione, acetic anhydride, acetonitrile, acetyl chloride, and anhydrous methanol were obtained from Sigma (St. Louis, MO) and used as received. 2 nm and 5 nm citrate capped gold nanoparticles were purchased from Ted Pella, Inc. (Redding, CA). Angiotensin I (DRVYIHPFHL), Bradykinin (RPPGFSPFR), Bradykinin 1-8 (RPPGFSPF), and Bradykinin 2-9 (PPGFSPFR) were purchased from American Peptide Co. (Sunnyvale, CA) and was prepared in 18 MΩ deionized water (Barnstead, Dubuque, IA).

Results

We first examined the in-source decay (ISD) fragmentation pattern for a series of Angiotensin peptides (Ac-Angiotensin I, Angiotensin I, Angiotensin I methyl ester) using 2 and 5 nm AuNPs. ISD of peptides using 2 nm AuNPs (data not shown) give very few peptide fragment ions compared to ISD of peptides using 5 nm AuNPs. Fragmentation efficiency increases as the basicity of the peptide increases (*i.e.*, Ac-Angiotensin I < Angiotensin I < Angiotensin I methyl ester); we and other groups have previously suggested that peptide composition is important for ionization.[85, 139] ISD of Ac-Angiotensin I yields very few fragment ions (data not shown). LDI mass spectra of Angiotensin I obtained using 5 nm AuNPs is shown in Figure 50, and Figure 52 contains spectra for Angiotensin I methyl ester. ISD of Angiotensin I shows a moderate amount of fragmentation; the parent ion spectrum contains numerous $[M + alkali]^+$ ions (see inset). Although most of the fragment ions appear to arise from the $[M + Na]^+$ ion, *i.e.*, the most abundant species contain Na^+. Fragment ions consist primarily of a- and y- type ions, with some side chain cleavages, and a few other ions. The highest abundance peaks are the $y_9 + Na$ and $b_9 + Na + K – H$ ions. See Figure 51 for a more detailed view of the mass spectrum.

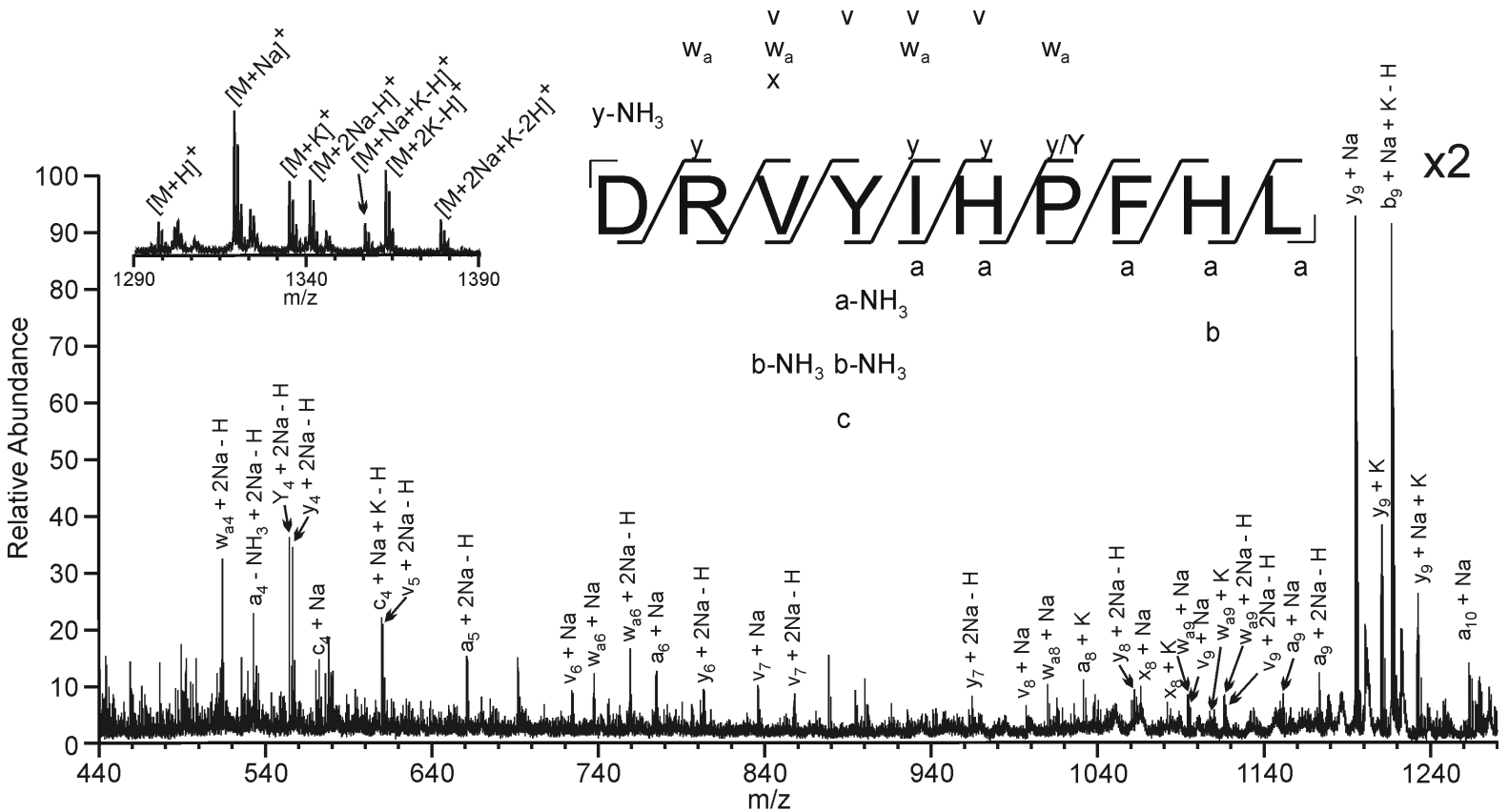

Figure 50. Positive ion ISD fragment ion LDI-TOF mass spectrum of Angiotensin I using 5 nm citrate capped AuNPs, with parent ion region of the mass spectrum inset.

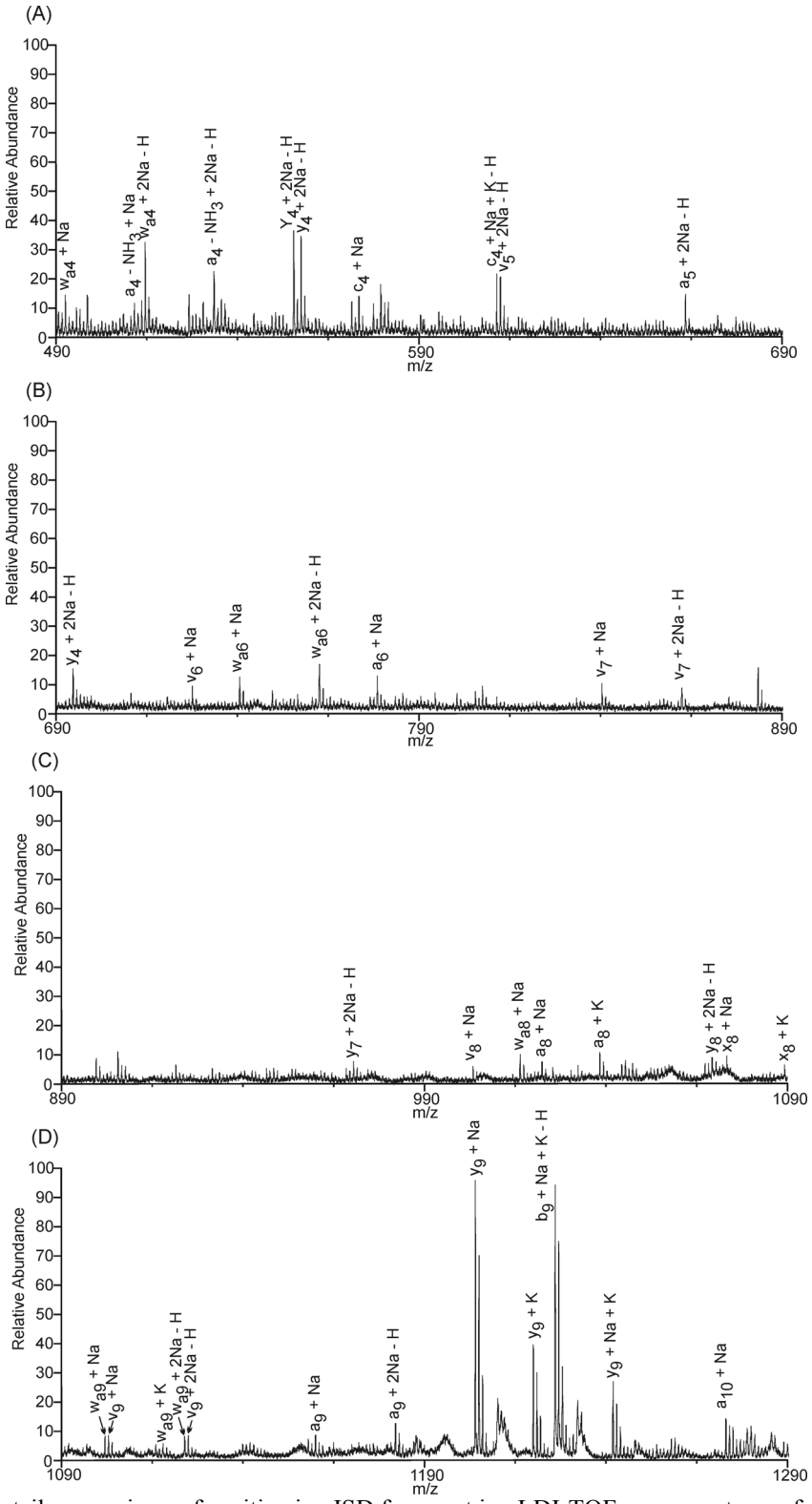

Figure 51. Detail zoom views of positive ion ISD fragment ion LDI-TOF mass spectrum of Angiotensin I using 5 nm citrate capped AuNPs.

Figure 52A shows the fragment ion region of the mass spectrum for Angiotensin I methyl ester. The parent ion spectrum (Figure 52B) consists primarily of the $[M + Na]^+$ ion, which has an overall abundance four times that of the signal from fragment ions. All of the fragment ions in Figure 52A are indentified as either sodium or potassium adducts, likely because the intact peptide exists as either $[M + Na]^+$ or $[M + K]^+$. The fragment ion spectrum shows a nearly complete a-, y-, and v- ion series, along with b-, c-, d-, Y-, x-, z-, w- type ions, and a few radical species. As this spectrum is congested, detailed views of the spectrum are provided in Figure 53; peaks denoted "#" represent contaminants from the AuNPs. In general, the most abundant peaks in the mass spectrum are w-, y- and a-type ions, with radical species and c- and x-type ions having the lowest relative abundances. Specifically, fragment ions with the highest abundances are centered around the proline residue (y_4 + Na and w_{a4} + Na), the isoleucine residue (w_{a6} + Na, y_6 + Na, a_5 + Na, and d_{a5} + Na), and the valine residue (y_8 + Na and a_3 + Na). Figures 52C and 52D show an expanded view of the a_5 + Na and z_3 + Na ions, respectively (black line). The red line represents the calculated isotopic distribution for the ion. The ^{13}C peak for the a_5 + Na and z_3 + Na ions are significantly higher than the predicted distribution, suggesting that another ion is present of the mass a_5 + Na + 1, and z_3 + Na + 1, which corresponds to the radical species of these ions.

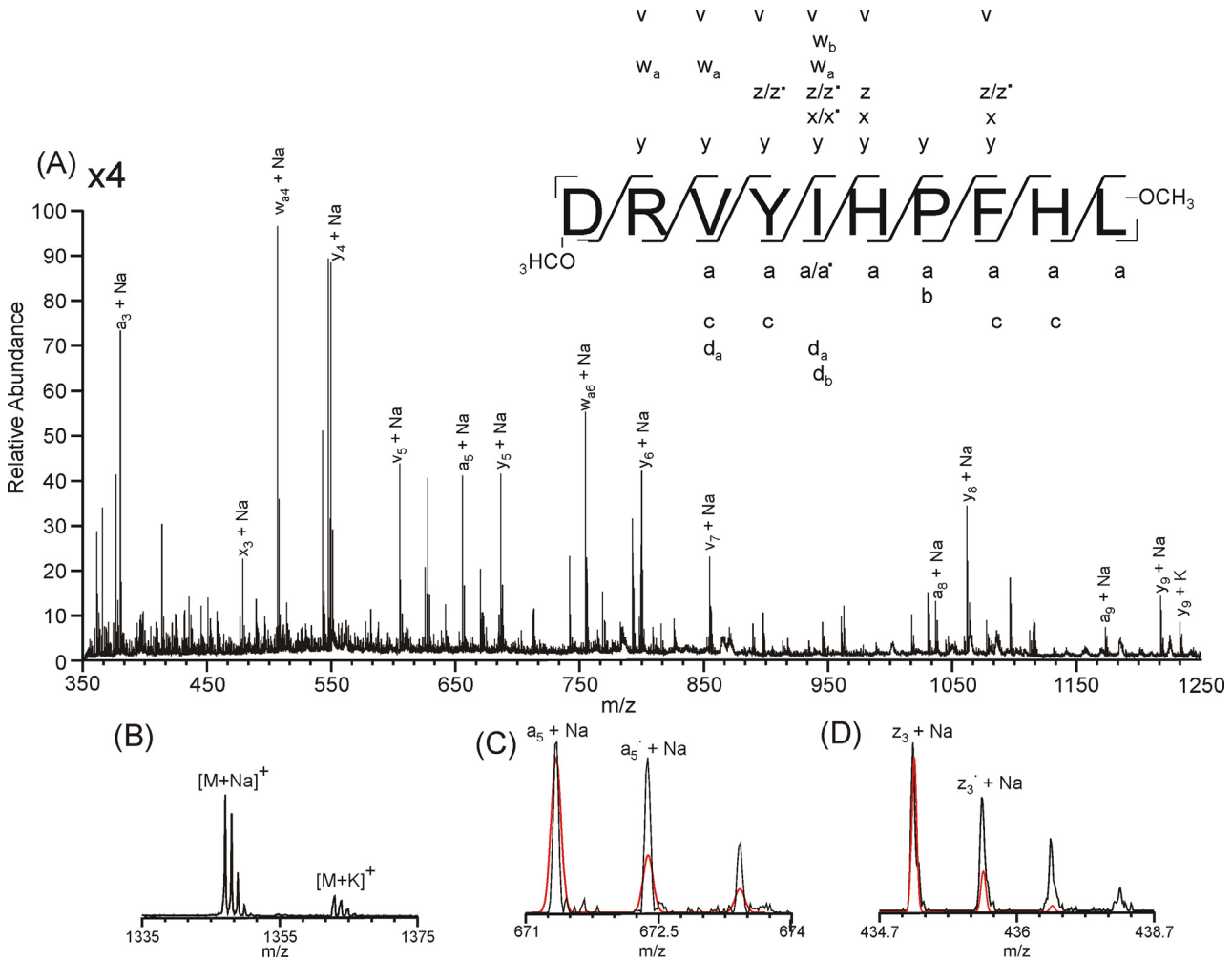

Figure 52. Positive ion LDI-TOF mass spectra of Angiotensin I methyl ester using 5 nm citrate capped AuNPs. (A) ISD fragment ion region of the mass spectrum, (B) parent ion region of the mass spectrum, (C) experimental (black line) and theoretical (red line) isotopic distribution of the a_5 + Na ion, (D) experimental (black line) and theoretical (red line) isotopic distribution of the z_3 + Na ion.

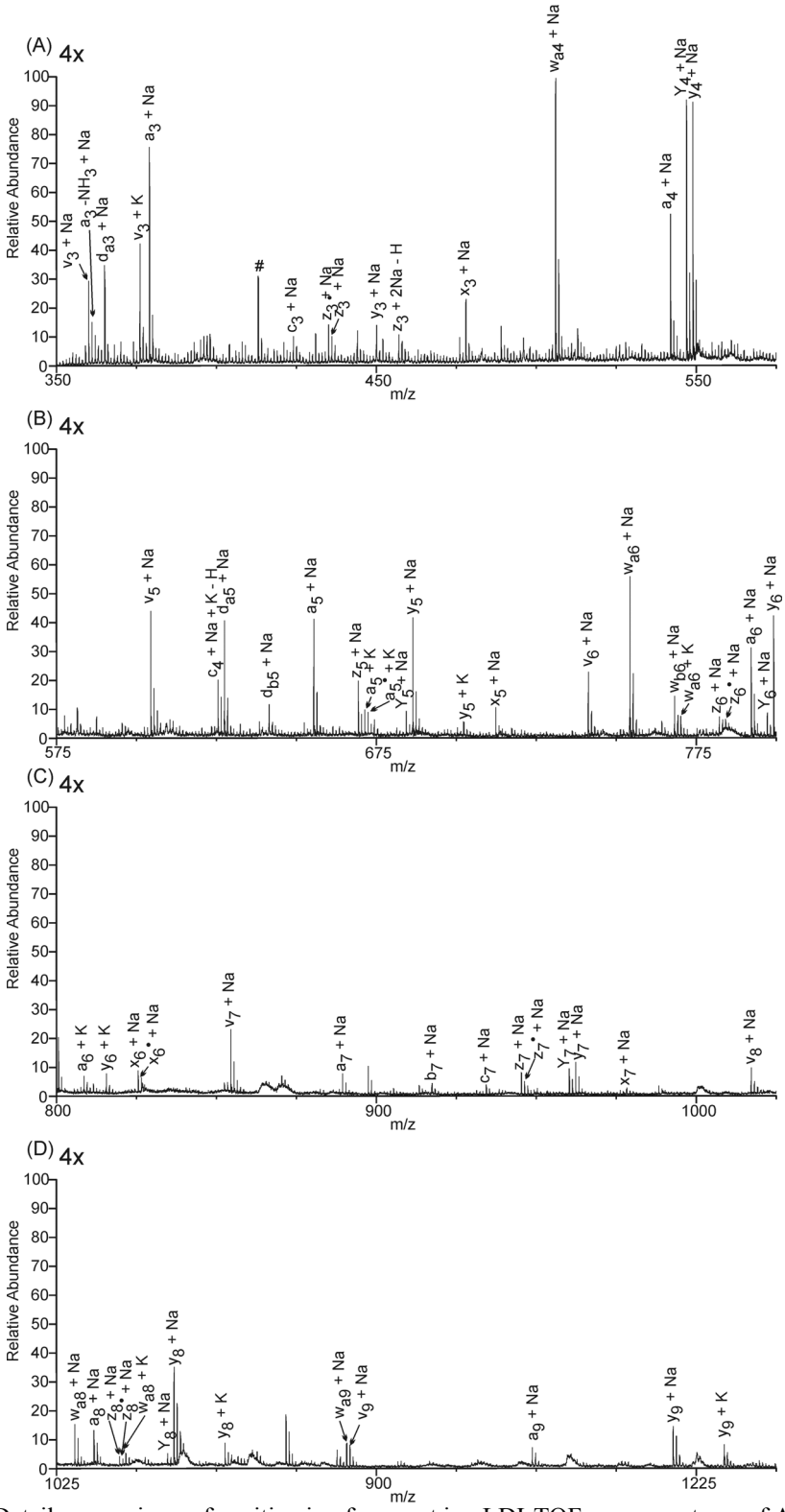

Figure 53. Detail zoom views of positive ion fragment ion LDI-TOF mass spectrum of Angiotensin I methyl ester using 5 nm citrate capped AuNPs.

Interesting fragmentation behavior is observed for the peptide Angiotensin I methyl ester and further work shown here will focus on this peptide. Figure 54 shows the fragment ion spectrum of Angiotensin I methyl ester using 5 nm AuNPs with fructose added. Detailed views of the spectrum are provided in Figure 55; peaks denoted "#" represent contaminants from the AuNPs. Figure 54B shows the parent ion region of the mass spectrum, and Figures 54C and 54D show the zoom region of the a_5 + Na and x_6 + Na ions (black line), with the calculated isotopic distribution shown by the red line. Some significant changes with respect to no fructose addition are observed. Fewer side chain cleavages, specifically v-type ions, are observed. No radical species are observed and more Y-type ions are observed. In general, ions that are formed by multiple reactions (*e.g.*, a- and Y-type ions, side chain cleavages) are decreased from 71% of the fragment ion peak area with no fructose to 47% with fructose added.

A series of Bradykinin peptides was also examined (*e.g.*, RPPGFSPFR, RPPGFSPF, PPGFSPFR), and ISD spectra using 5 nm citrate capped AuNPs are shown in Figure 56; peaks denoted "#" represent contaminants from the AuNPs. In the initial experiment done the intact ion was primarily the $[M + H]^+$ ion, so the data shown have added NaCl in order to generate more $[M + Na]^+$ ions, which results in increased ISD. Very few differences are observed in the fragmentation pattern of these three peptides. Location of the arginine has very little effect on fragmentation efficiency; a nearly complete a-ion series, and numerous y-ions are present for both Bradykinin 1-8 and Bradykinin 2-9.

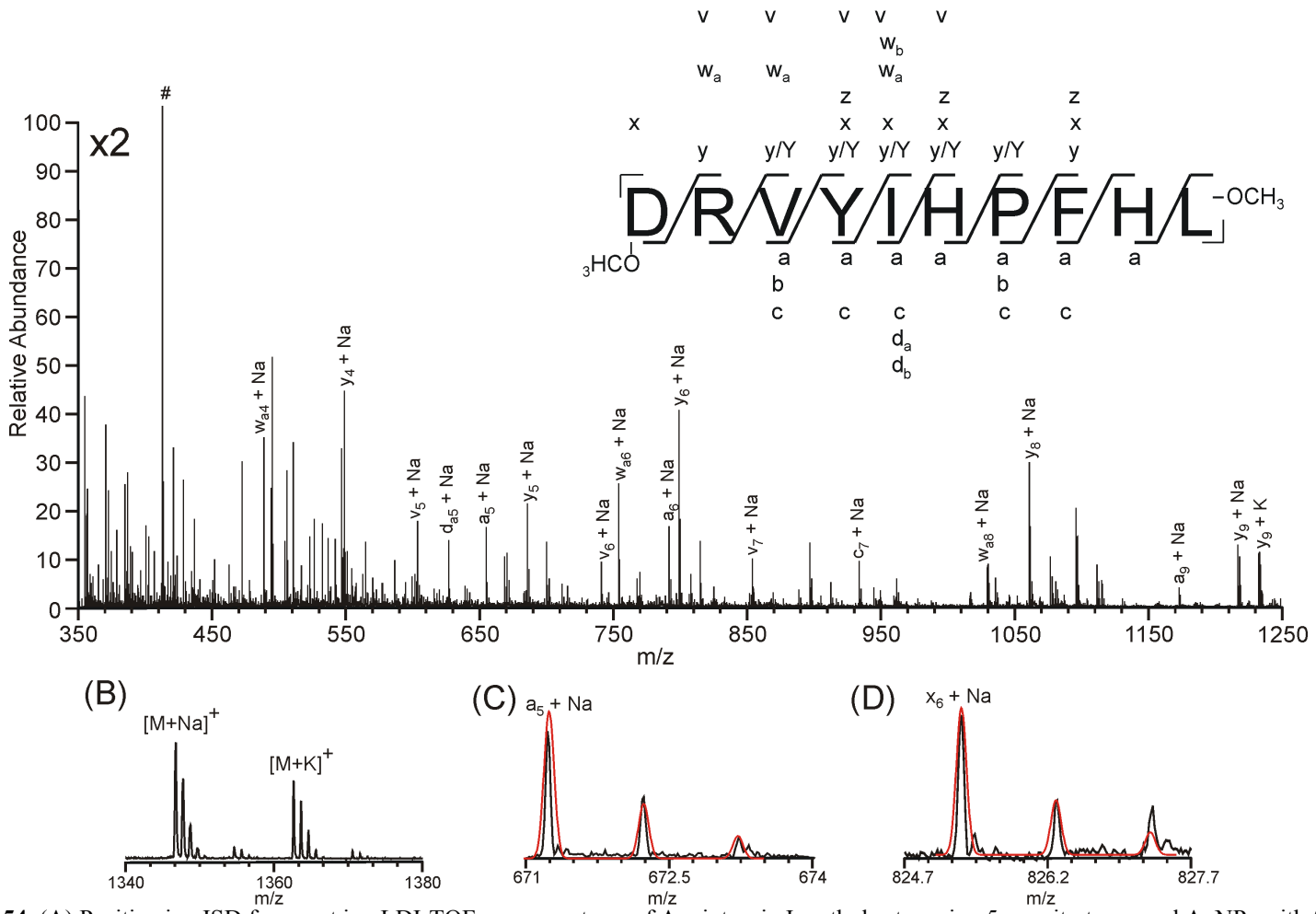

Figure 54. (A) Positive ion ISD fragment ion LDI-TOF mass spectrum of Angiotensin I methyl ester using 5 nm citrate capped AuNPs with fructose added, (B) the parent ion region of the mass spectrum, (C) expanded view of the a_5 + Na ion, with theoretical isotopic distribution (red line), and (D) expanded view of the x_6 + Na ion, with theoretical isotopic distribution (red line).

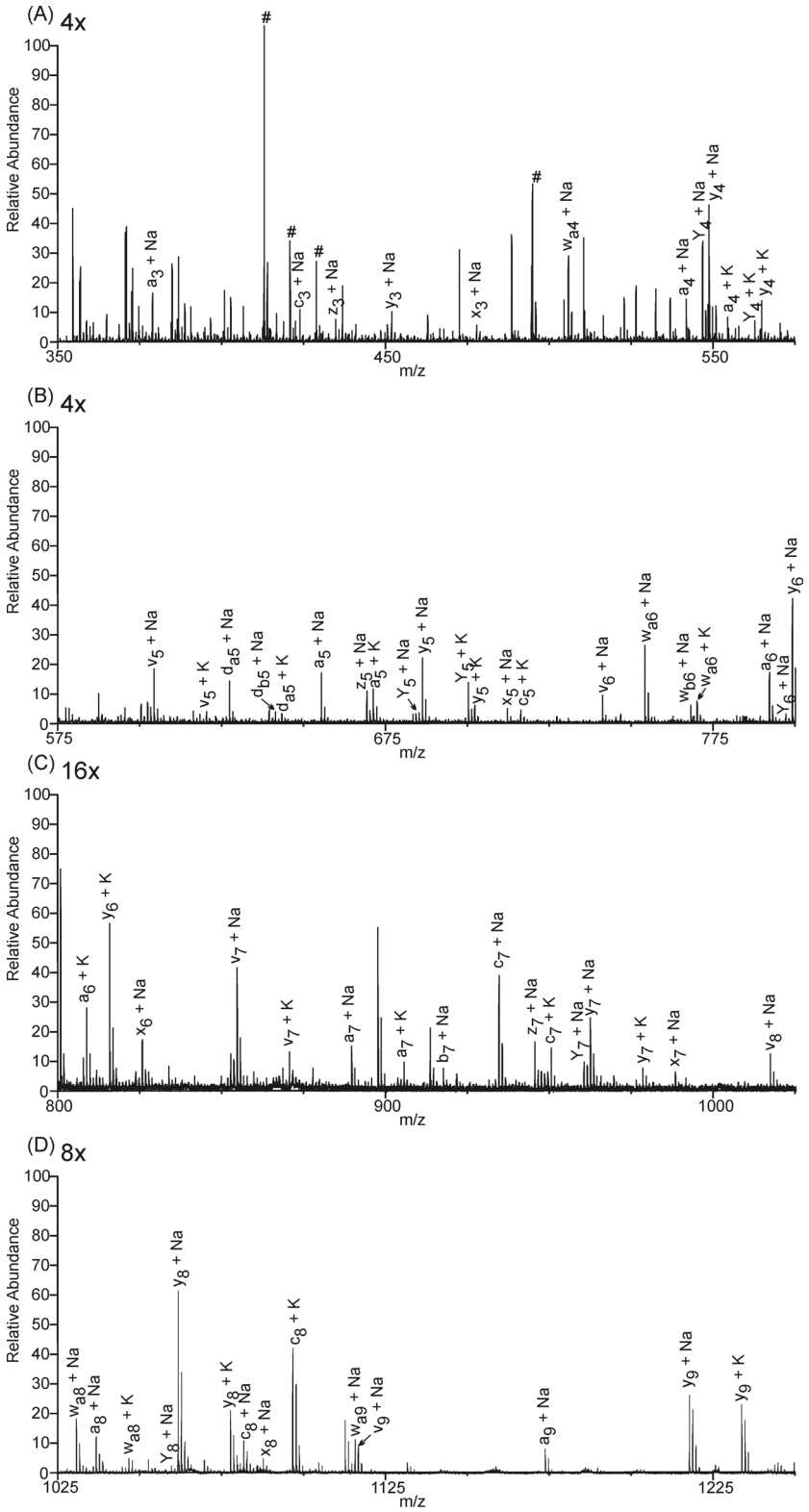

Figure 55. Detail zoom view of positive ion ISD fragment ion LDI-TOF mass spectrum of Angiotensin I methyl ester using 5 nm citrate capped AuNPs with fructose added.

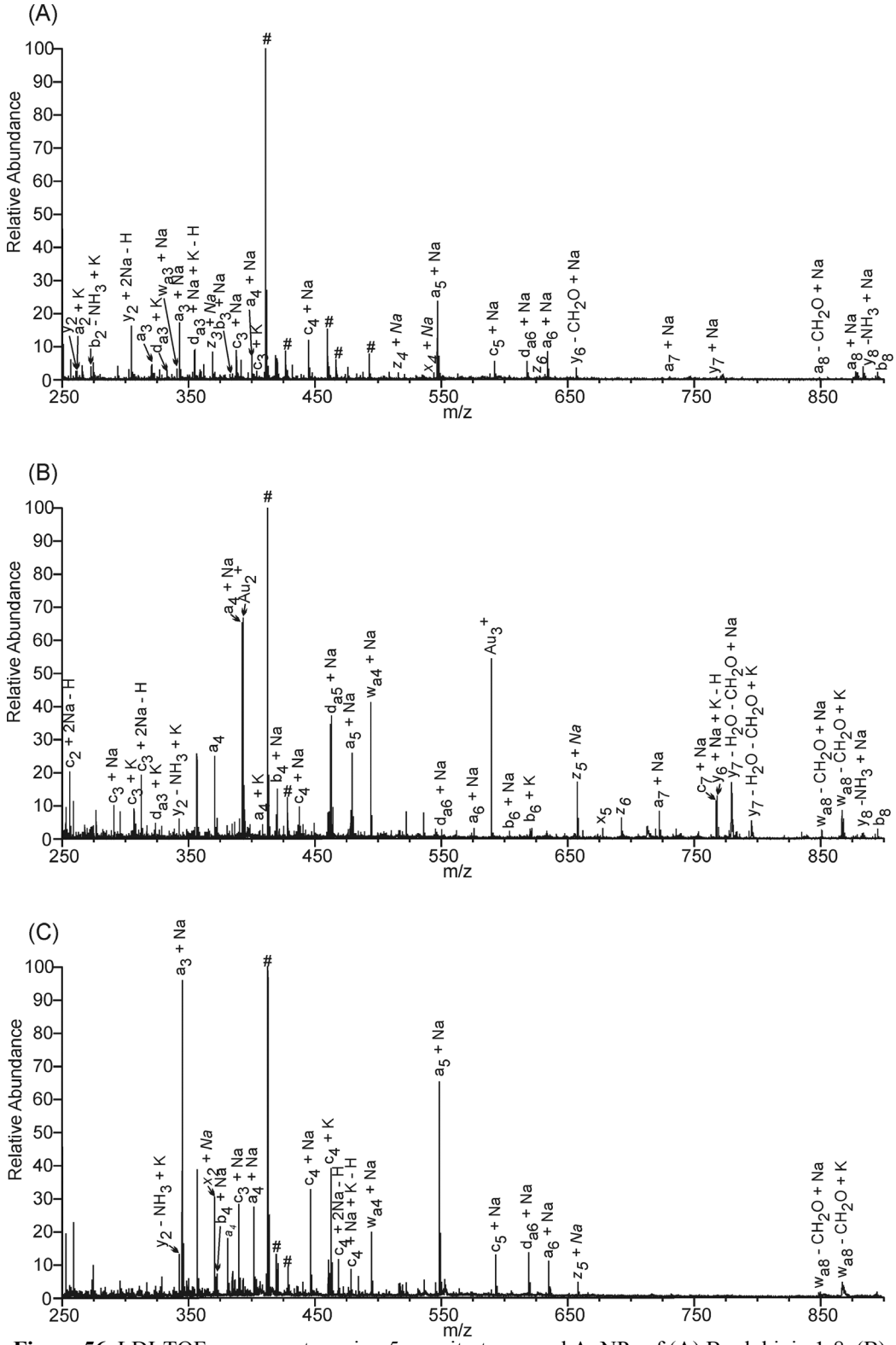

Figure 56. LDI-TOF mass spectra using 5 nm citrate capped AuNPs of (A) Bradykinin 1-8, (B) Bradykinin 2-9, and (C) Bradykinin.

We have also investigated desorption/ionization from Teflon, with glycerol added, and using derivitized AuNPs. Desorption/ionization from a Teflon surface produces intact $[M + Na]^+$ and $[M + K]^+$, but no ISD is observed (see Figure 57, peaks denoted "#" represent contaminants from the AuNPs). AuNPs with surfaces modified from citrate to tiopronin or glutathione give intact alkali-adducted peptide, and small numbers of fragment ions (see Figure 58, peaks denoted "#" represent contaminants from the AuNPs). Finally, addition of 5% glycerol to the AuNP-peptide solution results in few fragment ions compared to no glycerol added. Interestingly, if 5% glycerol and fructose are combined, more fragmentation is observed than with 5% glycerol, but less than if fructose is added (see Figure 59).

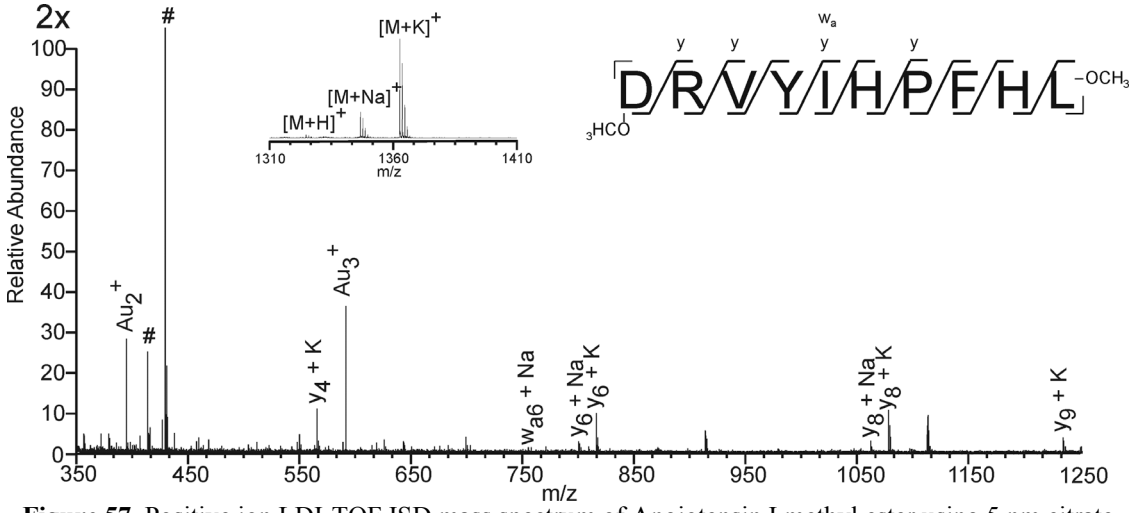

Figure 57. Positive ion LDI-TOF ISD mass spectrum of Angiotensin I methyl ester using 5 nm citrate capped AuNPs on a Teflon surface, with inset of parent ion region of the mass spectrum.

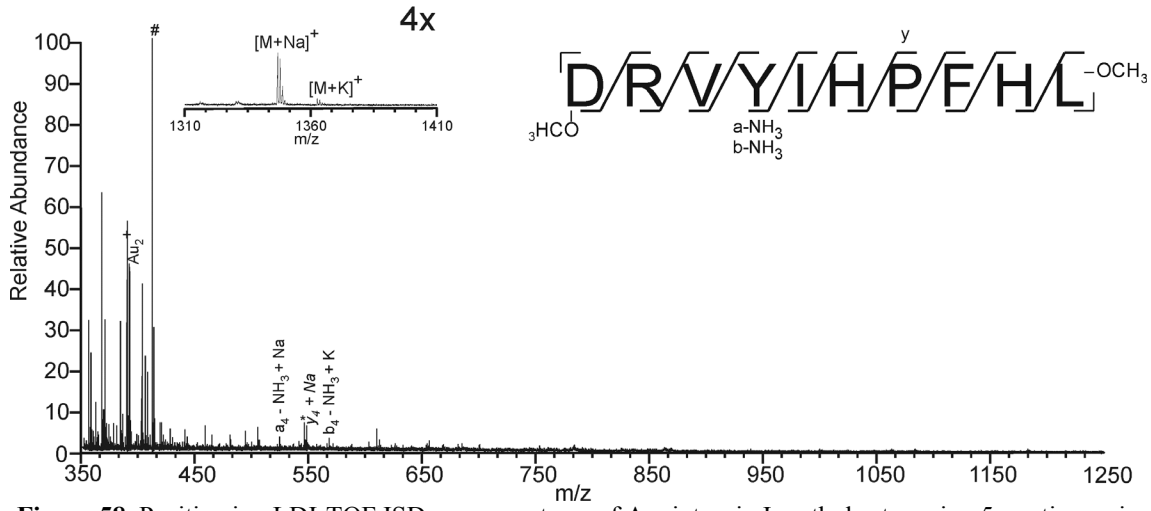

Figure 58. Positive ion LDI-TOF ISD mass spectrum of Angiotensin I methyl ester using 5 nm tiopronin modified AuNPs, with inset of parent ion region of mass spectrum**.**

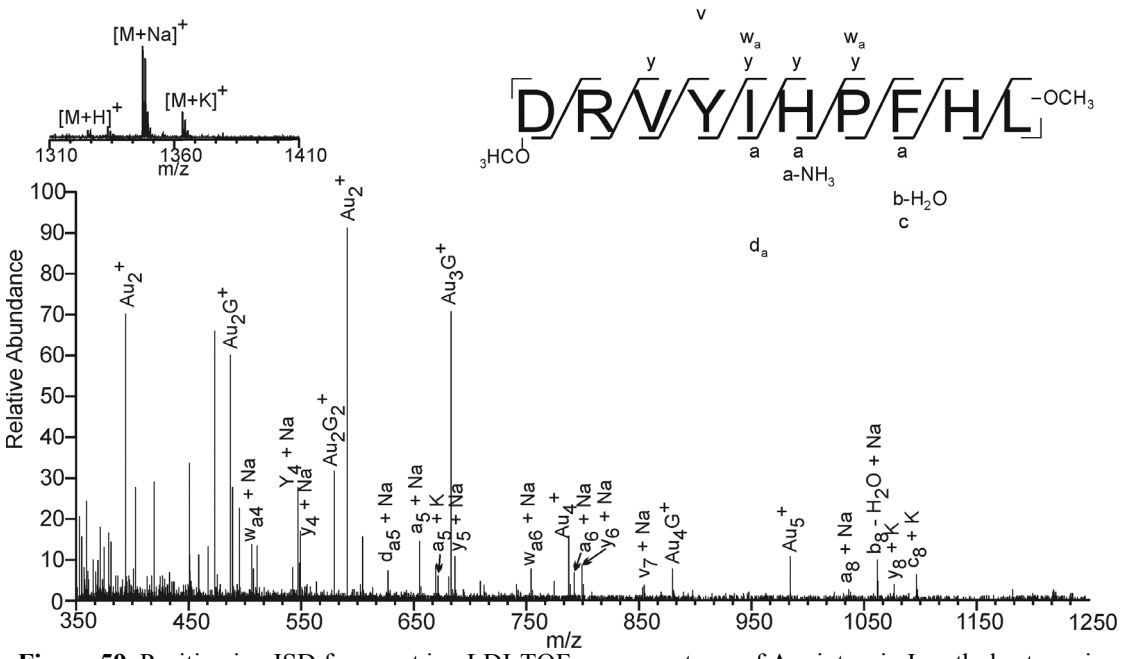

Figure 59. Positive ion ISD fragment ion LDI-TOF mass spectrum of Angiotensin I methyl ester using 5 nm citrate capped AuNPs, in 5% glycerol and the parent ion region of the mass spectrum inset.

For comparison, Figure 60 shows the CID mass spectrum of the $[M + Na]^+$ ion of Angiotensin I methyl ester. A nearly complete a- and y- ions series are observed, with a

few side chain cleavages. Table 3 shows a comparison of fragment ion peak areas for the peptide Angiotensin I methyl ester for: (i) CID of the $[M + Na]^+$ ion, (ii) ISD using 2 nm AuNPs, (iii) ISD using 5 nm AuNPs, and (iv) ISD using 5 nm AuNPs with fructose added. For all methods a- and y- type ions and side chain cleavages are the 3 most abundant ion types; however, subtle differences ion type and abundance are present. For example, side chain cleavages are the most abundant ion type for 5 nm AuNPs: 39.1% are v-type ions, 41.4% are w-type ions, and 19.5% are d-type ions.

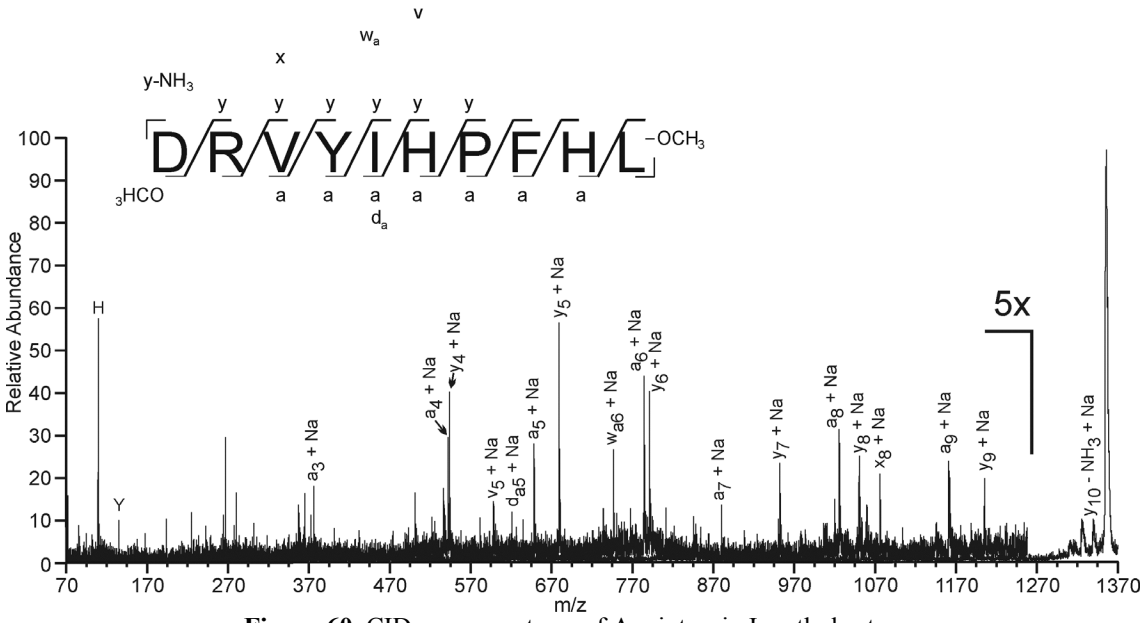

Figure 60. CID mass spectrum of Angiotensin I methyl ester.

Table 3. Ion current component analysis, percentages of peak area by component.

	a ions	b ions	c ions	x ions	y ions	z ions	Side chain
CID	37 .1	5.0	4.6	2.5	28.1	0	22.7
2 nm AuNPs	21.7	3.9	1.1	2.6	36.3	0.4	24.1
5 nm AuNPs	28.3	1.2	3.4	3.4	21.6	2.9	37.5
5 nm AuNPs w/ fructose	13.5	4.8	8.0	3.0	35.8	3.6	25.56

Discussion

We show here the first example of ISD fragmentation using AuNPs for LDI-MS. The fragmentation pattern observed is atypical in terms of the variety of different ion types are occurring together. For example, CID spectra typically yield a-, b-, and y- type ions, whereas photodissociation and SID result in a- and x- type and side chain fragment ions, and ECD/ETD yield almost exclusively c- and z- type ions. While our previous reports have generally shown that trends in LDI ion yields are independent of AuNP size,[99, 139] that is not the case here. Spectra obtained from 2 nm AuNPs contain very low abundances of ISD (data not shown), whereas 5 nm AuNPs yield a high abundance of ISD. There are a number of important points represented here: (i) NP induced ISD of $[M + Na]^+$ ions yield more fragment ions than do $[M + H]^+$ ions, (ii) the type of ions that are present in high abundance (*i.e.*, unexpected fragment ion types dominate the mass spectrum, specifically the w_{a4} + Na ion), and (iii) the presence radical species. There are a number of mechanistic issues that are relevant to each of these points, as peptide fragmentation behavior has been well studied, and we will draw on previous mechanisms.[42, 121, 141-143] Of particular interest are experiments that have investigated alkali metal cationized peptides,[144-147] and experiments that generate radical ions, such as ETD/ECD[43-45] and photodissociation.[46-49, 122, 148] There have also been a number of recent articles that have focused on derivitizing peptides to generate specific radical sites, which then induce radical dominated dissociation reactions and selective cleavage.[149-151] While the fragmentation that we observe is largely non-selective (meaning a nearly complete series of a-, y-, and v-type ions are observed which do not

appear to be residue specific or charge-directed fragmentation processes), we do observe a number of product ions that appear to be derived by radical initiated reactions.

The issue of ISD fragmentation from metal cationized species will be addressed first. Most of the fragment ions that are observed here are identified as either sodium or potassium adducts, which can be a result of the intact peptide existing as either $[M + Na]^+$ or $[M + K]^+$ or the energy for dissociation of $[M + Na]^+$ is lower than the energy for dissociation of $[M + H]^+$. Since most fragmentation mechanisms in the literature focus on the $[M + H]^+$ ion, comparisons made herein will be made to the $[M + H]^+$ ion, provided the mechanism is still logical for a $[M + Na]^+$ or $[M + K]^+$ ion. One of our key observations is that ISD of Angiotensin I methyl ester is more prominent than that for the free acid Angiotensin I (Figures 50 and 52). . With the free acid it is most likely that the Na^+ or K^+ will be sequestered at the carboxylate terminus,[146, 152] or complexed by the amide backbone oxygens.[153] Since the methyl ester does not have a carboxylate terminus, the Na^+ or K^+ is likely sequestered by the amide backbone. Multiple $[M +$ alkali$]^+$ ions are observed for Angiotensin I, and a limited amount of fragmentation is observed (Figure 50). For the methyl ester, an extensive amount of fragment ions are observed, and many have the charge on the C-terminus; these data suggest that even though the peptide is a methyl ester, the cation is localized near or at the C-terminus. This is in contrast to experiments done by Dongré *et al.*[114] and Shields *et al.*[137] where a complete ion series was only observed when the terminal amino acid acts as a fixed charge site, *i.e.*, when the terminus strongly binds the charge, the majority of ions in the fragment ion spectrum will be derived from that terminus. In other experiments done

with a series of Bradykinin peptides (*e.g.*, RPPGFSPFR, RPPGFSPF, PPGFSPFR) we found that when the parent ion is primarily the protonated peptide, poor ISD occurs. Addition of NaCl results in more $[M + Na]^+$, and also better ISD. Location of the arginine has very little effect on fragmentation efficiency; as Figure 56 showed, a nearly complete a-ion series, and numerous y-ions are present for both Bradykinin 1-8 and Bradykinin 2-9.

Next, the issue of several interesting fragment ions that are observed in the ISD spectrum of Angiotensin I methyl ester (Figure 52A). First, the presence and high relative abundance of the w_{a4} + Na ion, which is perhaps one of the most significant results reported here. This ion is a result of two bonds being cleaved, the N-C_α bond in the proline reside, and the C-C bond in the proline side chain. This fragment ion has only been reported in one other instance, by Cooper *et al.,* who utilized hot-ECD (3 -13 eV electrons) to fragment peptides, [154] although the ion was not observed as a sodium adduct. Also of interest is the y_4 + Na ion which has a high relative abundance. This fragment ion occurs C-terminal to the proline, and preferential cleavage near a proline residue has been extensively investigated, and is termed the proline effect.[141, 155-157]

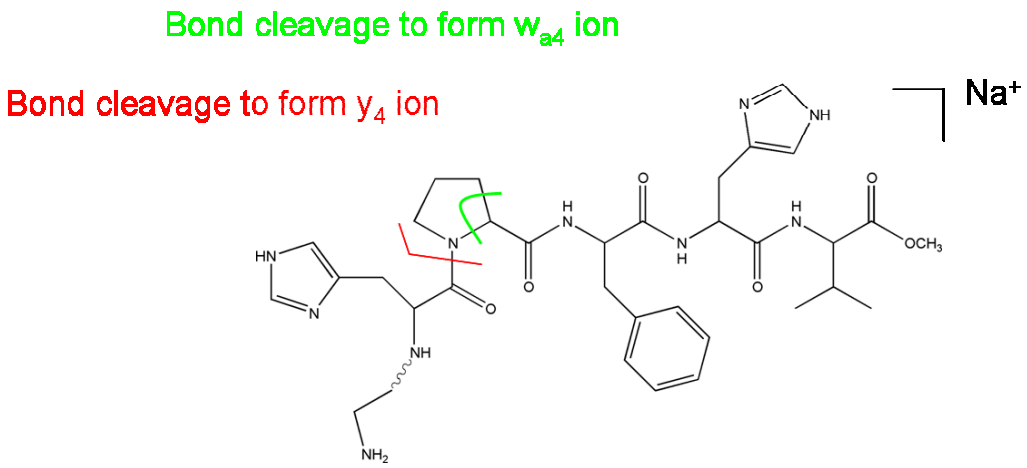

Figure 61. Bond cleavage site for w_{a4} and y_4 fragment ions from the peptide Angiotensin I methyl ester.

Also relevant is a study by Ly and Julian, who suggest that abstraction of an H atom from proline will be followed by homolytic cleavage of the peptide bond, which results in a y-type ion (which is stable), and a b-type radical that is not stable and will rapidly lose CO to yield a radical a-type ion. They conclude that radical directed dissociation at proline residues will give a- and y- type ions, not b- and y- type ions, which are characteristic of CID.[149] This explanation also accounts for the presence of y_4 + Na. We do observe a_7 + Na and b_7 + Na, which are the corresponding proline containing fragment ions, so it is difficult to say if this radical directed mechanism is most likely, or if it is simply a result of the proline effect.

The Y_4 + Na ion is present with high relative abundance, and other Y-type ions are observed as well. Several mechanisms for Y-type ion formation have previously been proposed. Han and co-workers have shown that a radical driven fragmentation process of z˙-ions results in Y-ions.[158] They suggest that the z˙-ions undergo a

McLafferty rearrangement, and then have homolytic cleavage of the amide bond which results in Y- and b˙-type ions. They also suggest that proline-containing z˙-ions have a characteristic cleavage at the amide bond N-terminal to the proline, resulting in Y- or y-type ions that contain proline. This is a possible mechanism for the Y_4- ion, and the preferential cleavage accounts for the high relative abundance of this ion.

Other fragment ions with high abundances occur near the isoleucine residue (w_{a6} + Na, y_6 + Na, a_5 + Na, and d_{a5} + Na), and the valine residue (y_8 + Na and a_3 + Na). Both of these amino acids have been shown to be involved in radical directed cleavage. Hodyss *et al.* suggest that hydrogen abstraction from an aliphatic side chain (*e.g.*, isoleucine, valine, leucine, alanine) followed by β-cleavage along the backbone can produce c- and z-type ions, as well as a- and x-type fragments. They also postulate that many hydrogen atoms in a peptide (both along the backbone and in side chains) have low bond dissociation energies, and may be abstracted readily,[150] and other radical driven processes can follow. This mechanism fits wells with our observation of y- and a-type ions near isoleucine and valine. The side chain cleavages that occur near the isoleucine and valine residue could be the result of several different reactions. Johnson *et al.*[140, 159] and Cui *et al.*[122] have both proposed d-ion formation as the result of secondary reactions of a˙ species. While none of the d-ions here have corresponding possible a˙ precursors, all d-ions have a-ion precursors. Johnson *et al.* also suggested that a˙ species rapidly dissociate into a-ions, which explains the lack of a˙-ions. Both authors also proposed w-ion formation from either z- or z˙-type ions. The w_{a6} + Na and w_{a8} + Na ions both have possible z˙-ion precursors present in the mass spectrum.

ISD of Angiotensin I methyl ester with addition of fructose (Figure 54) results in several key changes in the mass spectrum: (i) no radical species are observed and (ii) fewer secondary reactions are observed overall. These two observations are likely related to each other, as we have suggested that radical species initiate a number of these secondary reactions. Fructose has traditionally been added to MALDI samples to reduce ISD fragmentation. Beavis and co-workers suggested that rapid decomposition of the sugar molecule into CO and H_2O results in rapid collisional cooling, yielding fewer fragment ions.[80] Within the framework of the cluster ionization model as well,[160, 161] addition of fructose may decrease the amount of internal energy within a peptide ion, giving fewer secondary fragment ions. A recent study on electron attachment to fructose suggested that fructose can form a stable radical species, especially with some loss of water to the molecule.[162] During ionization using AuNPs, loss of water to a fructose molecule will make it more susceptible to accepting an electron and forming a stable radical specie, thereby reducing the amount of radicals that are reactive towards the peptide.

Experiments that were done using modified AuNPs, on Teflon surface, and with glycerol addition (see Figures 57-59) are important because they all suggest that thermal heating is a necessary part of the desorption/ionization process. Citrate capped AuNPs are electrostatically stabilized, and citrate can readily be displaced by other species that may have an affinity for the AuNP surface (*e.g.*, amines and carbonyl oxygens),[77] or thiols can covalently bind to the AuNP surface.[25] Covalent modification of the surface with tiopronin makes it difficult for analyte to displace the tiopronin, resulting in little to

no direct contact of analyte with the AuNP surface. Thus, direct electronic interactions between the peptide and NP are less likely, and heating is the main contribution for desorption/ionization. Additionally, AuNPs modified with glutathione (data shown for AuNPs modified with tiopronin is also representative of AuNPs modified with glutathione) do not result in any peptide fragmentation. However, it is difficult to separate these variables and determine if fragmentation is suppressed because of a change in NP surface chemistry or the radical scavenging ability of glutathione. LDI done from a Teflon coated target reduces the amount of photoelectrons[163, 164] and will also likely reduce electronic processes occurring from the AuNP. Additionally, since Teflon is an insulator, heat will be localized near the AuNP resulting in prompt NP fragmentation. Less energy will available to transfer to the nearby analyte molecules, resulting in no peptide fragmentation. The mass spectrum for LDI from a Teflon coated target also shows several Au-cluster species, which is in contrast to LDI from a stainless steel target; this also supports the statement of an increase in AuNP fragmentation. Finally, glycerol is a good heat dissipater, and since we only observe ionization with very little fragmentation, this suggests that only enough energy for desorption/ionization is getting to the peptides, with much of the heat being dissipated to the surrounding medium.

Summary

This chapter illustrates three key issues regarding ISD of peptides when using AuNPs for LDI. First, metal cationized peptides fragment better than protonated

peptides; specifically, the methyl ester peptide fragments better than the free acid peptide, and more C-terminal fragment ions are produced, suggesting that the metal is sequestered near the C-terminus. Second, fragment ions that are not typically present in ISD are observed here, and several interesting fragment ions (*e.g.*, w_{a4} + Na) are observed in high abundance. Third, in the methyl ester ISD spectrum, numerous radical species are observed. When fructose is added, a reduction in radical species and overall ISD is observed, suggesting that fructose is reducing the amount of reactive radicals. These data suggest that radical species are important for fragmentation of peptides when using AuNPs. However, unique types of fragmentation are observed (*i.e.*, x-type ions and side chain cleavages) that are similar to prompt photodissociation experiments done in our laboratory. The abundant v-type ions that are observed here for $[M + Na]^+$ ions has also been demonstrated in our lab for $[M + alkali]^+$ using CID. Therefore, it is likely that multiple processes are actually directing the fragmentation described in this chapter. In order to gain a better understanding of what is initiating these processes further work needs to be done. Specifically, the fragmentation pattern of the peptide used in this chapter (Angiotensin I methyl ester) needs to be determined using photodissociation and further investigation is needed using radical scavenging species and a better understanding of their interaction with AuNPs.

CHAPTER V

IN-SOURCE DECAY FRAGMENTATION OF COPPER-ADDUCTED PEPTIDES USING GOLD NANOPARTICLES AS MATRICES FOR LDI-MS

Introduction

Previous chapters in this dissertation have focused on various physico-chemical properties relating to AuNPs and the subsequent effects on desorption/ionization of biomolecules. The effects of NP size have been addressed in several chapters, with evidence for differences in desorption/ionization trends and peptide ion internal energies presented. Specifically, in Chapter V peptide ion energetics with regard to NP size and sample preparation were investigated. The addition of reactive or unreactive species on the AuNP surface, namely halides and oxyanions, was described in Chapter IV. Here we investigate the addition of transition metal cations to AuNPs, with interest in cation-NP interactions and peptide ion energetics.

Little is known about the interaction of copper cations with gold surfaces, but several studies have investigated the addition of copper ions on NP formation and provide some insight. Singh and coworkers reported that addition of Cu during AuNP synthesis catalyzes the formation of unique thin flat ordered structures; copper was not incorporated into the final NP material.[109] Sun *et al.* showed that cuboid and decahedral AuNPs can be formed and controlled by addition of Cu^{2+}; the adsorption of Cu^{2+} to different facets of the growing AuNP crystal was suggested as the mechanism of formation.[165] Leonard *et al.* and Sra *et al.* suggested that during formation of

intermetallic AuCu or $AuCuSn_2$ materials excess Cu^{2+} is associated with the AuNP surface. As the material is reduced, the Cu^{2+} is incorporated into the intermetallic species.[166, 167] Lastly, a recent report from Shlyahovsky *et al.* describes association of Cu^{2+} ions with the AuNP surface and subsequent reduction of the Cu^{2+} by NADH, which results in deposition of Cu^0 on the AuNP surface.[168] Overall we conclude from these studies that Cu^{2+} likely associates with the AuNP surface.

Also pertinent to this study are the effects of transition metal cations on LDI or MALDI-MS experiments. A significant amount of research has been done regarding Cu-ion addition in MALDI.[137, 169-175] Typically, Cu^{2+} is added, but only a singly charged ion is observed in the mass spectrum. Either reduction of the metal ion and addition to a neutral molecule (Equation 1) or deprotonation of the molecule and addition to a doubly charged cation (Equation 2) must occur.

$$M + Cu^{+} \rightarrow [M + Cu]^{+} \qquad (1)$$

$$[M - H]^{-} + Cu^{2+} \rightarrow [(M - H)^{-} + Cu^{2+}] \qquad (2)$$

Different explanations have been given for gas-phase charge reduction of Cu^{2+} to Cu^{+} in MALDI. Karas *et al.* suggest that electron capture by the metal cation results in reduction; this model assumes that photoelectrons are produced from the MALDI target during the ionization event.[161] Knochenmuss *et al.* and Zhang *et al.* have both suggested that gas-phase charge exchange between the metal cation and other neutral species result in metal reduction.[176,177]

The previous chapter discussed fragmentation of $[M + alkali]^{+}$ species, and some information about location of the metal cation was determined. Determination of Cu-ion

complexation site has been well studied by mass spectrometry[170-172, 174, 178-180] and other techniques, so the primary focus of this chapter is (i) to determine if/how Cu addition affects the desorption/ionization process when using AuNPs, (ii) to determine if peptide ion fragmentation is affected by Cu addition, and (iii) use any peptide fragmentation information to infer peptide ion energies.

Experimental

Mass spectrometry experiments using AuNPs were performed on an Applied Biosystems Voyager DE-STR (Foster City, CA) with a Spectra-Physics (Irvine, CA) N_2 laser at 337 nm. Experiments were performed in the positive ion reflected mode averaging spectra over 200 laser shots with internal calibration. All of the mass spectra shown used laser energies at 10-15% above the threshold for ionization.

The molar matrix-to-analyte ratios of AuNP to analyte was $1:10^6$-10^8, which has previously been determined to be within the optimum range.[99, 139] Samples were prepared by mixing solutions containing the AuNPs with solutions containing analyte and any additives, and immediately deposited onto a stainless steel plate and vacuum dried. Relatively high sample loadings were used in order to observe in-source decay (~10-20 pmol of analyte).

Copper salts were added in experimentally determined optimum ratios. For Val^4-Angiotensin III and Bradykinin 1-8 using 2 nm AuNPs, the ratio was 3800 Cu ions:1 peptide molecule. For Bradykinin 1-8, Angiotensin I methyl ester, and ACTH(18-39) using 5 nm AuNPs, the ratio was 35000 Cu ions:1 peptide molecule, and for Val^4-

Angiotensin III using 5 nm AuNPs, the ratio was 80000 Cu ions:1 peptide molecule. Other metal salts were added in the same ratios.

Modification of peptides was done according to literature procedures, and has been previously described in Chapter II.[82,83] Modification of AuNPs was done according to previously published procedures.[139]

Roepstorff[41] and Biemann[140] fragmentation nomenclature is employed here and can be reviewed in Chapter I. Data analysis of fragmentation efficiency was performed by taking the peak area of the desired fragment ion or group of fragment ions divided by the peak area of all peaks in the fragment ion area, *i.e.*, the area of all peaks with a lower *m/z* than the intact parent ion.

Copper sulfate, copper acetate, copper acetylacetonate, silver nitrate, nickel acetate, fructose, acetic anhydride, acetonitrile, acetyl chloride, and anhydrous methanol were obtained from Sigma (St. Louis, MO) and used as received. 2 nm and 5 nm citrate capped gold nanoparticles were purchased from Ted Pella, Inc. (Redding, CA). Val^4-Angiotensin III (RVYVHPF), Bradykinin 1-8 (RPPGFSPF), ACTH(18-39) (RPVKVYPNGAEDESAEAFPLEF) and Angiotensin I (DRVYIHPFHL) were purchased from American Peptide Co. (Sunnyvale, CA) and were prepared in 18 MΩ deionized water (Barnstead, Dubuque, IA).

Results and Discussion

Figure 62 contains the UV-Visible absorption spectra for 5 nm citrate capped AuNPs with added $CuSO_4$ and added $CuSO_4$ and peptide. Addition of Cu^{2+} results in a

significant red shift of the SPR band. This is expected if Cu^{2+} adsorbs to the surface, as ion adsorption would result in a change in the electronic density of the NP which would change the SPR band.[24, 181] The addition of peptide and $CuSO_4$ results in a very slight red-shift (less than 1 nm) compared to just $CuSO_4$ addition.

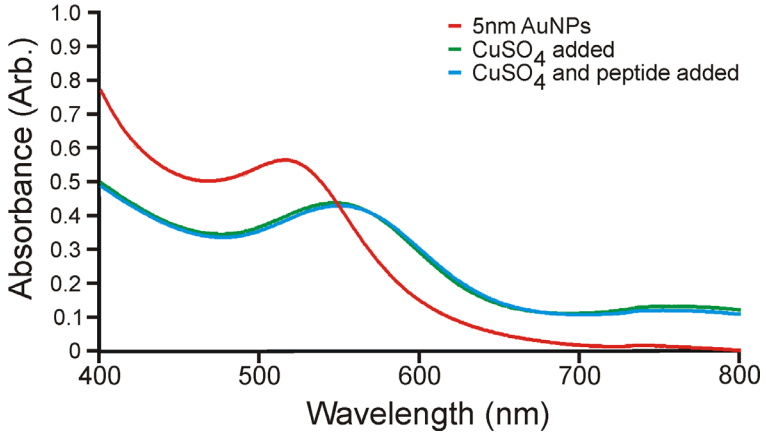

Figure 62. UV-Visible absorption spectra of 5 nm citrate capped AuNPs with added $CuSO_4$ and peptide.

Addition of Cu^{2+} to a peptide-AuNP mixture yields abundant peptide fragment ions. ISD of Angiotensin I methyl ester with added $CuSO_4$ using either 2 or 5 nm AuNPs was evaluated. Consistent with previous results (Chapter VI), the yield of fragment ions using 2 nm AuNPs is relatively low, and data are not shown here. Figure 63 shows the ISD spectrum for addition of $CuSO_4$ to Angiotensin I methyl ester using 5 nm AuNPs. The inset shows the parent ion region of the mass spectrum and the $[M + Cu]^+$ ion is the dominant peak, with small amounts of $[M + alkali]^+$, $[M + H]^+$ and $[M + 2Cu - H]^+$

ions. Figure 64 contains detailed zoom spectra with all peaks labeled, as the spectrum shown in Figure 63 is congested.

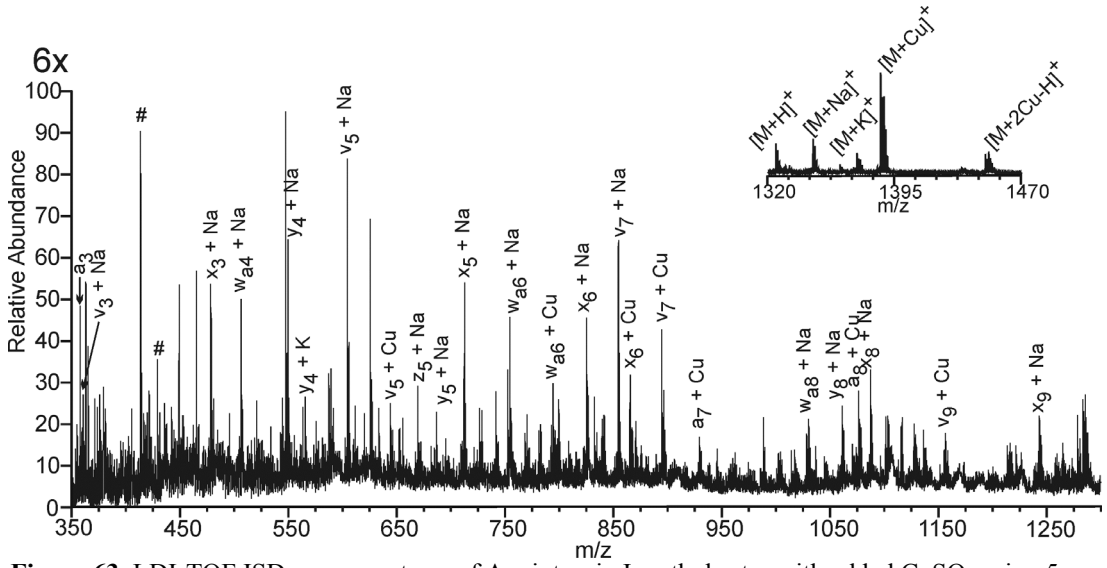

Figure 63. LDI-TOF ISD mass spectrum of Angiotensin I methyl ester with added $CuSO_4$ using 5 nm citrate capped AuNPs, inset is the parent ion spectrum.

Interestingly, very few fragment ions contain copper, only 22.7% of the fragment ion current. Of the copper-complexed fragment ions, 80% of the peak area corresponds to C-terminal fragment ions. This suggests that the Cu ion is sequestered near the C-terminus, which is not consistent with previous reports where the Cu ion was sequestered at the arginine side chain, the amino acid with the highest affinity for Cu.[137, 173] Compared to ISD of $[M + Na]^+$ (see Figure 52) there are some significant changes in the ISD spectrum with Cu addition. Table 4 lists the differences in ion type that are present; the main differences are the decrease in a- and y-type ions and the increase in x-type ions.

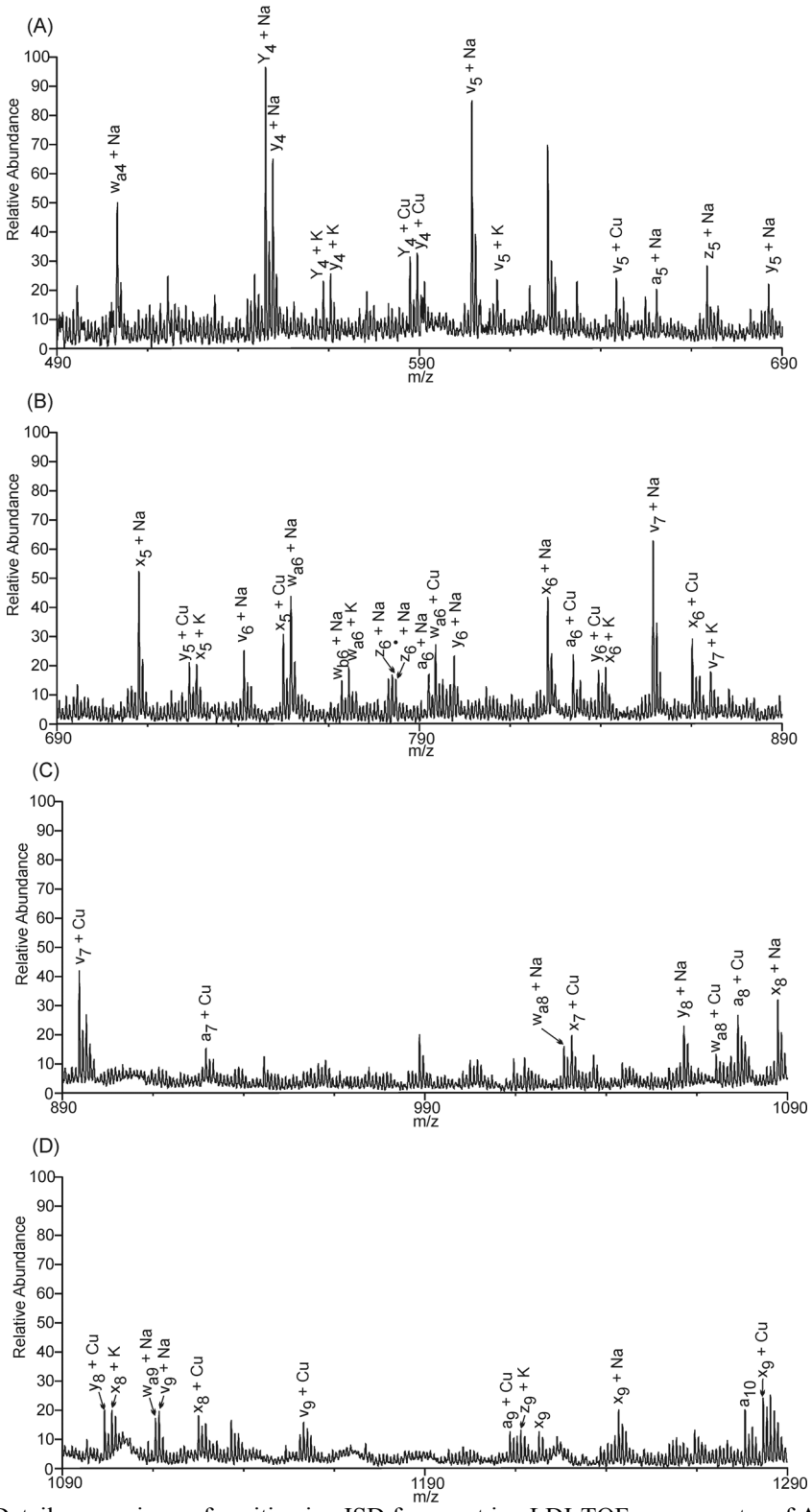

Figure 64. Detail zoom views of positive ion ISD fragment ion LDI-TOF mass spectra of Angiotensin I methyl ester with added $CuSO_4$.

Table 4. Percentage of ion current by ion type for Cu addition and no Cu addition.

	a-ions	b-ions	c-ions	x-ion	y-ions	z-ions	Side chain
no Cu^{2+} addition	28.35	1.21	3.4	3.37	21.63	2.87	37.5
Cu^{2+} addition	12.87	0	1.8	26.06	14	2.65	32.38

ISD of the peptide ACTH(18-39) (RPVKYPNGAEDESAEAFPLEF) with added Cu^{2+} also results in an increase in x-type ions, and also a partial series of a-type ions (see Figures 65 and 66; the spectra contained in Figure 66 are the detailed views of Figure 65). There are very few Cu containing fragment ions here, but more than 90% of the Cu containing fragment ions have the charge retained on the N-terminus, which is consistent with previous work.[137, 175]

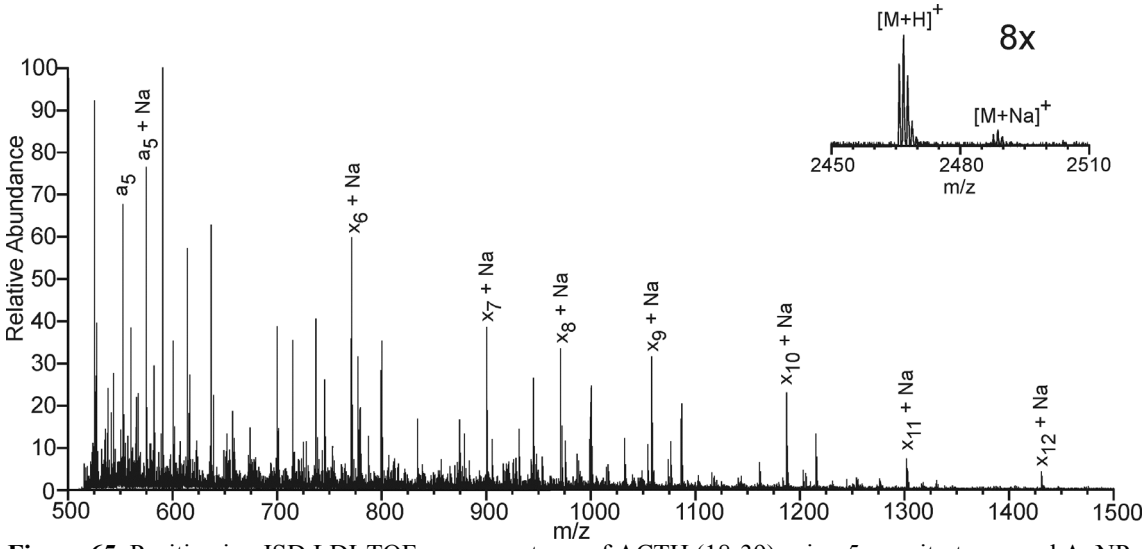

Figure 65. Positive ion ISD LDI-TOF mass spectrum of ACTH (18-39) using 5 nm citrate capped AuNPs with added $CuSO_4$.

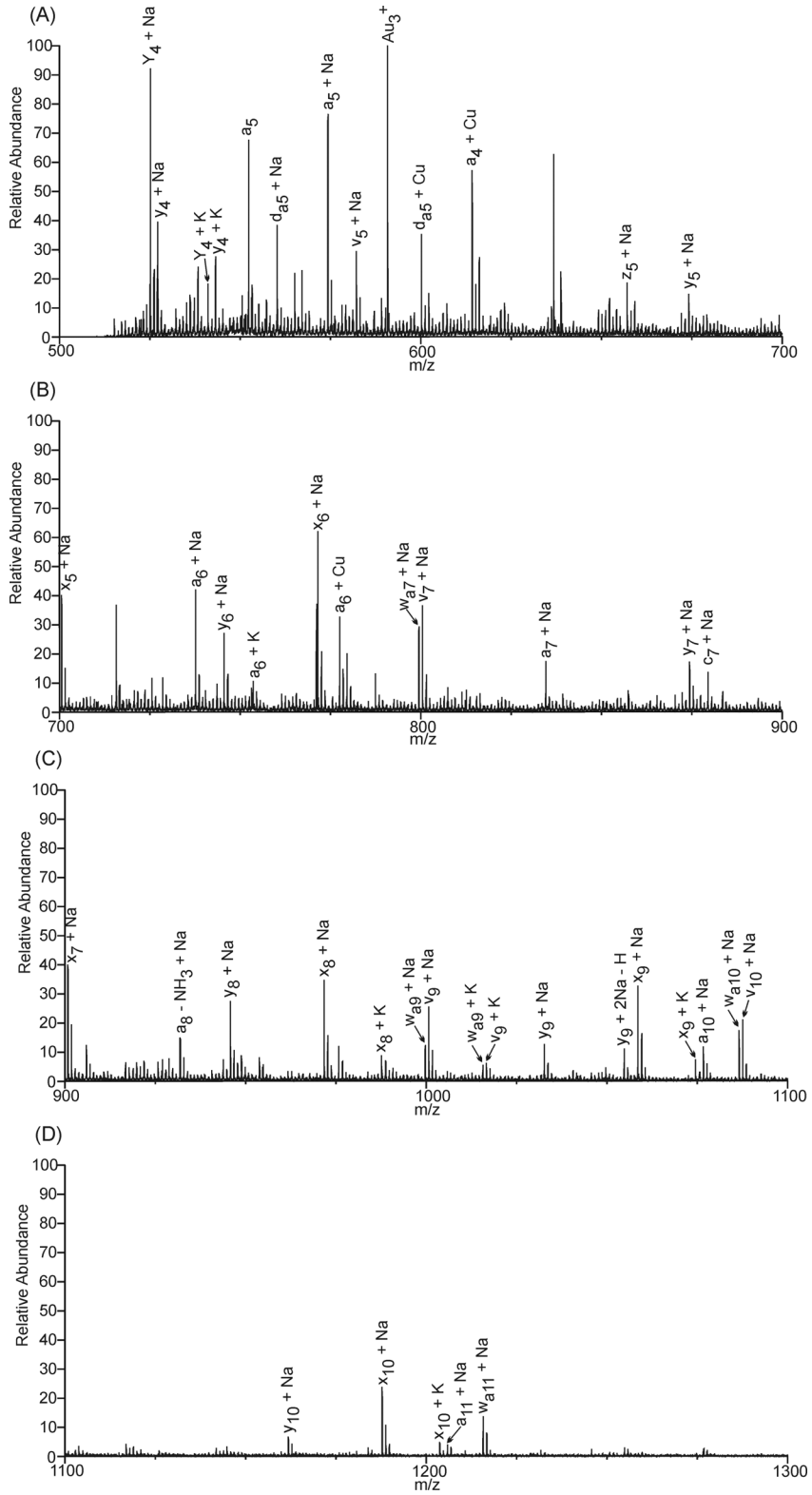

Figure 66. Detail zoom views of positive ion ISD LDI-TOF mass spectrum of ACTH (18-39) using 5 nm citrate capped AuNPs with added $CuSO_4$.

Interestingly, the peptides Bradykinin 1-8 (RPPGFSPF) and Val^4-Angiotensin III (RVYVHPF) do not show an increase in x-type ions, and fewer Cu containing fragment ions are observed compared to Angiotensin I methyl ester and ACTH(18-39). Chapter IV discussed radical initiated cleavage reactions, and that is also likely here, as x-type ions typically only are observed in photodissociation experiments which can generate large numbers of radicals.[122] Also note that the Cu-ion may be directing the cleavage, and when reduction of Cu^{2+} to Cu^{+} occurs, over 12 eV of energy is released that may contribute to the fragmentation process.[177] Further discussion pertaining to the mechanism of ion formation and fragmentation is held until Chapter VI, as the mechanism for ion formation is discussed in length there.

The following experiments describe changes in experimental conditions to evaluate the efficiency of fragmentation and what factors influence fragmentation.

Cu^{2+} vs. Cu^{+} effects

The effects of the solution charge of the added copper salt was also investigated. Figures 67A and 67B show the ISD mass spectra of Bradykinin 1-8 with addition of Cu^{2+} and Cu^{+}, respectively, using 5 nm AuNPs. The main differences observed between the two copper oxidation states are: (i) very few fragment ions overall are observed for Cu^{+} addition compared to Cu^{2+} addition and (ii) no peptide fragment ions contain Cu with Cu^{+} addition, even though there is more $[M + Cu]^{+}$ present compared to Cu^{2+} addition.

As mentioned previously, the oxidation state of a Cu ion complexed to the peptide is typically Cu^{+}, suggesting that a reduction process must occur when Cu^{2+} is added initially. The process by which Cu^{2+} is reduced to Cu^{+} may be important, as the reduction process may lead to the generation of radical species, as Equation 3 shows. Alternatively, radical species may be responsible for the reduction, as Equation 4 shows.

$$M + Cu^{2+} \rightarrow M^{+\bullet} + Cu^{+} \qquad (3)$$

$$M^{\bullet} + Cu^{2+} \rightarrow M^{+} + Cu^{+} \qquad (4)$$

The absence of radical species in the Cu^{2+} and Cu^{+} spectra do not confirm either reduction process, however as Chapter IV suggested, radical initiated cleavage events do not always show high abundances of radical species. It is unlikely that much Cu^{+} survives the reduction process, which accounts for the low abundances of parent and fragment ions for Cu^{+} addition.

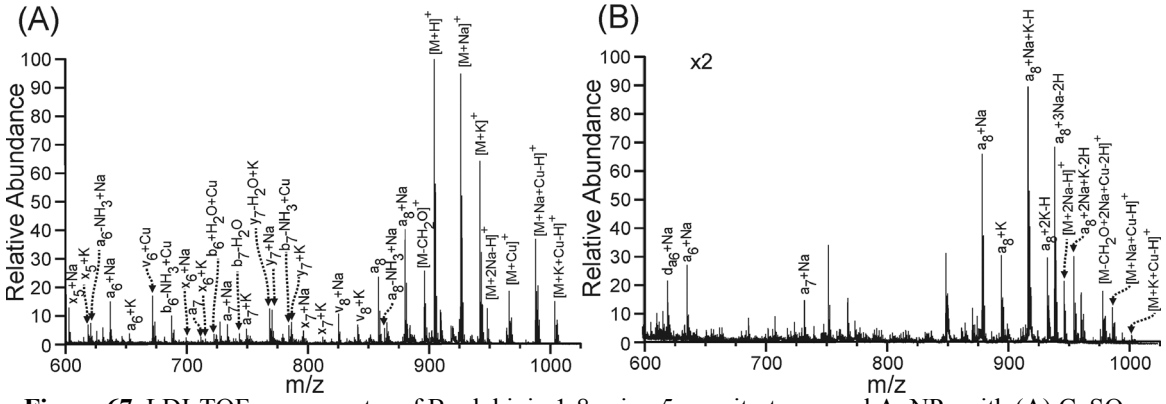

Figure 67. LDI-TOF mass spectra of Bradykinin 1-8 using 5 nm citrate capped AuNPs with (A) $CuSO_4$ added and (B) $CuCH_3COO$ added.

Copper ligand effects

Just as the charge of Cu in solution can affect the fragmentation pattern, the ligand is also of interest. Copper (II) acetylacetonate (CuAcac) stabilizes the Cu^{2+} ion and reduces the likelihood of reduction in solution; the structure is shown in Figure 68.

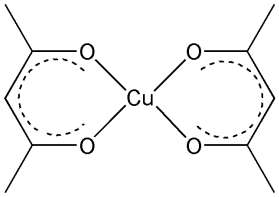

Figure 68. Structure of Copper Acetylacetonate.

Figure 69 shows the fragmentation pattern of Val^4-Angiotensin III using 5 nm AuNPs with added $CuSO_4$ and CuAcac, respectively. For addition of CuAcac (Figure 69B), fragment ion abundances do not differ significantly from $CuSO_4$ addition (Figure 69A). However, ion abundances of the protonated fragment ions are dramatically decreased with CuAcac addition compared to $CuSO_4$ addition. This is likely because the abundance of the $[M + H]^+$ ion is high for $CuSO_4$ addition, and only low abundances are present for CuAcac addition. Since fragmentation still occurs with CuAcac addition it appears that this ligand does not protect the Cu^{2+} ion from being reduced. Martinez-Diaz and Torres observed that in fast-atom bombardment MS processes, reduction of Cu^{2+} was also accompanied by ligand loss (fragmentation) of the molecule that was complexed to the Cu.[182] Fragmentation of the acetylacetonate ligand would allow the Cu ion to be reduced more readily, and participate in peptide fragmentation reactions.

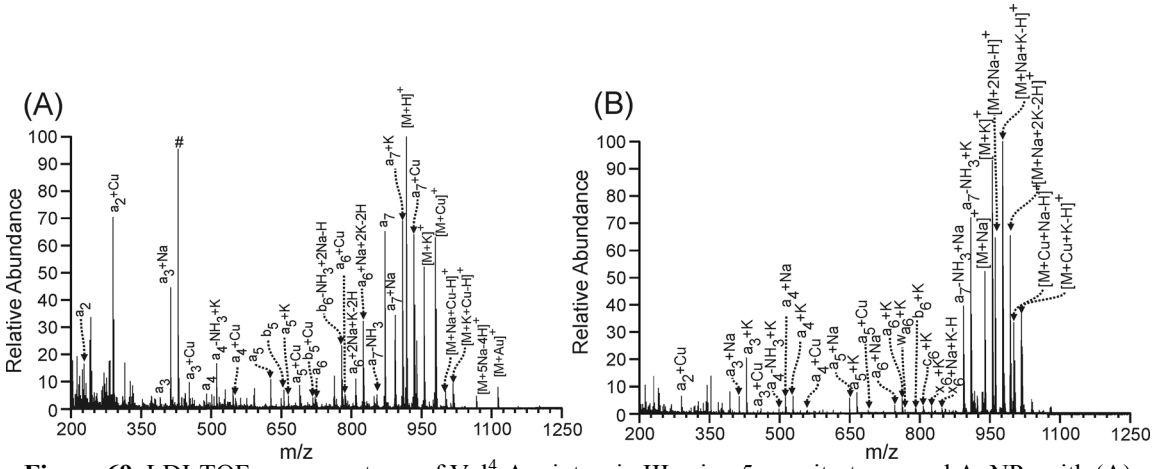

Figure 69. LDI-TOF mass spectrum of Val[4]-Angiotensin III using 5 nm citrate capped AuNPs with (A) added $CuSO_4$ and (B) added copper acetylacetonate.

In the negative ion LDI spectrum of Val[4]-Angiotensin III with CuAcac addition (Figure 70) Au_xCu^- species and several analyte ions are observed, including the [M – 2H + Cu]$^-$ ion. It is not clear why this phenomenon is occurring here, as Cu^{2+} as $CuSO_4$ does not produce this effect. However, this is further evidence for Cu^{2+} ion being on the AuNP surface and participating in reduction-oxidation reactions.

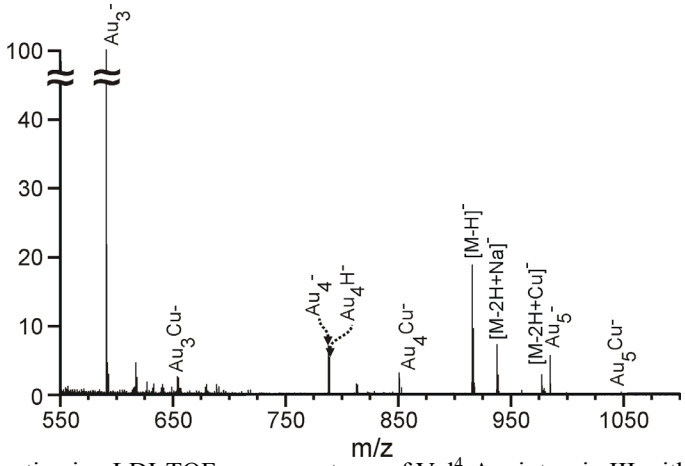

Figure 70. Negative ion LDI-TOF mass spectrum of Val[4]-Angiotensin III with added copper acetylacetonate using 5 nm citrate capped AuNPs.

Continuous extraction mode

Given the results from Cu(I) and Cu(II) salts, and reports from other researchers, it appears that electrons may be playing a part in fragmentation efficiency. Figure 71 shows the positive ion LDI mass spectrum of Val^4-Angiotensin III using 2nm AuNPs and added $CuSO_4$ in continuous extraction mode (see Figure 4A, Chapter I). Here, positive ions are extracted from the source immediately after the laser pulse (in contrast to delayed extraction, where ions are extracted up to a few hundred nanoseconds after the laser pulse) and electrons will go back to the sample plate.[91] No fragmentation is observed, suggesting that electrons may play a role in fragmentation or reduction processes. Zhang *et al.* showed that under continuous extraction conditions no significant decrease in copper reduction was observed compared to delayed extraction conditions.[177] Given that we still observe $[M + Cu]^+$, this is consistent with their work. ISD takes place on a short timescale which can not be monitored by continuous extraction.

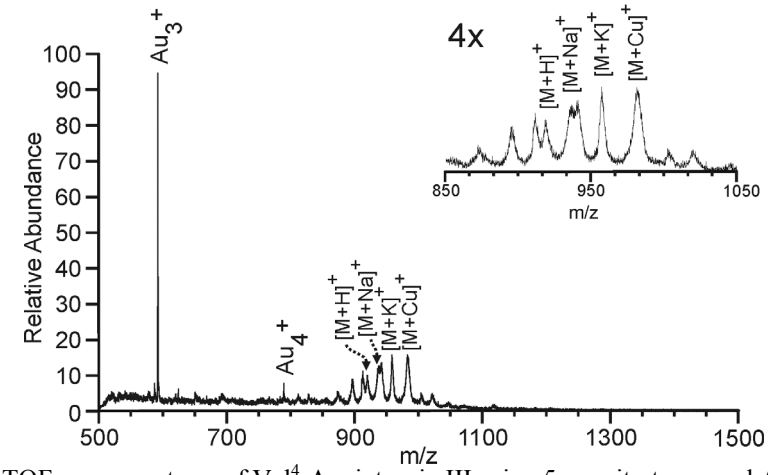

Figure 71. LDI-TOF mass spectrum of Val^4-Angiotensin III using 5 nm citrate capped AuNPs with added $CuSO_4$ in continuous extraction mode.

Effects of other metal salts

Other salts that were investigated are $Ni(CH_3COO)_2$ and $AgNO_3$. Figure 72 shows Ag^+ addition to Val^4-Angiotensin III using 2 and 5 nm AuNPs. LDI using 2 nm AuNPs (Figure 72A) results in low abundances of a-ions and a few side chain cleavages are observed. LDI using 5 nm AuNPs yields a-, b-, y-ions and side chain cleavages. Overall, silver addition results in less fragmentation than either nickel or copper salts, and very little silver adduction to fragment ions is observed. Silver has previously been shown to complex with sulfur and non-sulfur containing peptides, but with a higher affinity for sulfur containing amino acids; CID showed a high abundance of silver containing fragment ions.[183] It is unclear why so few silver adducted peptides are observed here when there is a relatively high abundance of the $[M + Ag]^+$ ion. Several other interaction may be occurring, such as Ag^+ interaction with the AuNP or gas-phase charge transfer reactions during fragmentation that neutralize the Ag^+ ion.

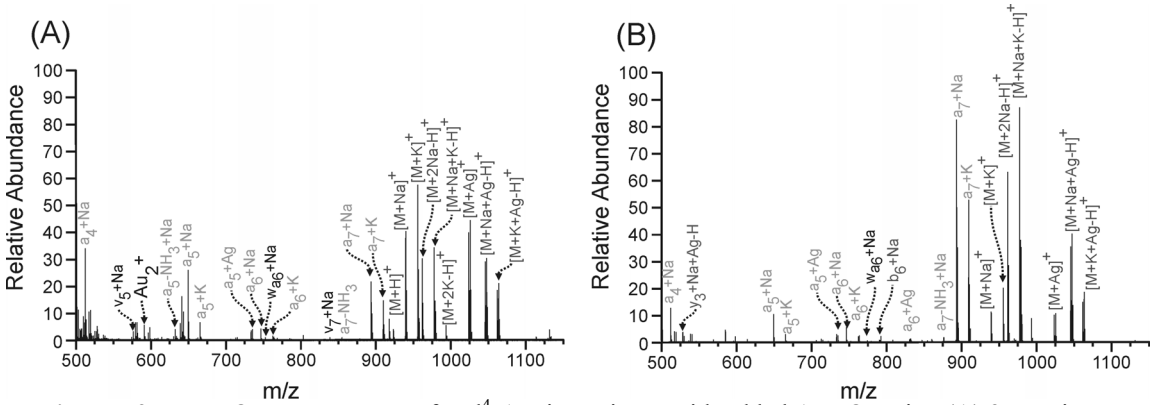

Figure 72. LDI-TOF mass spectra of Val^4-Angiotensin III with added $AgNO_3$ using (A) 2 nm citrate capped AuNPs and (B) 5 nm citrate capped AuNPs.

Figure 73 shows LDI spectra of Bradykinin 1-8 with Ni^{2+} addition, using 2 nm (Figure 73A) and 5 nm (Figure 73B) citrate capped AuNPs. For LDI using 2 nm AuNPs, $[M + Ni]^+$ ions are observed, but very few fragment ions contain nickel. LDI using 5 nm AuNPs results in no $[M + Ni]^+$ ions. Very little is known about Ni-peptide complexes in the gas-phase [184, 185] as most studies have been done in the solution-phase. The data presented here does not give any significant results for the fragmentation of Ni-adducted peptides.

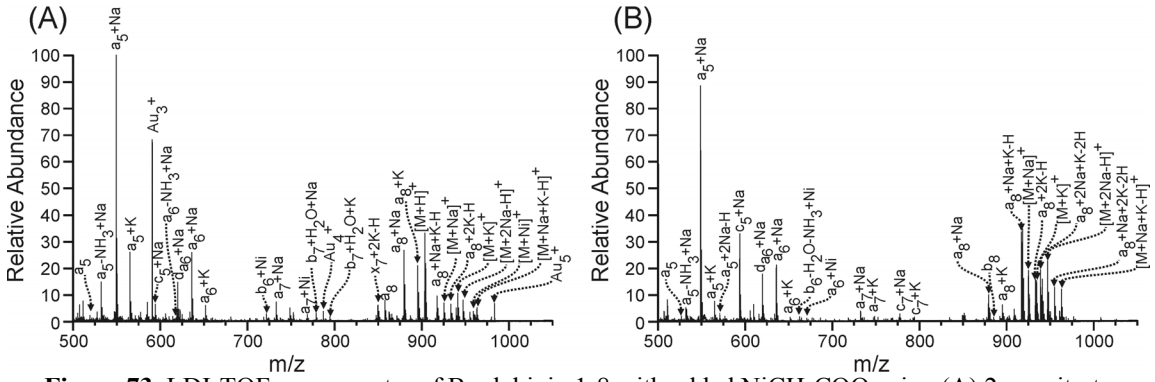

Figure 73. LDI-TOF mass spectra of Bradykinin 1-8 with added $NiCH_3COO$ using (A) 2 nm citrate capped AuNPs and (B) 5 nm citrate capped AuNPs.

Summary

The addition of Cu salts to AuNPs for LDI-MS results in ISD and is similar ISD of $[M + alkali]^+$ ions, with the exception of an increase in x-type ions for some peptides. The charge state of Cu was shown to change fragmentation efficiencies, with a lower

abundance of fragment ions for Cu^{+} compared to Cu^{2+}. The fragmentation mechanism relates closely to topics in Chapter VI and will be discussed more thoroughly there.

There are differences observed in peptide fragmentation for Ag^{+} and Ni^{+} addition compared to Cu^{2+} and Cu^{+} addition. For Ag^{+}, a substantial amount of Ag-peptide complex is observed, but few fragment ions that contain Ag are observed. This suggests that enough Ag^{+} survives the initial reduction process to form a complex with the peptide, but none stays complexed during fragmentation. Either these peptide complexes are more stable and do not fragment, or the Ag^{+} is reduced during that process. For Ni^{+}, very little peptide is complexed with the metal, suggesting that most of the Ni^{+} is reduced during the desorption/ionization event, or the metal-peptide complex is not as stable and does not survive the desorption/ionization event. Overall this chapter has shown that transition metal cations can also affect the desorption/ionization process, and promote ISD similarly to no transition metal addition.

CHAPTER VI

EVIDENCE FOR PRE-FORMED IONS USING GOLD NANOPARTICLES AS MATRICES FOR LDI-MS

Introduction

A number of questions must be addressed when discussing desorption/ionization mechanisms using NP materials. What happens to the NPs upon laser irradiation? How do NP and analyte interact upon laser irradiation? How do materials leave the surface of the LDI target? While the exact details of what happens during the desorption/ionization are difficult to determine, there are a number of reports that when taken together can provide a general model. Note that this is not a unified model and not all observations that occur during ionization can be explained by the proposed model. The use of NPs complicates a desorption/ionization mechanism, as not as much is known about NP behavior in this type of system, but there are a few reports that can help to define a general model.

Since the late 1980s when Tanaka and coworkers[2] and Karas and Hillenkamp[1] introduced MALDI as an ionization method there has been discussion centered around how ionization occurs. Experiments done to determine initial ion velocity are of interest, as they can provide some evidence as to what happens after laser irradiation. Upon laser irradiation some of the electronic excitation energy is converted into translational and vibrational energy of the matrix analyte molecules. Several groups have shown that the initial ion velocity is in the direction normal to the sample surface, suggesting that ions

are rapidly leaving the surface of the MALDI target. [186-190] When the matrix is excited by the laser, a rapid expansion of material occurs and forms a dense plume. Zhigilei and Garrison[191-193] have performed several molecular dynamics simulations on velocity and directions of clusters emitted from a surface, and as laser fluence increases, the amount of material increases. Large clusters of material can be ablated and neutral evaporation occurs during cluster emission.[191-194] Mechanisms proposed for desorption/ionization (DI)[195, 196] and laser desorption/ionization (LDI)[197] also use the ideas of cluster formation and desolvation. Taken together, these data suggest that clusters of material are generated and that MALDI is fundamentally an ablation process, with the role of the matrix to transfer energy to the analyte. While large clusters of material have not been detected in any MALDI experiments, one experiment has detected analyte ions clustered with matrix molecules by changing the pressure in the source. This suggests that at higher gas pressures (where collisional cooling of the ions or clusters can occur), cluster decay can be stopped at an intermediate stage.[160, 198] Additionally, high molecular weight clusters generated by MALDI have been trapped in a quadrupole ion trap and shown to be weakly bound molecules that readily dissociate.[199, 200] Figure 74 shows a cartoon of matrix molecules (blue hexagons) and analyte molecules (green circles) on a surface together; upon laser irradiation, small charged clusters of matrix and analyte are formed, and are held together by hydrogen bonds and coulombic interactions.[161] The clusters that result are in an excited state and contain enough energy to desolvate into molecular species by way of evaporation of neutral molecules, or chemical reactions may occur that result in more stable molecular species.[195-197] If any clusters exist that are initially

highly charged, they will not survive in the plume, but will undergo charge reduction by trapped electrons with are formed upon matrix photoionization processes.[161] This general picture of the cluster model accounts for most of the observations made during the MALDI process, and further discussion can be found in an article by Karas and coworkers.[161]

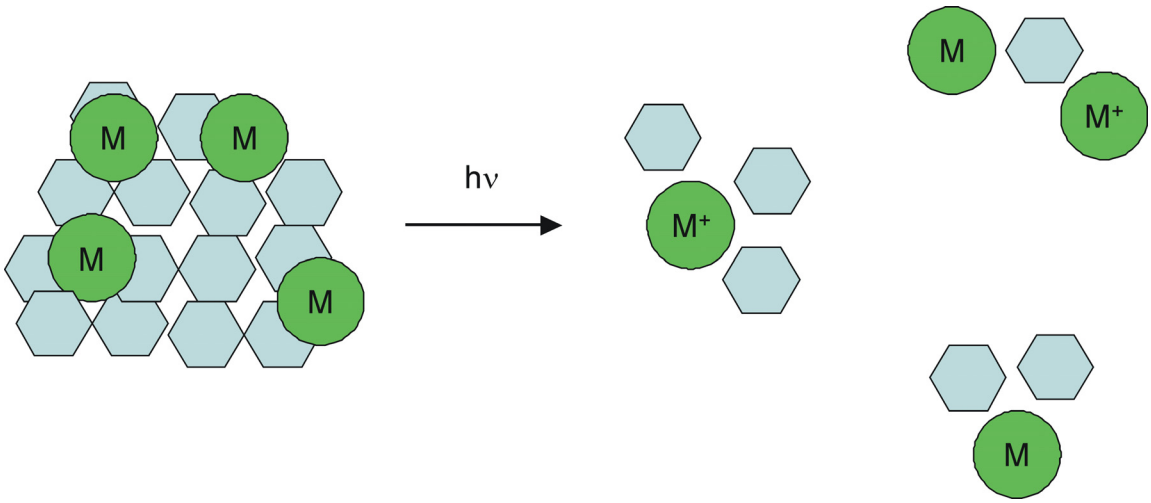

Figure 74. Cartoon of MALDI cluster ionization model.

Beuhler *et al.* and Winkler *et al.* suggest another model for desorption/ionization that came from studies using field desorption mass spectrometry.[201, 202] Both papers state that a certain amount of energy is required to break the bonds that attach analyte molecules (or ions) to a solid surface. If energy from the desorption/ionization event is deposited solely in the surface attachment bonds and does not get distributed into the internal degrees of freedom of the analyte, then a molecule (or ion) is desorbed from the surface. If the energy from desorption/ionization does get distributed to the internal degrees of freedom of the analyte molecule (or ion), then fragmentation or surface

decomposition processes can occur because of the increased internal energy of the ion. Beuhler *et al.* also concludes that molecules that exist as ions of the surface (*i.e.*, pre-formed ions) desorb more readily than molecules that must undergo gas-phase charge exchange to be ionized.[201]

However, the work in this dissertation utilizes NPs and not organic acid matrices or field desorption from surfaces, so consideration of the behavior of NPs upon laser irradiation is also important. When a NP is irradiated with a laser, electrons are photoejected from the NP[203-206] and some accumulation of electrons at or near the NP surface occurs.[204] The electrons that are immediately ejected from the NP are "hot" electrons, with estimated energies of 1-3 eV.[206] Any electrons that are not photoejected from the NP are rapidly thermalized by electron-phonon scattering, a process which occurs within a few picoseconds.[204, 205] Electron accumulation or ejection leads to charging of the NP surface which results in rapid (< 50 ps) fragmentation of the NP.[204] Energy that is put into phonon modes is transferred into the surrounding media over 10-100 ps.[203, 204]

Throughout this dissertation there has been mention of possible desorption/ionization mechanisms, with specific reference to the cluster ionization model and desorption of pre-formed ions. This chapter reviews the previous experiments that are relevant to these models, and presents several more experiments which further support these statements. Finally, the various desorption/ionization theories that have been discussed are brought together at the end of this chapter to present a mechanism for desorption/ionization when using NPs.

Experimental

Mass spectrometry experiments using AuNPs were performed on an Applied Biosystems Voyager DE-STR (Foster City, CA) equipped with a Spectra-Physics (Irvine, CA) N_2 laser (337 nm). Experiments were performed in the positive ion reflected mode using 200 laser shots with internal calibration. All of the mass spectra shown used laser energies 10-15% above the threshold for ionization. Tandem mass spectrometry was done on an Applied Biosystems 4700 Proteomics Analyzer (Foster City, CA). Collision-induced dissociation tandem mass spectra were acquired using 10-20% greater laser power than MS acquisition. Collision gas was used was at the medium air pressure setting (4×10^{-7} torr) with 1 kV collision energy.

Laser energy measurements were taken using an Ophir Nova Power/Energy meter coupled to a PE-10 Ophir Pyroelectric head (Ophir Laser Measurement Group, North Logan, UT). Measurements were taken in increments of 50 arbitrary units on the rotatable variable neutral density filter wheel of the Voyager DE-STR. Values were recorded every 200 shots from a total of 1400 laser shots per setting point in the lower energy region (0.77 - 1.92 μJ) of the laser, and every 100 arbitrary units on the higher energy region of the laser (1.92 - 51.89 μJ). The process was repeated twice and the average calculated. Data shown here uses laser energy instead of laser fluence (laser energy/area · time), as accurate laser spot size data is very difficult to acquire.

AuNP-to-analyte ratios were optimized for each peptide and was determined to be 1 AuNP: 10^6 analyte molecules for these peptides, which is consistent with previous reports.[99, 139] Samples were prepared by mixing solutions containing the AuNPs with

solutions containing analyte and any additives, and immediately deposited onto a stainless steel plate and vacuum dried. Sample loadings of 10-20 pmol of analyte were used.

Modification of Angiotensin I to Angiotensin I methyl ester was done according to literature procedures, and was reported in detail in Chapter II.[82,83] Modification of AuNPs was done according to previously described procedures.[139] Modification of Leucine-Enkephalin to a fixed-charge derivative [trimethylammonium acetyl (TMAA)] was done according to literature procedures.[114] Briefly, the peptide was iodoacetylated by dissolving 1 mg of peptide in 1 mL of water and reacting it with a 10-fold molar excess of iodoacetic anhydride for 15 minutes in an ice bath; the resulting solution was allowed to warm back up to room temperature. The peptide was lyophilized and then dissolved in 500 μL of a 25% wt solution of trimethylamine and reacted for 30 minutes at room temperature. The resulting product was lyophilized and re-suspended in water at a concentration of 1 mg/mL. The reaction scheme is shown in Figure 75.

Acetic anhydride, acetonitrile, acetyl chloride, anhydrous methanol, iodoacetic anhydride, trimethylamine, and crystal violet were obtained from Sigma (St. Louis, MO) and used as received. 2 nm and 5 nm citrate capped gold nanoparticles were purchased from Ted Pella, Inc. (Redding, CA). Angiotensin I (DRVYIHPFHL) and Leucine-Enkephalin (YGGFL) were purchased from American Peptide Co. (Sunnyvale, CA).

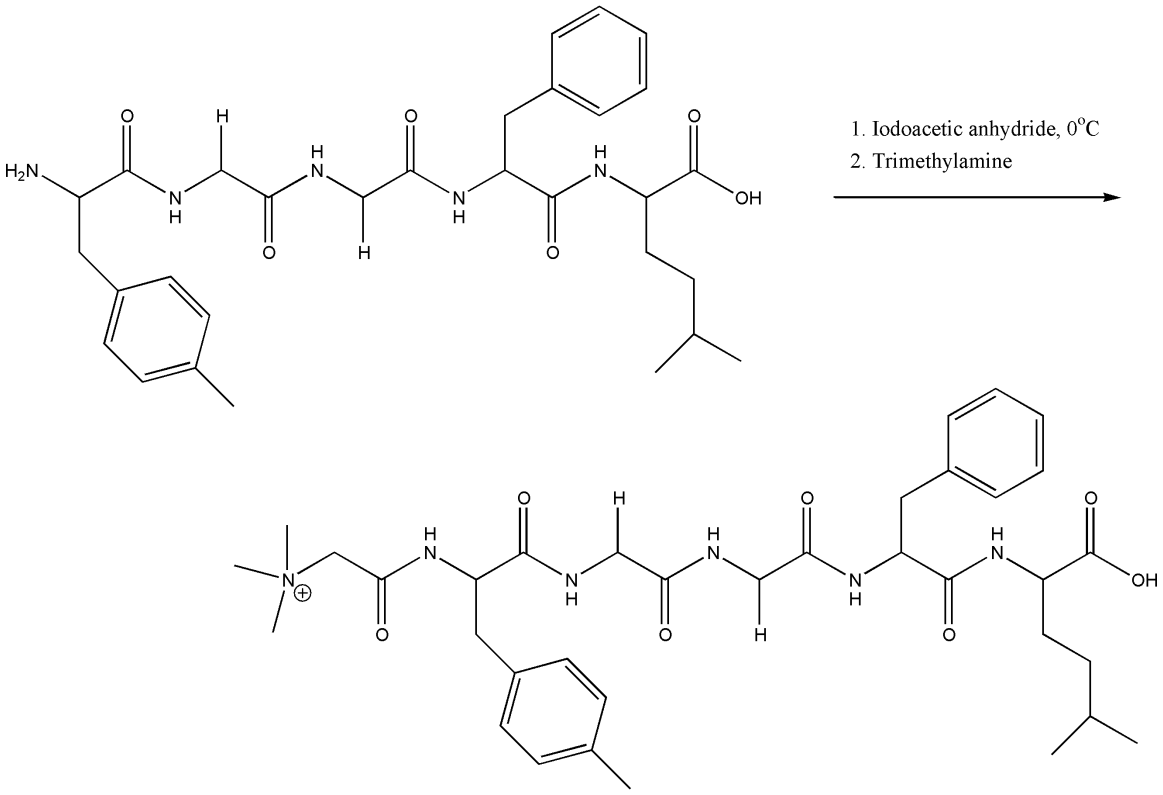

Figure 75. Reaction scheme for modification of the peptide N-terminus to a trimethylammonium acetyl group.

Results and Discussion

Several of the experimental results already shown in this dissertation support the theory that desorption/ionization when using AuNPs is a thermal desorption of pre-formed ions. The differences in analyte desorption/ionization for 2, 5, and 10 nm AuNPs are an important observation. 2 nm AuNPs desorb/ionize analyte readily, with little peptide fragmentation observed (see Figures 12A, 14, 16 for examples of this). 5 nm AuNPs ionize peptides, but do result in some peptide fragmentation; it is very difficult to desorb/ionize peptides with 5 nm AuNPs and not get some fragmentation (see Figures 50 and 52). When using 10 nm AuNPs, only low relative abundances of intact peptide

molecules desorb/ionize and ISD is not observed (see Figure 12C). Different amounts of thermal energy are produced from each of the size distributions of AuNPs, and the radius of heating is different. This means that different amounts of energy will be deposited into the peptide, and some will be desorbed/ionized intact, and some will undergo fragmentation. For fragmentation to occur, higher internal energies are needed (see Figure 7). If too much energy is present, then very little intact or fragment ions may be observed. We suggest that this is why differences in ionization are observed for 2, 5, and 10 nm AuNPs.

The importance of AuNP-to-analyte ratios was discussed in Chapter II. As Figure 14 shows, ion signal from $[M + alkali]^+$ ions decreases as AuNP-to-analyte ratio increases. The main contribution of alkali in solution is from the AuNPs (a consequence of the synthesis), and so by increasing the AuNP-to-analyte ratio, the amount of alkali per peptide in a given area is reduced, resulting in less alkali adduction. The distribution of ions that are desorbed/ionized reflect the composition of ions in solution, suggesting that desorption/ionization of pre-formed ions is occurring.

Differences in ionization of similar peptide species also suggest a pre-formed ion mechanism. As stated in Chapter II (Figure 16), the desorption/ionization efficiency of a series of Angiotensin peptides (Angiotensin I, Angiotensin I methyl ester, acetylated Angiotensin I) increases with peptide basicity. Previous work done in MALDI-MS experiments has shown that the amino acid composition is important for desorption/ionization and since arginine having the highest proton affinity it is likely the site of protonation.[85, 86] Also, modifying the peptide to increase or reduce its overall

basicity will likely affect desorption/ionization, as Chapter II showed (see Figure 16). The effects of pH can also be attributed to a pre-formed ion mechanism. As Figure 18 shows, when the solution pH drops, more $[M + H]^+$ ions are desorbed/ionized. With a lower pH additional protons are available as a source for protonation, and more molecules are likely protonated on the LDI target, and are thus desorbed/ionized. Finally, most mass spectra obtained using AuNPs show some abundance of small gold cluster species (*i.e.*, Au_2^+, Au_3^+, Au_5^+). This observation fits well with the previously mentioned study by Kamat and coworkers,[204] who showed that NPs fragment upon laser irradiation.

Chapter III also presented data that supports the theory of pre-formed ions (see Figures 36 and 41). The enhancement of the $[M - H]^-$ ion with F^-, Cl^-, and oxyanion addition likely occurs because of reactions that happen in solution prior to the NP-peptide sample being deposited on the LDI target plate.

Peptide ion fragmentation was observed in Chapters IV and V. As discussed earlier, the model proposed by Beuhler *et al.* suggests that desorption of molecules (or ions) depends on how tightly bound the molecule is to the surface of a sample target.[201] When more energy is present in the system, then molecules and ions can undergo fragmentation or surface decomposition reactions. Data was shown in Chapter V where the addition of Cu^{2+} ions to the AuNPs results in increased peptide ion fragmentation, specifically for x-type ions. The Cu^{2+} ions likely adsorb to the AuNP surface and peptide molecules will also likely interact with the Cu ions. Increases in fragmentation may be

the result of the peptide being folded around the Cu^{2+} ions in a specific manner or more efficient energy transfer to the peptide molecule through the Cu^{2+} ion.

Crystal violet

The dye molecule crystal violet was chosen to investigate desorption/ionization of an ion with a fixed charge site. Figure 76 shows the UV-Visible absorption spectrum and structure of crystal violet. Figure 77 shows a representative mass spectrum of desorption/ionization of crystal violet using 2 nm and 5 nm AuNPs, where the M^+ ion is the dominant peak.

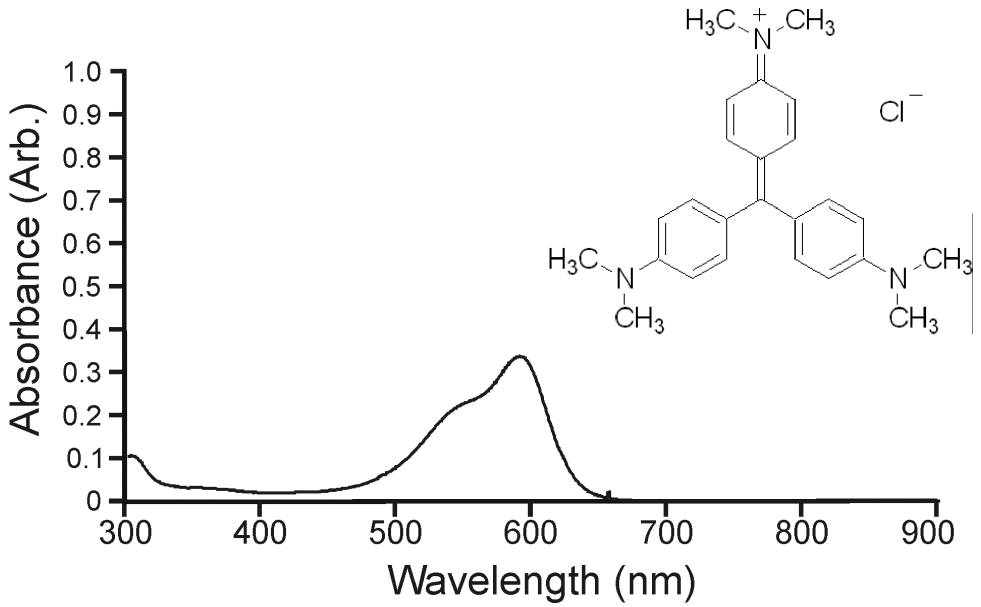

Figure 76. UV-Visible absorption spectrum and structure of crystal violet.

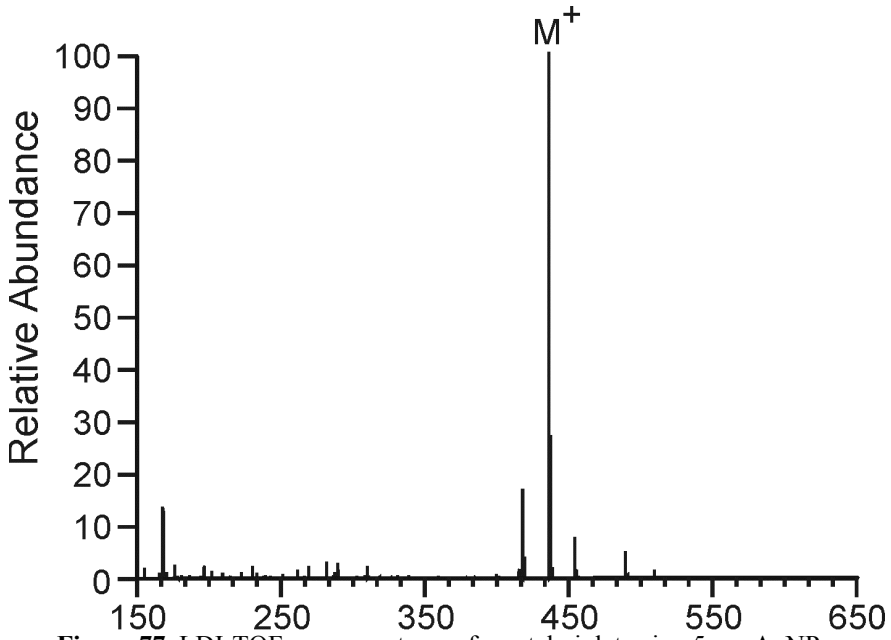

Figure 77. LDI-TOF mass spectrum of crystal violet using 5 nm AuNPs.

Different AuNP-to-analyte ratios were mixed to determine if the viable range for desorption/ionization differs from peptides, which was shown in Chapter II. The lowest ratio where analyte was detected was 1 AuNP: 10^2 analyte molecules, although a significant amount of chemical noise is present, and analyte abundances are low. A series of mass spectra were collected using different laser energies to determine the trend of ionization. Figure 78 shows a plot of peak area (for the M^+ ion of crystal violet) vs. laser energy per pulse. The greatest increase in peak area is observed for a ratio of 1 AuNP: 10^4 analyte molecules. This is in contrast to peptides, where 1 AuNP: 10^6 analyte molecules typically gives the highest peak areas. This may be occurring because crystal violet is a much smaller molecule than a peptide, which would require less energy for desorption/ionization of the molecule. This observation fits with the Beuhler *et al.* theory of energy required to break the bonds of the molecule interacting with the target plate,

which was discussed earlier.[201] A smaller molecule like crystal violet does not have as many interactions holding it to the surface compared to a larger peptide molecule, which would result in less energy required for desorption of the ion.

Figure 79 shows a plot of peak area vs. laser energy using 5 nm AuNPs. Here, the greatest increase in peak area is observed using a ratio of 1 AuNP: 10^5 analyte molecules. Also, several AuNP-to-analyte ratios show a drop in peak area. The mass spectra from 1 AuNP: 10^5 analyte molecules and lower ratios are more congested, meaning more peaks are present in the low mass region, but no peaks correspond to fragment ions of crystal violet.

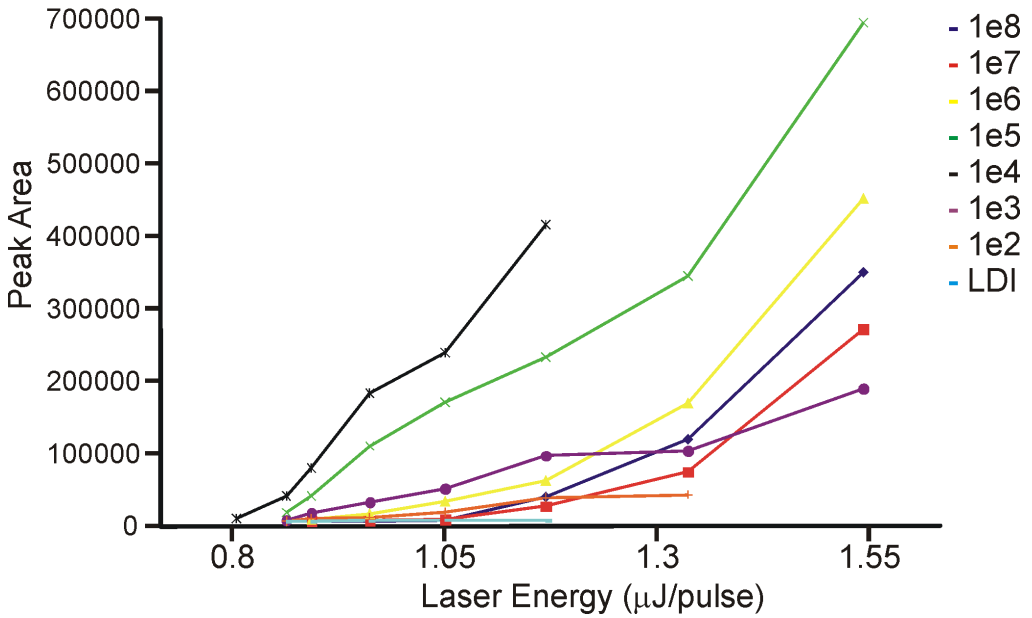

Figure 78. Peak areas of crystal violet at varying AuNP-to-analyte ratios and laser energies using 2 nm citrate capped AuNPs.

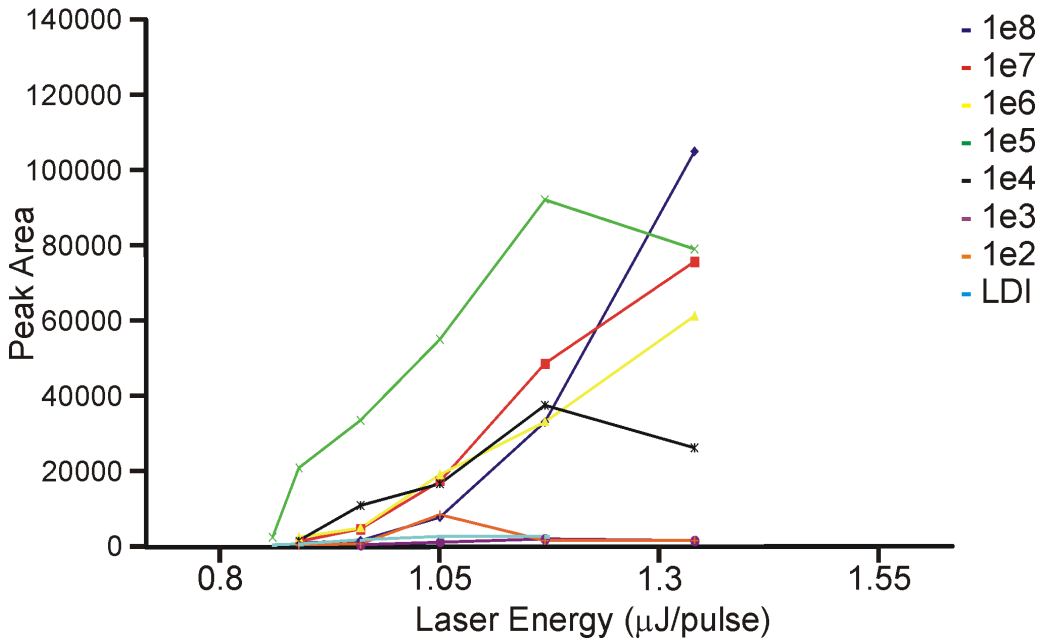

Figure 79. Peak areas of crystal violet at varying AuNP-to-analyte ratios and laser energies using 5 nm citrate capped AuNPs.

Figure 80 is a plot of peak areas vs. laser energy at different AuNP-to-analyte ratios using 2 nm AuNPs when fructose has been added. As discussed previously, fructose can act to cool ions and reduce internal energy. The green line shows peak areas for 1 AuNP: 10^5 analyte molecules and no fructose addition. The other three lines are for addition of 10^1, 10^2, and 10^3 molecules of fructose to 1 AuNP: 10^5 analyte molecules, respectively. There is a significant decrease in peak area when fructose is added, suggesting overall fewer ions are desorbed/ionized, which could be correlated to the internal energy of the analyte molecule.

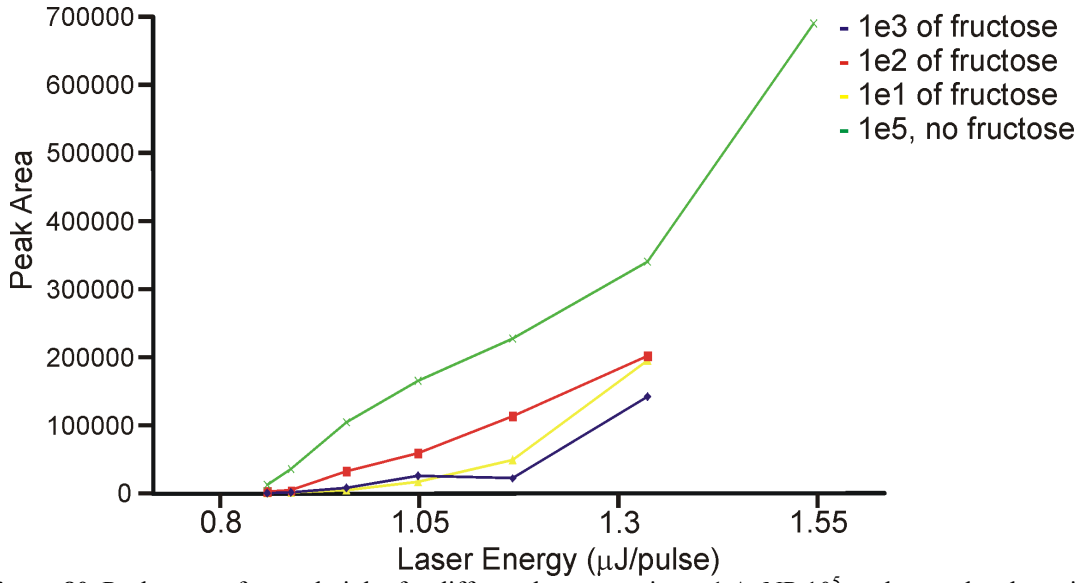

Figure 80. Peak areas of crystal violet for different laser energies at 1 AuNP:10^5 analyte molecules using 2 nm citrate capped AuNPs, with fructose added.

TMAA modified peptide

Given the differences in energies for desorption/ionization of a small pre-formed ion such as crystal violet and peptides, we have modified a peptide to have a fixed charge on the N-terminus for better comparison. Figure 81 shows a representative mass spectrum for trimethylammonium acetyl (TMAA) modified YGGFL using either 2 or 5 nm AuNPs. The intact molecule is the dominant peak in the mass spectrum, with some gold-cluster peaks also present.

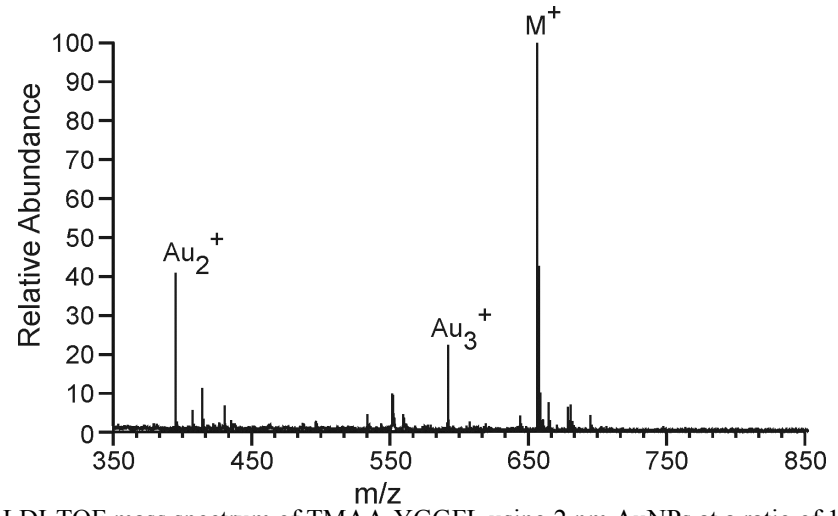

Figure 81. LDI-TOF mass spectrum of TMAA-YGGFL using 2 nm AuNPs at a ratio of 1 AuNP: 10^6 analyte molecules, where 10 pmol was deposited on the sample plate.

Figure 82 shows a comparison of peak areas vs. laser energy for YGGFL and TMAA-YGGFL using 2 nm and 5 nm AuNPs. Figure 82A shows desorption/ionization of YGGFL using 2 nm AuNPs with ratios of 1 AuNP: 10^6 – 10^7 analyte molecules. Using 5 nm AuNPs (Figure 82B) desorption/ionization occurs for ratios of 1 AuNP: 10^6 – 10^7 analyte molecules. Figure 82C and 82D shows desorption/ionization of TMAA-YGGFL using 2 nm and 5 nm AuNPs, respectively for ratios of 1 AuNP: 10^5 – 10^7 analyte molecules. Modification of the peptide YGGFL to the fixed charge TMAA-YGGFL results in three key differences: (i) desorption/ionization occurs at lower AuNP-to-analyte ratios for TMAA-YGGFL, (ii) lower laser energies are needed for desorption/ionization of TMAA-YGGFL, and (iii) TMAA-YGGFL results in larger peak areas compared to YGGFL. Figure 83 shows a direct comparison of peak area vs. laser energy for YGGFL and TMAA-YGGFL at various AuNP-to-analyte ratios. An increase in peak area is observed for the fixed charge peptide derivative compared to the

unmodified peptide. Compared to crystal violet, laser energies needed for desorption/ionization of YGGFL and TMAA-YGGFL are significantly higher, which was discussed previously.

Lastly, laser energies were increased to determine if any ISD occurs with TMAA-YGGFL. No ISD was observed; this result is reasonable, as fragmentation would have to occur by charge-remote homolytic bond cleavages, which require higher activation energies.[114, 142]

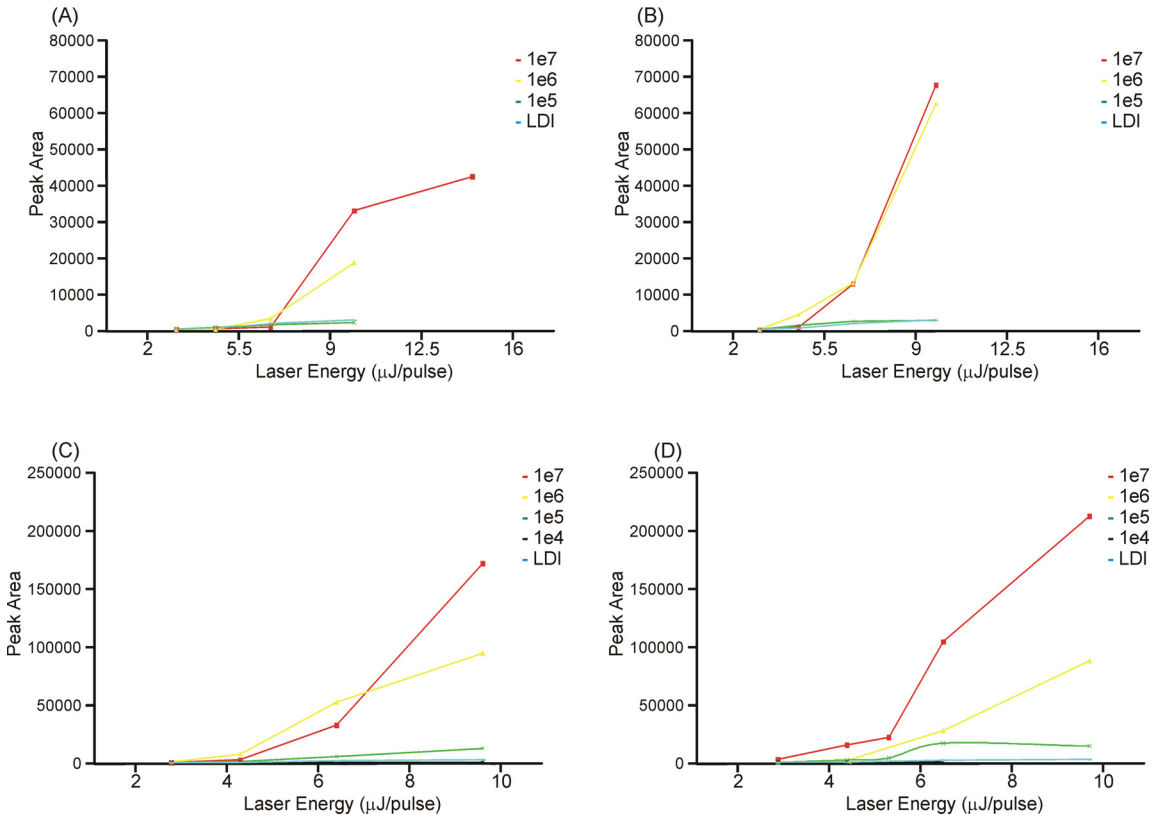

Figure 82. Peak areas of YGGFL for different laser energies at varying AuNP-to-analyte ratios using (A) 2 nm citrate capped AuNPs and (B) 5 nm citrate capped AuNPs and peak areas of TMAA-YGGFL using (C) 2 nm citrate capped AuNPs and (D) 5 nm citrate capped AuNPs.

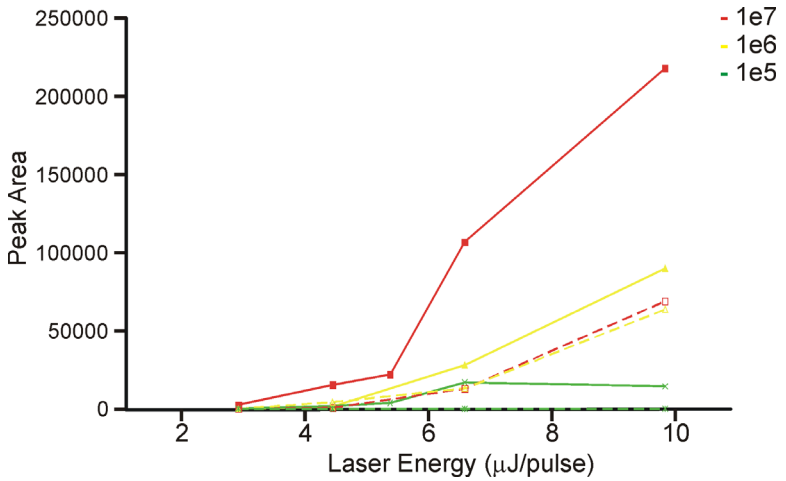

Figure 83. Comparison of peak areas at different laser energies for YGGFL (dashed lines) and TMAA-YGGFL (solid lines) at various AuNP-to-analyte ratios using 5 nm citrate capped AuNPs.

Proposed mechanism for ion formation

Based on the findings of various researchers who have described the cluster model and other pre-formed ion mechanisms, along with the data presented in this chapter, a general mechanism of ion formation can be proposed. Figure 84 shows a cartoon of the possible interaction of analyte molecules with a NP (left), where a large number of analyte molecules are present for each NP. Upon laser irradiation (right) smaller clusters of the NP, analyte, and possibly electrons or other species (water, salt, etc.) may be present. Several key things happen during laser irradiation: (i) the NPs are heated and eject electrons which eventually results in fragmentation of the NP, (ii) energy (as heat) from the NP is transferred to the analyte molecules/ions, which can simply be desorbed from the surface as a pre-formed ion, or if enough internal energy is present, the molecules/ions can fragment, (iii) clusters of material that are composed of NP, analyte, and other species present in the sample leave the surface of the LDI target,

and (iv) the clusters of material become smaller via neutral evaporation or further transfer of energy between components of the cluster which results in single ions that are detected by the mass spectrometer.

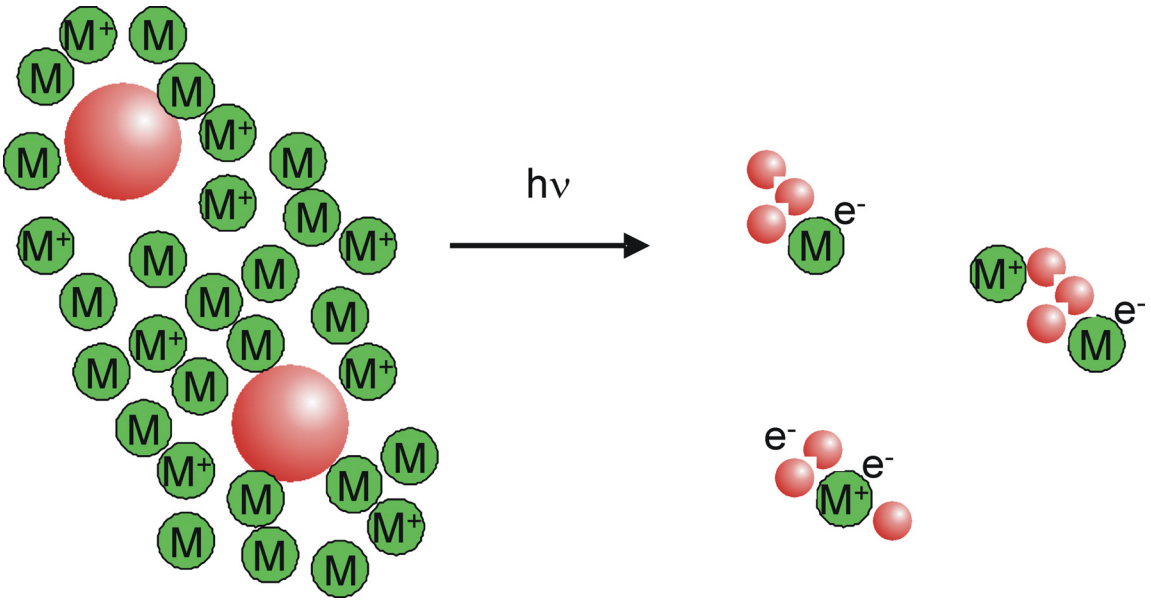

Figure 84. Cartoon of desorption/ionization with NPs.

Summary

Throughout this dissertation results have suggested that desorption of pre-formed ions is occurring. This chapter aimed to summarize those results, and add a few select experiments that support this theory. The desorption of a molecule with a fixed charge provides strong evidence for this. Differences in ion abundances and laser energies required for desorption (*e.g.*, for the peptide YGGFL and the modified peptide TMAA-YGGFL) also support this theory.

CHAPTER VII

SUMMARY AND CONCLUSIONS

Gold nanoparticles (AuNPs) have emerged as valuable and versatile research tools in chemistry and related fields. In particular, NPs have become useful for laser desorption/ionization mass spectrometry (LDI-MS) to facilitate desorption/ionization of biomolecules. The initial goal of the research presented in this dissertation was to define parameters that are important for desorption/ionization of biomolecules. Many different solution parameters were explored, and some were found to enhance ionization, while others proved detrimental. Specifically, controlling the AuNP-to-analyte ratio, pH, peptide composition, and AuNP size are important parameters for ionization.

A better understanding of basic conditions for ionization led to investigation of effects of passivating the AuNP surface using halides and oxyanions. The presence of NaF, NaCl, NaBr, and NH_4X (X = F, Cl, Br, I) were shown to not significantly affect analyte ion abundances, whereas addition of NaI strongly suppressed analyte ion yields. The LDI ion yields from AuNPs treated with β-mercaptoethanol, glutathione or tiopronin were much less sensitive to the presence of NaI, suggesting that covalently bound ligands protect the NP from halide adsorption. In addition, peptide $[M - H]^-$ ion yields were significantly higher from AuNPs treated with oxyanions (NO_3^- and SO_4^{2-}); however, thiolate functionalized AuNPs did not show increased negative ion yields, suggesting that these ligands also protect the NP surface from oxyanion physisorption.

The results from Chapters II and III on modifying solution and NP conditions led to further questions about the desorption/ionization process. In-source decay (ISD) of peptides using gold nanoparticles (AuNPs) for laser desorption/ionization mass spectrometry (LDI MS) was investigated in Chapter IV with the goal of gaining insight into internal energy distributions of peptide molecules, and peptide fragmentation mechanisms. Fragment ions were observed for a series of Angiotensin peptides, with the highest ion abundances for Angiotensin I methyl ester (compared to Angiotensin I (free acid) and acetylated Angiotensin I), and many different types of fragment ions were observed including side-chain cleavages and radical species. Addition of fructose reduced the number of radical species and in general less ISD was observed. These results suggest that peptide molecules have a distribution of internal energies, with intact and fragment ions being observed. A radical initiated mechanism for fragmentation was proposed. Next, questions regarding how the energy is deposited in analyte molecules were addressed. Chapter VI reiterated numerous points that suggest a pre-formed ion desorption mechanism (*e.g.*, AuNP-to-analyte ratios, pH, peptide composition, and AuNP size), and additional experiments showed that molecules with a fixed charge desorb/ionize more readily than those without.

Overall, the data presented in this dissertation have provided insight on a number of important issues: (i) sample preparation is extremely important for consistent results and ion type, (ii) NPs must be intact for desorption/ionization to occur, (iii) differing amounts of energy are imparted to biomolecules based on NP size and surface structure, (iv) in general desorption/ionization appears to be of pre-formed ions.

Future work using AuNPs for LDI-MS could proceed in many different directions. Many of the experiments that were done in this dissertation that pertain to energy transfer and internal energy of peptide ions were done using 5 nm AuNPs, and all of the work in this dissertation was done using a laser at 337 nm. The effects of pumping the plasmon band would provide more information about energy transfer into peptides and perhaps help to refine the desorption/ionization mechanism proposed here. Other experiments that pertain to ion energetics would involve comparing photodissociation data to that presented here. Also, using a so-called 'thermometer ion' under strictly controlled experimental conditions for desorption/ionization would further the understanding of fragmentation processes and ion energetics.

Also of interest are other transition metals, or expansion of the work started here. Silver is known to complex with sulfur containing ligands, and thiols also have an affinity for gold surfaces. While thiols will not typically dissociate from gold surfaces, bridging interactions between the NP and cation could be achieved, and more ordered analyte-NP structures could be investigated, and perhaps shed more light on how interaction between the peptide and AuNP is important. Interaction between the AuNP and transition metal cations also begs the question of how different alloy materials may affect the desorption/ionization process.

Several experiments in this dissertation were not successful, such as alkanethiol coated AuNPs or mixtures with a tryptic digest. While biomolecules are not miscible with alkanethiols, there is potentially utility for analysis of other molecule classes (*e.g.*, lipids, organic molecules). The ability to desorb/ionize a complex mixture such as a

tryptic digest would also be useful for biological mass spectrometry, and any selective ionization that may occur when using AuNPs could also be investigated. Modification of the AuNP surface was briefly explored in this dissertation, but because of the versatile chemistry of AuNPs, selective analyte capture experiments could easily be designed for a specific purpose.

REFERENCES

(1) Karas, M.; Hillenkamp, F. *Anal. Chem.* **1988**, *60*, 2299-2301.

(2) Tanaka, K.; Waki, H.; Ido, Y.; Akita, S.; Yoshida, Y.; Yoshida, T. *Rapid Comm. Mass Spectrom.* **1988**, *2*, 151-153.

(3) Dai, Y.; Whittal, R. M.; Li, L. *Anal. Chem.* **1996**, *68*, 2494-2500.

(4) Westman, A.; Huth-Fehre, T.; Demirev, P.; Sundqvist, B. U. R. *J. Mass Spectrom.* **1995**, *30*, 206-211.

(5) Amado, F. M. L.; Domingues, P.; Graça Santana-Marques, M.; Ferrer-Correia, A. J.; Tomer, K. B. *Rapid Comm. Mass Spectrom.* **1997**, *11*, 1347-1352.

(6) Strupat, K.; Karas, M.; Hillenkamp, F. *Int. J. Mass Spectrom. Ion Proc.* **1991**, *111*, 89-102.

(7) Vorm, O.; Roepstorff, P.; Mann, M. *Anal. Chem.* **1994**, *66*, 3281-3287.

(8) Gusev, A. I.; Wilkinson, W. R.; Proctor, A.; Hercules, D. M. *Anal. Chem.* **1995**, *67*, 1034-1041.

(9) Figueroa, I. D.; Torres, O.; Russell, D. H. *Anal. Chem.* **1998**, *70*, 4527-4533.

(10) Fitzgerald, M. C.; Parr, G. R.; Smith, L. M. *Anal. Chem.* **1993**, *65*, 3204-3211.

(11) Sunner, J.; Dratz, E.; Chen, Y.-C. *Anal. Chem.* **1995**, *67*, 4335-4342.

(12) Dale, M. J.; Knochenmuss, R.; Zenobi, R. *Anal. Chem.* **1996**, *68*, 3321-3329.

(13) Schurenberg, M.; Dreisewerd, K.; Hillenkamp, F. *Anal. Chem.* **1999**, *71*, 221-229.

(14) Wei, J.; Buriak, J. M.; Siuzdak, G. *Nature* **1999**, *399*, 243-246.

(15) Go, E. P.; Apon, J. V.; Luo, G.; Saghatelian, A.; Daniels, R. H.; Sahi, V.; Dubrow, R.; Cravatt, B. F.; Vertes, A.; Siuzdak, G. *Anal. Chem.* **2005**, *77*, 1641-1646.

(16) Wen, X.; Dagan, S.; Wysocki, V. H. *Anal. Chem.* **2007**, *79*, 434-444.

(17) Finkel, N. H.; Prevo, B. G.; Velev, O. D.; He, L. *Anal. Chem.* **2005**, *77*, 1088-1095.

(18) Kauppila, T. J.; Talaty, N.; Salo, P. K.; Kotiaho, T.; Kostiainen, R.; Cooks, R. G. *Rapid Comm. Mass Spectrom.* **2006**, *20*, 2143-2150.

(19) Chen, Y.; Vertes, A. *Anal. Chem.* **2006**, *78*, 5835-5844.

(20) Lai, E. P. C.; Owega, S.; Kulczycki, R. *J. Mass Spectrom.* **1998**, *33*, 554-564.

(21) Li, Y.; McIver, J. R. T.; Hemminger, J. C. *J. Chem. Phys.* **1990**, *93*, 4719-4723.

(22) Chen, Y.; Luo, G.; Diao, J.; Chornoguz, O.; Reeves, M.; Vertes, A. *J. Phys.: Conf. Series* **2007**, *59*, 548-554.

(23) Hoheisel, W.; Schulte, U.; Vollmer, M.; Träger, F. *Appl. Phys. A* **1990**, *51*, 271-280.

(24) Moores, A.; Goettmann, F. *New J. Chem.* **2006**, *30*, 1121-1132.

(25) Daniel, M. C.; Astruc, D. *Chem. Rev.* **2004**, *104*, 293-346.

(26) Faraday, M. *Philos. Trans. R. Soc. London* **1857**, *147-181*, 145.

(27) Link, S.; El-Sayed, M. A. *Annu. Rev. Phys. Chem.* **2003**, *54*, 331-366.

(28) Creighton, J. A.; Eadon, D. G. *J. Chem. Soc. Faraday Trans.* **1991**, *87*, 3881-3891.

(29) Mie, G. *Ann. Phys.* **1908**, *25*, 329-371.

(30) Kreibig, U.; Vollmer, M. *Optical Properties of Metal Clusters*; Springer: New York, 1995.

(31) Perenboom, J. A. A. J.; Wyder, P.; Meier, F. *Phys. Reports* **1981**, *78*, 173-292.

(32) Link, S.; El-Sayed, M. A. *Int. Rev. Phys. Chem.* **2000**, *19*, 409-453.

(33) Stephens, W. *Phys. Rev.* **1946**, *69*, 691-698.

(34) Cameron, A. E.; Eggers, D. F., Jr. *Rev. Sci. Instrum.* **1948**, *19*, 605-607.

(35) Wiley, W. C.; McLaren, J. B. *Rev. Sci. Instrum.* **1955**, *16*, 1150-1157.

(36) Cotter, R. J. *Time-of-Flight Mass Spectrometry: Instrumentation and Applications in Biological Research*; American Chemical Society: Washington, D.C., 1997.

(37) de Hoffmann, E.; Stroobant, V., Eds. *Mass Spectrometry: Principles and Applications*, 2nd ed.; Wiley: Chichester, 1999.

(38) Zhou, J.; Ens, W.; Standing, K. G.; Verentchikov, A.; Sundqvist, B. U. R. *Rapid Comm. Mass Spectrom.* **1992**, *6*, 671-678.

(39) Beavis, R. C.; Chait, B. T. *Chem. Phys. Lett.* **1991**, *181*, 479-484.

(40) Pan, Y.; Cotter, R. J. *Org. Mass Spectrom.* **1992**, *27*, 3-8.

(41) Roepstorff, P.; Fohlmann, J. *J. Biomed. Mass Spectrom.* **1984**, *11*, 601-605.

(42) Biemann, K.; Martin, S. A. *Mass Spectrom. Rev.* **1987**, *6*, 1-75.

(43) Zubarev, R. A.; Kelleher, N. L.; McLafferty, F. W. *J. Am. Chem. Soc.* **1998**, *120*, 3265-3266.

(44) McLafferty, F. W.; Horn, D. M.; Breuker, K.; Ge, Y.; Lewis, M. A.; Cerda, B.; Zubarev, R. A.; Carpenter, B. K. *J. Am. Soc. Mass Spectrom.* **2001**, *12*, 245-249.

(45) Zubarev, R. A.; Kruger, N. A.; Fridriksson, E. K.; Lewis, M. A.; Horn, D. M.; Carpenter, B. K.; McLafferty, F. W. *J. Am. Chem. Soc.* **1999**, *121*, 2857-2862.

(46) Zhang, L.; Cui, W.; Thompson, M. S.; Reilly, J. P. *J. Am. Soc. Mass Spectrom.* **2006**, *17*, 1315-1321.

(47) Thompson, M. S.; Cui, W.; Reilly, J. P. *Angew. Chem. Int. Ed.* **2004**, *43*, 4791-4794.

(48) Solouki, T.; Russell, D. H. *Appl. Spectroscopy* **1993**, *47*, 211-217.

(49) Morgan, J. W.; Russell, D. H. *J. Am. Soc. Mass Spectrom.* **2006**, *17*, 721-729.

(50) Rosenstock, H. M.; Wallenstein, M. B.; Wahrhaftig, A. L.; Eyring, H. *Proc. Natl. Acad. Sci* **1952**, *38*, 667-678.

(51) McLafferty, F. W.; Turecek, F. *Interpretation of Mass Spectra*, 4th ed.; University Science Books: Mill Valley, California, 1993.

(52) McCombie, G.; Knochenmuss, R. *J. Am. Soc. Mass Spectrom.* **2006**, *17*, 737-745.

(53) Keller, B. O.; Li, L. *J. Am. Soc. Mass Spectrom.* **2006**, *17*, 780-785.

(54) Wang, J.; Chen, R.; Ma, M.; Li, L. *Anal. Chem.* **2008**, *80*, 491-500.

(55) Horneffer, V.; Glückmann, M.; Krüger, R.; Karas, M.; Strupat, K.; Hillenkamp, F. *Int. J. Mass Spectrom.* **2006**, *249/250*, 426-432.

(56) Schwartz, S. A.; Reyzer, M. L.; Caprioli, R. M. *J. Mass Spectrom.* **2003**, *38*, 699-708.

(57) Nuwaysir, L. M.; Wilkins, C. L. *Proc. SPIE* **1991**, *1437*, 112-123.

(58) Koomen, J. M.; Russell, W. K.; Hettick, J. M.; Russell, D. H. *Anal. Chem.* **2000**, *72*, 3860-3866.

(59) Cohen, S. L.; Chait, B. T. *Anal. Chem.* **1996**, *68*, 31-37.

(60) Sheeley, S. A.; Rubakhin, S. S.; Sweedler, J. V. *Anal. Bioanal. Chem.* **2005**, *382*, 22-27.

(61) Laugesen, S.; Roepstorff, P. *J. Am. Soc. Mass Spectrom.* **2003**, *14*, 992-1002.

(62) Beavis, R. C.; Chaudhary, T.; Chait, B. T. *Org. Mass Spectrom.* **1992**, *27*, 156-158.

(63) Armstrong, D. W.; Zhang, L. K.; He, L.; Gross, M. L. *Anal. Chem.* **2001**, *73*, 3679-3686.

(64) Jespersen, S.; Niessen, W. M. A.; Tjaden, U. R.; van der Greef, J. *J. Mass Spectrom.* **1998**, *33*, 1088-1093.

(65) André, M.; Karas, M. *Anal. Bioanal. Chem.* **2007**, *389*, 1047-1053.

(66) Fukuzawa, S.; Asanuma, M.; Tachibana, K.; Hirota, H. *Anal. Chem.* **2005**, *77*, 5750-5754.

(67) Zhang, N.; Li, L. *Anal. Chem.* **2002**, *74*, 1729-1736.

(68) Gobom, J.; Nordhoff, E.; Mirgorodskaya, E.; Ekman, R.; Roepstorff, P. *J. Mass Spectrom.* **1999**, *34*, 105-116.

(69) Zhang, N.; Li, L. *Rapid Comm. Mass Spectrom.* **2004**, *18*, 889-896.

(70) Börnsen, K. O.; Gass, M. A. S.; Bruin, G., J. M.; von Adrichem, J. H. M.; Biro, M. C.; Kresbach, G. M.; Ehrat, M. *Rapid Comm. Mass Spectrom.* **1997**, *11*, 603-609.

(71) Dogruel, D.; W. Nelson, R.; Williams, P. *Rapid Comm. Mass Spectrom.* **1996**, *10*, 801-804.

(72) Kjellstrom, S.; Jensen, O. N. *Anal. Chem.* **2004**, *76*, 5109-5117.

(73) Li, Y. C. L.; Cheng, S.-w.; Chan, T.-W. D. *Rapid Comm. Mass Spectrom.* **1998**, *12*, 993-998.

(74) Kim, J. S.; Kim, J. Y.; Kim, H. J. *Anal. Chem.* **2005**, *77*, 7483-7488.

(75) Brust, M.; Walker, M.; Bethell, D.; Schiffrin, D. J.; Wyhman, R. *J. Chem. Soc., Chem. Comm.* **1994**, 801-802.

(76) Enustun, B. V.; Turkevich, J. *J. Am. Chem. Soc.* **1963**, *85*, 3317-3328.

(77) Wangoo, N.; Bhasin, K. K.; Mehta, S. K.; Suri, C. R. *J. Coll. Interf. Sci.* **2008**, *323*, 247-254.

(78) Cheng, S.-w.; Dominic Chan, T.-W. *Rapid Comm. Mass Spectrom.* **1996**, *10*, 907-910.

(79) Li, Y. C. L.; Cheng, S.-w.; Dominic Chan, T.-W. *Rapid Comm. Mass Spectrom.* **1998**, *12*, 993-998.

(80) Beavis, R. C.; Lindner, J.; Grotemeyer, J.; Schlag, E. W. *Chem. Phys. Lett.* **1988**, *146*, 310-314.

(81) Koster, C.; Castoro, J. A.; Wilkins, C. L. *J. Am. Chem. Soc.* **1992**, *114*, 7572-7574.

(82) Reid, G.; Simpson, R.; O'Hair, R. J. *J. Am. Soc. Mass Spectrom.* **1998**, *9*, 945-956.

(83) Cox, K. A.; Gaskell, S. J.; Morris, M.; Whiting, A. *J. Am. Soc. Mass Spectrom.* **1996**, *7*, 522-531.

(84) Basu, S.; Panigrahi, S.; Praharaj, S.; Ghosh, S. K.; Pande, S.; Jana, S.; Pal, T. *New J. Chem.* **2006**, *30*, 1333-1339.

(85) Zhu, Y. F.; Lee, K. L.; Tang, K.; Allman, S. L.; Taranenko, N. I.; H., C. C. *Rapid Comm. Mass Spectrom.* **1995**, *9*, 1315-1320.

(86) Krause, E.; Wenschuh, H.; Jungblut, P. R. *Anal. Chem.* **1999**, *71*, 4160-4165.

(87) Baumgart, S.; Lindner, Y.; Kühne, R.; Oberemm, A.; Wenschuh, H.; Krause, E. *Rapid Comm. Mass Spectrom.* **2004**, *18*, 863-868.

(88) Nishikaze, T.; Takayama, M. *Rapid Comm. Mass Spectrom.* **2006**, *20*, 376-382.

(89) Valero, M.-L.; Giralt, E.; Andreu, D. *Lett. Peptide Sci.* **1999**, *6*, 109-115.

(90) Shields, S. J., Texas A&M University, College Station, 1998.

(91) Barbacci, D. C.; Edmondson, R. D.; Russell, D. H. *Int. J. Mass Spectrom. Ion Proc.* **1997**, *165/166*, 221-235.

(92) Williams, T. L.; Fenselau, C. *Eur. Mass Spectrom.* **1998**, *4*, 379-383.

(93) Shipway, A. N.; Katz, E.; Willner, I. *ChemPhysChem* **2000**, *1*, 18-52.

(94) Nuzzo, R. G.; Allara, D. L. *J. Am. Chem. Soc.* **1983**, *105*, 4481-4483.

(95) Ulman, A. *Chem. Rev.* **1996**, *96*, 1533-1554.

(96) Bain, C. D.; Troughton, E. B.; Tao, Y.-T.; Evall, J.; Whitesides, G. M.; Nuzzo, R. G. *J. Am. Chem. Soc.* **1989**, *111*, 321-335.

(97) Bain, C. D.; Evall, J.; Whitesides, G. M. *J. Am. Chem. Soc.* **1989**, *111*, 7155-7164.

(98) Bain, C. D.; Whitesides, G. M. *J. Am. Chem. Soc.* **1989**, *111*, 7164-7175.

(99) McLean, J. A.; Stumpo, K. A.; Russell, D. H. *J. Am. Chem. Soc.* **2005**, *127*, 5304-5305.

(100) Gao, P.; Weaver, M. J. *J. Phys. Chem.* **1986**, *90*, 4057-4063.

(101) Magnussen, O. M.; Ocko, B. M.; Adzic, R. R.; Wang, J. X. *Phys. Rev. B* **1995**, *51*, 5510-5513.

(102) Huheey, J. E.; Keiter, E. A.; Keiter, R. L. *Inorganic Chemistry: Principles of Structure and Reactivity*, 4th ed.; HarperCollins: New York.

(103) Clementi, E.; Raimondi, D. L. *J. Chem. Phys.* **1963**, *38*, 2686-2689.

(104) Breuker, K.; Knochenmuss, R.; Zenobi, R. *Int. J. Mass Spectrom.* **1998**, *176*, 149-159.

(105) Russell, W. K.; Chen, L.; Russell, D. *J. Am. Soc. Mass Spectrom.* **2008**, *Manuscript in preparation*.

(106) Rodriguez, J. F.; Harris, J. E.; Bothwell, M. E.; Mebrahtu, T.; Soriaga, M. P. *Inorg. Chim. Acta* **1988**, *148*, 123-131.

(107) Cheng, W.; Dong, S.; Wang, E. *Angew. Chem. Int. Ed.* **2003**, *42*, 449-452.

(108) Wanner, M.; Gerthsen, D. *Colloid Polym. Sci.* **2004**, *282*, 1126-1132.

(109) Singh, S.; Pasricha, R.; Bhatta, U. M.; Satyam, P. V.; Sastry, M.; Prasad, B. L. V. *J. Mater. Chem.* **2007**, *17*, 1614-1619.

(110) Devanathan, M. A. V.; Fernando, M. J. *Trans. Faraday Soc.* **1962**, *58*, 368.

(111) Barclay, D. J.; Anson, F. C. *J. Electroanal. Chem.* **1970**, *28*, 71-79.

(112) Fink, J.; Kiely, C. J.; Bethell, D.; Schiffrin, D. J. *Chem. Mater.* **1998**, *10*, 922-926.

(113) Cumberland, S. L.; Strouse, G. F. *Langmuir* **2002**, *18*, 269-276.

(114) Dongre, A. R.; Jones, J. L.; Somogyi, A.; Wysocki, V. H. *J. Am. Chem. Soc.* **1996**, *118*, 8365-8374.

(115) Tsaprailis, G.; Nair, H.; Somogyi, A.; Wysocki, V. H.; Zhong, W.; Futrell, J. H.; Summerfield, S. G.; Gaskell, S. J. *J. Am. Chem. Soc.* **1999**, *121*, 5142-5154.

(116) Tsaprailis, G.; Somogyi, Á.; Nikolaev, E. N.; Wysocki, V. H. *Int. J. Mass Spectrom.* **2000**, *195-196*, 467-479.

(117) Wysocki, V. H.; Tsaprailis, G.; Smith, L. L.; Breci, L. A. *J. Mass Spectrom.* **2000**, *35*, 1399-1406.

(118) Burlet, O.; Orkiszewski, R. S.; Ballard, K. D.; Gaskell, S. J.; Bertrand, M. J. *Rapid Comm. Mass Spectrom.* **1992**, *6*, 658-662.

(119) Mabud, M. A.; Dekrey, M. J.; Graham Cooks, R. *Int. J. Mass Spectrom. Ion Proc.* **1985**, *67*, 285-294.

(120) Cooks, R. G.; Ast, T.; Mabud, M. A. *Int. J. Mass Spectrom. Ion Proc.* **1990**, *100*, 209-265.

(121) McCormack, A. L.; Somogyi, A.; Dongre, A. R.; Wysocki, V. H. *Anal. Chem.* **1993**, *65*, 2859-2872.

(122) Cui, W.; Thompson, M. S.; Reilly, J. P. *J. Am. Soc. Mass Spectrom.* **2005**, *16*, 1384-1398.

(123) Chu, I. K.; Rodriquez, C. F.; Lau, T. C.; Hopkinson, A. C.; Siu, K. W. M. *J. Phys. Chem. B* **2000**, *104*, 3393-3397.

(124) Chu, I. K.; Rodriguez, C. F.; Hopkinson, A. C.; Siu, K. W. M.; Lau, T.-C. *J. Am. Soc. Mass Spectrom.* **2001**, *12*, 1114-1119.

(125) Ke, Y.; Verkerk, U. H.; Shek, P. Y. I.; Hopkinson, A. C.; Siu, K. W. M. *J. Phys. Chem. B* **2006**, *110*, 8517-8523.

(126) Hopkinson, A. C.; Siu, K. W. M. In *Principles of Mass Spectrometry Applied to Biomolecules*; Laskin, J., Lifshitz, C., Eds.; John Wiley and Sons: New York, 2006.

(127) Wee, S.; O'Hair, R. A. J.; McFadyen, W. D. *Int. J. Mass Spectrom.* **2006**, *249-250*, 171-183.

(128) Karnezis, A.; Barlow, C. K.; O'Hair, R. A. J.; McFadyen, W. D. *Rapid Comm. Mass Spectrom.* **2006**, *20*, 2865-2870.

(129) Laskin, J.; Yang, Z.; Lam, C.; Chu, I. K. *Anal. Chem.* **2007**, *79*, 6607-6614.

(130) Brown, R. S.; Lennon, J. J. *Anal. Chem.* **1995**, *67*, 3990-3999.

(131) Brown, R. S.; Feng, J.; Reiber, D. C. *Int. J. Mass Spectrom. Ion Proc.* **1997**, *169/170*, 1-18.

(132) Reiber, D. C.; Grover, T. A.; Brown, R. S. *Anal. Chem.* **1998**, *70*, 673-683.

(133) Kocher, T.; Engstrom, A.; Zubarev, R. A. *Anal. Chem.* **2005**, *77*, 172-177.

(134) Kish, M. M.; Ohanessian, G.; Wesdemiotis, C. *Int. J. Mass Spectrom.* **2003**, *227*, 509-524.

(135) Liao, P.-C.; Huang, Z.-H.; Allison, J. *J. Am. Soc. Mass Spectrom.* **1997**, *8*, 501-509.

(136) Cheng, C.; Gross, M. L. *Mass Spectrom. Rev.* **2000**, *19*, 398-420.

(137) Shields, S. J.; Bluhm, B. K.; Russell, D. H. *J. Am. Soc. Mass Spectrom.* **2000**, *11*, 626-638.

(138) Wysocki, V. H.; Tsaprailis, G.; Smith, L. L.; Breci, L. A. *J. Mass Spectrom.* **2000**, *35*, 1399-1406.

(139) Stumpo, K. A.; Russell, D. H. *J. Phys. Chem. C* **2008**, *Submitted*.

(140) Johnson, R. S.; Martin, S. A.; Biemann, K. *Int. J. Mass Spectrom. Ion Proc.* **1988**, *86*, 137-154.

(141) Hunt, D. F.; Yates, J. R.; Shabanowitz, J.; Winston, S.; Hauer, C. R. *Proc. Natl. Acad. Sci* **1986**, *83*, 6233-6237.

(142) Ballard, K. D.; Gaskell, S. J. *Int. J. Mass Spectrom. Ion Proc.* **1991**, *111*, 173-189.

(143) Somogyi, Á.; Wysocki, V. H.; Mayer, I. *J. Am. Soc. Mass Spectrom.* **1994**, *5*, 704-717.

(144) Mallis, L. M.; Russell, D. H. *Anal. Chem.* **1986**, *58*, 1076-1080.

(145) Mallis, L. M.; Russell, D. H. *Int. J. Mass Spectrom. Ion Proc.* **1987**, *78*, 147-178.

(146) Grese, R. P.; Cerny, R. L.; Gross, M. L. *J. Am. Chem. Soc.* **1989**, *111*, 2835-2842.

(147) Teesch, L. M.; Orlando, R. C.; Adams, J. *J. Am. Chem. Soc.* **1991**, *113*, 3668-3675.

(148) Hettick, J. M.; McCurdy, D. L.; Barbacci, D. C.; Russell, D. H. *Anal. Chem.* **2001**, *73*, 5378-5386.

(149) Ly, T.; Julian, R. R. *J. Am. Chem. Soc.* **2008**, *130*, 351-358.

(150) Hodyss, R.; Cox, H. A.; Beauchamp, J. L. *J. Am. Chem. Soc.* **2005**, *127*, 12436-12437.

(151) Masterson, D. S.; Yin, H.; Chacon, A.; Hachey, D. L.; Norris, J. L.; Porter, N. A. *J. Am. Chem. Soc.* **2004**, *126*, 720-721.

(152) Tang, X.; Ens, W.; Standing, K. G.; Westmore, J. B. *Anal. Chem.* **1988**, *60*, 1791-1799.

(153) Leary, J. A.; Zhou, Z.; Ogden, S. A.; Williams, T. D. *J. Am. Soc. Mass Spectrom.* **1990**, *1*, 473-480.

(154) Cooper, H. J.; Hudgins, R. R.; Håkansson, K.; Marshall, A. G. *Int. J. Mass Spectrom.* **2003**, *228*, 723-728.

(155) Loo, J. A.; Edmonds, C. G.; Smith, R. D. *Anal. Chem.* **1993**, *65*, 425-438.

(156) Martin, S. A.; Biemann, K. *Int. J. Mass Spectrom. Ion Proc.* **1987**, *78*, 213-228.
(157) T. Vaisar, J. U. *J. Mass Spectrom.* **1996**, *31*, 1185-1187.

(158) Han, H.; Xia, Y.; McLuckey, S. A. *J. Prot. Res.* **2007**, *6*, 3062-3069.

(159) Johnson, R. S.; Martin, S. A.; Biemann, K.; Stults, J. T.; Watson, J. T. *Anal. Chem.* **1987**, *59*, 2621-2625.

(160) Karas, M.; Kruger, R. *Chem. Rev.* **2003**, *103*, 427-440.

(161) Karas, M.; Gluckmann, M.; Schäfer, J. *J. Mass Spectrom.* **2000**, *35*, 1-12.

(162) Thomas, S. *J. Chem. Phys.* **2007**, *126*, 124301.

(163) Knochenmuss, R. *Anal. Chem.* **2004**, *76*, 3179-3184.

(164) Dashtiev, M.; Frankevich, V.; Zenobi, R. *J. Phys. Chem. A* **2006**, *110*, 926-930.

(165) Sun, J.; Guan, M.; Shang, T.; Gao, C.; Xu, Z.; Zhu, J. *Crys. Growth Des.* **2008**, *8*, 906-910.

(166) Sra, A. K.; Schaak, R. E. *J. Am. Chem. Soc.* **2004**, *126*, 6667-6672.

(167) Leonard, B. M.; Bhuvanesh, N. S. P.; Schaak, R. E. *J. Am. Chem. Soc.* **2005**, *127*, 7326-7327.

(168) Shlyahovsky, B.; Katz, E.; Xiao, Y.; Pavlov, V.; Willner, I. *Small* **2005**, *1*, 213-216.

(169) Gatlin, C. L.; Rao, R. D.; Turecek, F.; Vaisar, T. *Anal. Chem.* **1996**, *68*, 263-270.

(170) Gatlin, C. L.; Turecek, F.; Vaisar, T. *J. Am. Chem. Soc.* **1995**, *117*, 3637-3638.

(171) Gatlin, C. L.; Turecek, F.; Vaisar, T. *J. Mass Spectrom.* **1995**, *30*, 1605-1616.

(172) Gatlin, C. L.; Turecek, F.; Vaisar, T. *J. Mass Spectrom.* **1995**, *30*, 1617-1627.

(173) Cerda, B. A.; Wesdemiotis, C. *J. Am. Chem. Soc.* **1995**, *117*, 9734-9739.

(174) Shields, S. J.; Bluhm, B. K.; Russell, D. H. *Int. J. Mass Spectrom.* **1999**, *182/183*, 185-195.

(175) Bluhm, B. K.; Shields, S. J.; Bayse, C. A.; Hall, M. B.; Russell, D. H. *Int. J. Mass Spectrom.* **2001**, *204*, 31-46.

(176) Knochenmuss, R.; Stortelder, A.; Breuker, K.; Zenobi, R. *J. Mass Spectrom.* **2000**, *35*, 1237-1245.

(177) Zhang, J.; Frankevich, V.; Knochenmuss, R.; Friess, S. D.; Zenobi, R. *J. Am. Soc. Mass Spectrom.* **2003**, *14*, 42-50.

(178) Gross, M. L. *Acc. Chem. Res.* **1994**, *27*, 361-369.

(179) Wen, D.; Yalcin, T.; Harrison, A. G. *Rapid Comm. Mass Spectrom.* **1995**, *9*, 1155-1157.

(180) Hoyau, S.; Ohanessian, G. *J. Am. Chem. Soc.* **1997**, *119*, 2016-2024.

(181) Underwood, S.; Mulvaney, P. *Langmuir* **1994**, *10*, 3427-3430.

(182) Martínez-Díaz, M. V.; Torres, T.; Schäfer, W. *Inorg. Chim. Acta* **1994**, *219*, 85-92.

(183) Li, H.; Siu, K. W. M.; Guevremont, R.; Le Blanc, J. C. Y. *J. Am. Soc. Mass Spectrom.* **1997**, *8*, 781-792.

(184) Reiter, A.; Adams, J.; Zhao, H. *J. Am. Chem. Soc.* **1994**, *116*, 7827-7838.

(185) Hu, P.; Gross, M. L. *J. Am. Chem. Soc.* **1993**, *115*, 8821-8828.

(186) Spengler, B.; Bökelmann, V. *Nucl. Instrum. Methods B* **1993**, *82*, 379-385.

(187) Zhang, W.; Chait, B. T. *Int. J. Mass Spectrom. Ion Proc.* **1997**, *160*, 259-267.

(188) Edy Ayala, E.; Vera, C. C.; Håkansson, P. *Rapid Comm. Mass Spectrom.* **1999**, *13*, 792-797.

(189) Beavis, R. C.; Chait, B. T. *Chem. Physics Lett.* **1991**, *181*, 479-484.

(190) Verentchikov, A.; Ens, W.; Martens, J.; Standing, K. G., Washington, D.C. 1992; ASMS; 360.

(191) Zhigilei, L. V.; Kodali, P. B. S.; Garrison, B. J. *Chem. Phys. Lett.* **1997**, *276*, 269-273.

(192) Zhigilei, L. V.; Kodali, P. B. S.; Garrison, B. J. *J. Phys. Chem. B* **1997**, *101*, 2028-2037.

(193) Zhigilei, L. V.; Garrison, B. J. *Rapid Comm. Mass Spectrom.* **1998**, *12*, 1273-1277.

(194) Dreisewerd, K.; Schürenberg, M.; Karas, M.; Hillenkamp, F. *Int. J. Mass Spectrom. Ion Proc.* **1995**, *141*, 127-148.

(195) Cooks, R. G.; Busch, K. L. *Int. J. Mass Spectrom. Ion Phys.* **1983**, *53*, 111-124.

(196) Michl, J. *Int. J. Mass Spectrom. Ion Phys.* **1983**, *53*, 255-272.

(197) Spengler, B.; Karas, M.; Bahr, U.; Hillenkamp, F. *J. Phys. Chem.* **1987**, *91*, 6502-6506.

(198) Verentchikov, A.; Smirnov, I.; Vestal, M., Dallas, TX, June 13-17, 1999.

(199) Cai, Y.; Peng, W. P.; Kuo, S. J.; Sabu, S.; Han, C. C.; Chang, H. C. *Anal. Chem.* **2002**, *74*, 4434-4440.

(200) Krutchinsky, A. N.; Chait, B. T. *J. Am. Soc. Mass Spectrom.* **2002**, *13*, 129-134.

(201) Beuhler, R. J.; Flanigan, E.; Greene, L. J.; Friedman, L. *J. Am. Chem. Soc.* **1974**, *96*, 3990-3999.

(202) Winkler, H. U.; Beuhler, R. J.; Friedman, L. *Biomed. Mass Spectrom.* **1976**, *3*, 201-206.

(203) Ahmadi, T. S.; Logunov, S. L.; El-Sayed, M. A. *J. Phys. Chem.* **1996**, *100*, 8053-8056.

(204) Kamat, P. V.; Flumiani, M.; Hartland, G. V. *J. Phys. Chem. B* **1998**, *102*, 3123-3128.

(205) Heilweil, E. J.; Hochstrasser, R. M. *J. Chem. Phys.* **1985**, *82*, 4762-4770.

(206) Feldstein, M. J.; Keating, C. D.; Liau, Y. H.; Natan, M. J.; Scherer, N. F. *J. Am. Chem. Soc.* **1997**, *119*, 6638-6647.

VITA

Katherine Anne Stumpo received her Bachelor of Science degree in chemistry with a biochemistry emphasis from the University of Northern Iowa in 2003. In the summer of 2003 she joined the Russell Research Group at Texas A&M University. She earned her Ph.D. in Chemistry in December of 2008.

Publications

Stumpo, Katherine A.; Russell, David H. "Anion Effects on Ionization Efficiency Using Gold Nanoparticles as Matrices for LDI-MS," *J. Phys. Chem. C*, 2**008**, Submitted.

McLean, John A.; Stumpo, Katherine A.; Russell, David H. "Size-Selected (2-10 nm) Gold Nanoparticles for Matrix Assisted Laser Desorption Ionization of Peptides," *J. Am. Chem. Soc.*, **2005**, *127*, 5304-5305.

Selected Presentations

Stumpo, Katherine A.; Russell, David H. "The Effects of Sample Preparation for Nanoparticulate Matrices in LDI-TOFMS," presented at the 55th American Society for Mass Spectrometry Conference, Indianapolis, IN, June 2007.

Stumpo, Katherine A.; Russell, David H. "Fragmentation of Cu-adducted peptides by MALDI TOFMS using Gold Nanoparticle Matrices," presented at 21st Asilomar Conference on Mass Spectrometry, Pacific Grove, CA, October 2006.

Stumpo, Katherine A.; Castellana, Edward T.; Russell, David H. "Surface Passivation of Gold Nanoparticles in MALDI Mass Spectrometry," presented at the 2006 Materials Research Society Spring Meeting, San Francisco, CA, April 2006.

Stumpo, Katherine A.; McLean, John A.; Russell, David H. "Quantum Dots as MALDI Matrices for Biological Mass Spectrometry," presented at the 53rd American Society for Mass Spectrometry Conference, San Antonio, TX, June 2005.

Kate may be reached at her permanent address: Kate Stumpo, c/o David Russell, Texas A&M University, Department of Chemistry, MS 3255, College Station, Texas, 77843